A Study on Aeolian Dust Outbreak in East Asia

A Dissertation Submitted to
the Graduate School of Life and Environmental Science,
the University of Tsukuba
in Partial Fulfillment of the Requirements
for the Degree of Doctor of Philosophy in Science

Yasunori KUROSAKI

Abstract

The impact of aeolian dust on climate has been recognized to be large due to radiative effect. *Intergovernmental Panel on Climate Change (IPCC)* [2001] also treats the aeolian dust as an important factor of climate change. However, the uncertainty of the effect of the aeolian dust is very large and the level of scientific understanding about the aeolian dust is classified as very low in *IPCC* [2001]. One of the major reasons of insufficient understanding is the inhomogeneous distribution of aeolian dust owing to their short lifetime. They are removed by rain typically within a week. As a result, the concentration of aeolian dust rises to its highest near its source just after its outbreak. The uncertainty still remains due to the difficulty of understanding the distribution of aeolian dust sources and the timing of aeolian dust outbreak.

Aeolian dusts are generated by strong surface winds, while land surface conditions largely affect aeolian dust outbreaks because the threshold wind velocity of aeolian dust outbreak has various values according to land surface conditions. Therefore, it is important to recognize the distribution of aeolian dust sources, land cover types (e.g., desert, grassland, forest, cultivation) around aeolian dust sources and threshold wind velocities according to land surface conditions.

This study focuses on the aeolian dust outbreak in East Asia, which is one of the major aeolian dust sources. The following three geographical characteristics are found to be essential for the aeolian dust outbreak in East Asia: (1) frequent synoptic disturbances in spring, (2) complicated distribution of land cover types, and (3) frequent snow covers in early spring. With regard to the first characteristic, it is well known that strong winds cause aeolian dust outbreaks when a synoptic disturbance passes over East Asia. With regard to the second characteristic, land cover types complicatedly distribute in East Asia in comparison with other aeolian dust sources such as Sahara Desert. This suggests that aeolian dust sources also complicatedly distribute in East Asia. With regard to the third characteristic, snow cover in early spring often prevents aeolian dust outbreaks in East Asia because arid and/or semiarid regions distribute in

relatively high latitude. These geographical characteristics make it difficult to understand the spatial and temporal distributions of aeolian dust outbreaks in East Asia.

The purposes in this study are to clarify (i) the relation between aeolian dust sources and land cover types, (ii) which largely control aeolian dust outbreaks, surface winds or land surface conditions, (iii) the spatial distribution of threshold wind velocities of aeolian dust outbreak, and (iv) the effect of snow cover on aeolian dust outbreak. For these purposes, this study conducts statistical analyses by use of surface meteorological data, land cover type data and snow cover data in East Asia for the period from March 1988 to June 2003. Conclusions are summarized as follows:

1. Aeolian dust sources in East Asia distribute in regions of Bare Desert, Semi Desert Shrubs, Grass/Shrub and Cultivation. The northern boundary of dust sources almost corresponds to the southern boundary of the Forest regions. The southern boundary of dust sources distribute around the southern boundaries of Bare Desert and Semi Desert Shrubs regions in middle and upper reaches of the Huang He River.

2. Aeolian dust outbreaks frequently occur at months of frequent strong winds around the Gobi Desert and in the Taklimakan Desert. The months of frequent dust outbreaks are limited in March, April and May around the Gobi Desert, while dust outbreaks frequently occur from March to July and/or August in the Taklimakan Desert. According to the correlation between strong wind frequency and dust outbreak frequency, the surface wind primarily controls dust outbreaks in March and April. This tendency is strong especially in the Taklimakan Desert. On the other hand, land surface conditions largely affect aeolian dust outbreaks in May around the Gobi Desert.

3. The minimum threshold velocity ($u_{t5\%}$) and the practical threshold velocity ($u_{t50\%}$) are defined in this study. The former ($u_{t5\%}$) is the threshold velocity at nearly the most favorable land surface condition for aeolian dust outbreak. The latter ($u_{t50\%}$) is the threshold velocity at a usual land surface condition. There is a tendency that

both kinds of threshold velocities (i.e., $u_{t5\%}$ and $u_{t50\%}$) decrease from the northeast (i.e., Mongolia and Inner Mongolia) to the southwest (i.e., the Taklimakan Desert). From the viewpoint of land cover type, they are the largest in the Grass/Shrub region, the next largest in the Semi Desert Shrubs region and the smallest in the Bare Desert region. Differences of threshold velocity ($\Delta u_t = u_{t50\%} - u_{t5\%}$) are large in Mongolia and small in the west of the Taklimakan Desert. This result indicates that land surface conditions are largely variable in Mongolia and almost constant in the west of the Taklimakan Desert.

4. This study statistically analyzed the relation between the threshold wind velocity of dust outbreak and snow cover in March and April. It is found that the threshold velocity linearly increases with snow cover fraction. The threshold velocity is well parameterized with snow cover fraction. This formulation improves the correlation between the strong wind frequency and the dust outbreak frequency in East Asia in March and April.

Key words: aeolian dust outbreak, threshold wind velocity, strong wind, land cover type, snow cover

Contents

List of Tables

List of Figures

the right axis. In a neutrally buoyant surface layer the wind velocity varies with height in a logarithmic profile as $u(z) = \{u_* \ln(z/z_0)\}/\kappa$, where u is the wind velocity at the height z, u_* is the friction velocity, z_0 is the roughness length, and κ is the von Karman constant (0.41). Threshold wind velocity (u_t) in the right axis is given through this equation where the reference height (z) and the roughness length (z_0) are set as 10 m and 0.001 m, respectively. 91

Chapter 1

Introduction

1.1 Aeolian dust

The "*dust*" can be defined as a suspension of solid particles in a gas, or a deposit of such particles [*Pye*, 1987]. There are several types of dust such as soil dust, cosmic dust, volcanic dust, industrial dust, and so on, while the dust treated in this study is soil dust.

The meaning of "*aeolian*" is "*pertaining to the action or the effect of the wind*" [*Glickman*, 2000] and/or "*borne, deposited, produced, or eroded by the wind*" [*Gove et al.*, 1981; Webster's Third New International Dictionary]. A life of the aeolian dust has three distinct phases: (1) the entrainment of particles by wind shear at surface ("*produced*" or "*eroded*"), (2) the transport of particles in the atmosphere by advection and turbulent diffusion ("*borne by wind*" or "airborne"), and (3) the deposition of particles through dry and wet removal ("*deposited*") (Fig. 1.1) [*Shao*, 2000]. The phase discussed in this study is the first one (i.e., "*produced*" or "*eroded*"). This phase can be expressed as an outbreak of aeolian dust. Hereafter, the phase of entrainment is called "*aeolian dust outbreak*" or "*dust outbreak*". The "*aeolian dust*" in this study is practically the same as the "*mineral dust*" used in other research, while this study chooses the "*aeolian dust*" because our target of discussion is not the component of dust particles but the outbreak of dust.

Soil particles are crudely divided into four categories referred to as gravel (2000 μm < d < 2 m), sand (63 < d < 2000 μm), silt (4 < d < 63 μm) and clay (d < 4 μm) [*Shao*, 2000]. Silt and clay particles are commonly called dust. Namely, the dust particles are tiny soil

particles, which can be suspended in the atmosphere. The particle size distribution in the surface soil is one of important keys in the process of aeolian dust outbreak (section 5.1). The difference of particle size is important in the discussion of radiative forcing (section 1.3) and dust transport (section 1.4).

1.2 Impact of aeolian dust on human society

A heavy aeolian dust is a disaster, which considerably damages agriculture, livestock farming, transportation, human health, and so on. One of major agricultural damages is soil degradation by wind erosion, which reduces agricultural productivity [*Middleton and Thomas*, 1997]. A visibility reduction and a huge dust deposition lead to closures of airports, stops of railroad services, road accidents, and so on. Fine particles cause respiratory diseases to livestock and humans.

On the contrary, the aeolian dust has positive aspects for human society. Minerals of aeolian dust neutralize acid rain [*Hedin and Likens*, 1996]. The aeolian dust plays an important role in the supply of nutrients to the oceans [*Squires*, 2001]. Depositions of minerals lead to large supplies of oceanic food. Furthermore, the suppression of greenhouse effect can be expected because phytoplankton absorbs carbon dioxide.

1.3 Impact of aeolian dust on climate

The aeolian dust is a kind of aerosols, which are particles of matter, solid or liquid, larger than a molecule but small enough to remain suspended in the atmosphere [*Canadian Society of Soil Science*, 2002]. The third assessment report of the Intergovernmental Panel on Climate Change (IPCC) [*IPCC*, 2001] evaluates the impacts of aerosols on climate, using the concept of radiative forcing, which is a change in the net radiative energy available to the global Earth-atmosphere system. According to this report, aerosols are known to influence significantly the radiative budget of the Earth/atmosphere. However, the levels of scientific understanding (LOSU) about

radiative forcings due to aerosols, especially aeolian dust, are very low, and there are still many uncertainties.

1.3.1 Mechanism

Radiative effects by aerosols occur in two distinct ways: (i) the direct effect, whereby aerosols themselves scatter and absorb solar and thermal infrared radiation, and (ii) the indirect effect, whereby aerosols modify the cloud microphysics and hence the radiative properties and amount of clouds.

The sources of aerosols are inhomogeneously distributed on the earth's surface. Most aerosols are found in the lower troposphere (below a few kilometers), and aerosols are largely and relatively rapidly removed by precipitation (typically within a week). Because of these, aerosols are distributed inhomogeneously in the troposphere, with maxima near the sources. The radiative forcings due to aerosols depend on these spatial distributions. In addition, they depend on the size, shape, and chemical composition of the particles as well. For example, the aeolian dust particles have various shapes [*Okada et al.*, 2001], and they are composed of many kinds of mineral matter   [*Pye*, 1988; *Yabuki et al*, 2002; *Kanayama et al.*, 2002]. Their shapes and components are different according to dust sources. Various aspects of the hydrological cycle (e.g., cloud formation) affect radiative forcings due to aerosols as well.

1.3.2 Level of scientific understanding (LOSU) and uncertainty of radiative forcing due to aeolian dust

According to *IPCC* [2001], most notable agents, which can cause climate change, are increases in the atmospheric concentrations of greenhouse gases and aerosols and variations in solar activity. They can alter the Earth's radiation-budget and hence climate. Figure 1.2 shows global, annual-mean radiative forcings (Wm^{-2}) due to a number of agents for the period from pre-industrial times (1750) to the present (late 1990s; about 2000). LOSU of radiative forcing due to greenhouse gases (e.g., CO_2, CH_4) is high, while those due to aerosols, including tropospheric aerosol indirect effect, are

low or very low. Especially as concerns mineral dust, in addition to very low LOSU, there is no central or best estimate value of radiative forcing, and the uncertainty of this is positively and negatively very large.

Greenhouse gases, of which LOSU are high, are long-lived and well-mixed (i.e., homogeneous spatial distribution). In contrast, aerosols are inhomogeneously distributed, and this fact makes LOSU of aerosols very low. Furthermore, the wide range of particle size distribution and many kinds of shapes and complex chemical compositions of aerosols cause LOSU to be very low.

1.4 Distribution of aeolian dusts

1.4.1 Global distribution of aeolian dust sources

Aeolian dusts account for a large proportion of aerosols, especially in sub-tropical and tropical regions. According to *IPCC* [2001], and *Tegen and Fung* [1995], the global source strength of aeolian dust is estimated to be a value between 1000 and 5000 Mt/year. According to *Pye* [1987], the major sources of aeolian dust are: (1) the sub-tropical deserts located in a broad belt from West Africa to Central Asia; and (2) semi-arid and sub-humid regions where dry, ploughed soils are exposed to severe winds at certain times of the year (Fig. 1.3). Global dust sources can be read roughly from Fig. 1.3, which shows deserts in arid and semi-arid erodible regions. However, this map does not show the precise distribution of aeolian dust sources. Dust source regions are not only deserts and dry ploughed cultivation regions but also dry lake beds, wadis, semi-arid desert fringes, deforestation regions, overgrazed lands and so on. On the contrary, even in a desert, there are both large and small dust sources. It is recognized that an old desert is usually not a large dust source because many fine soil particles (i.e., dust particles) have already been blown away by the wind over a long period, while a new desert (i.e., frontal region of desertification) is a large dust source because this region is rich in fine soil particles.

When and where wind erosion (i.e., aeolian dust outbreak) occurs depends upon the

mutual interaction between "*erosivity*" and "*erodibility*" factors [*Bullard* et al., 1997]. Erosivity refers to the forces that can liberate particles from the main soil mass and is controlled primarily by natural criteria such as frequency of strong winds, duration of wind, wind velocity, wind turbulence, and so on. Erodibility is the susceptibility of a soil to the loss of material, which is influenced by both physical soil characteristics and land use such as particle size and shape, organic material (binding) content, clay content, cohesiveness, infiltration capacity, moisture content, porosity and permeability, vegetation cover density, plant height and shape, presence of surface crusts and so on [*Middleton and Thomas*, 1997]. *Middleton and Thomas* [1997] provides a map of wind erosion severity (Fig. 1.4). Their map shows that the central regions of Sahara Desert are non-degraded, while the wind erosion severities is classed as high or very high in the fringes of Sahara Desert, including the Sahel.

Tegen and Fung [1995] conducted a numerical simulation of aeolian dust. They classified aeolian dust sources into natural sources and disturbed sources. Natural sources are deserts and sparsely vegetated soils, and disturbed sources are cultivated eroded soils (i.e., old cultivation regions) and uncultivated eroded soils (e.g., overgrazed regions), Saharan/Sahelian boundary shift, recently cultivated areas, and recently deforested areas. They gave a boundary condition of dust outbreaks as Fig. 1.5, and they obtained annual dust emission from natural and disturbed soils (Fig. 1.6).

Prospero et al. [2002] identified aeolian dust sources with the Nimbus 7 Total Ozone Mapping Spectrometer (TOMS) absorbing aerosol products. The TOMS instrument can estimate the total column of aerosols by an index, TOMS aerosol index (AI), which uses two channels of ultraviolet (UV) radiance (340 and 380 nm). When the TOMS instrument detects UV-absorbing aerosols (e.g., dust and smoke), AI is positive. On the contrary, when non-UV-absorbing aerosols (e.g., sulfate aerosols and sea-salt particles) are detected, AI is negative. In addition, when clouds are present, AI is near zero [*Herman et al.*, 1997; *Torres et al.*, 1998]. Aerosol optical thickness measurements in dusty regions are well correlated with positive values of TOMS AI [*Chiapello et al.*, 1999; *Hsu et al.*, 1999]. *Prospero et al.* [2002] shows the global distribution of aeolian

dust sources derived from TOMS AI (Fig. 1.7), and they obtained a result that the most active aeolian dust sources are associated with topographic lows or they are situated in close proximity to mountains and highlands. In mountainous regions (e.g., Afghanistan, Iran, Pakistan, and China), strong dust sources are often found in closed intermountain basins.

1.4.2 Aeolian dust sources in East Asia and long-range transport of East Asian dust

According to *Pye* [1987], *Middleton and Thomas* [1997], and *Tegen and Fung* [1995] cited in the previous section, East Asia (around the Gobi Desert and the Taklimakan Desert) is one of the major aeolian dust sources on the Earth (Figs. 1.3, 1.4, and 1.6). However, Fig. 1.7 obtained by TOMS AI data [*Prospero et al.*, 2002] shows that the Taklimakan Desert is a major dust source, while the region around the Gobi Desert is not a dust source. Although *Prospero et al.* [2002] obtained the above results, they regard the Gobi Desert as a major dust source. In their comments, dust storms around the Gobi Desert are caused by strong winter storms, while clouds accompanied by storms disturb the detection of an aeolian dust with TOMS, and the frequency of dusts detected by TOMS reduces. Indeed, true color images from satellites (e.g., SeaWiFS and MODIS images) show yellow dust clouds largely covered by white water cloud [e.g., *Husar et al.*, 2001; many images can be seen on http://visibleearth.nasa.gov/]. *Xuan* [1999] and *Xuan et al.* [2000] suggest that a zone in the central Gobi is subordinate only to the Taklimakan Desert in terms of emission intensity of Chinese dust sources. In addition, past studies show that frequent aeolian dusts occur around the Gobi Desert in spring by cold fronts that emerge from Siberia [e.g., *Littmann*, 1991; *Goudie and Middleton*, 1992; *Kurosaki and Mikami*, 2003].

Aeolian dust particles from East Asia are observed in the North Pacific Ocean [e.g., *Shaw*, 1980; *Duce et al.*, 1980; *Uematsu et al.*, 1983; *Gao et al.*, 1992]. Furthermore, transports of aeolian dust from East Asia to North America (i.e., trans-Pacific transport) are observed by satellite [*Husar et al.*, 1997, 2001]. Figure 1.8 [after *Husar et al.*, 2001]

shows a typical case of trans-Pacific dust transport, which occurred in April 1998, and the SeaWiFS images of this case are shown in Fig. 1.9. *Uno et al.* [2001] simulated this trans-Pacific dust transport (Fig. 1.10)[¶]. Another typical trans-Pacific dust transport, which occurred in April 2001, is simulated by *Takemura et al.* [2002], *Liu et al.* [2003], and so on.

These facts mean that the East Asian aeolian dust is a large-scale phenomenon, which can have an impact on the Earth's climate. *Prospero et al.* [2002] refers to regions from the west coast of North Africa, through the Middle East and Central Asia, China, into the Pacific Ocean as the "*global dust belt.*"

1.5 Objectives of this study

This study focuses on the aeolian dust outbreak in East Asia because it is important to understand the impact of aeolian dust on the Earth's climate. Aeolian dusts are generated by strong winds, while land surface conditions largely affect the aeolian dust outbreaks. As described in Chapter 3, the following three geographical characteristics are found to be essential for the aeolian dust outbreak in East Asia: (1) frequent synoptic disturbances in spring, (2) complicated distribution of land cover types (see section 2.2.1), and (3) frequent snow covers in early spring. With regard to the first characteristic, it is well known that strong winds cause aeolian dust outbreaks when a synoptic disturbance passes over East Asia. With regard to the second characteristic, land cover types complicatedly distribute in East Asia in comparison with other aeolian dust sources such as Sahara Desert. This suggests that aeolian dust sources also complicatedly distribute in East Asia. With regard to the third characteristic, snow cover in early spring often prevents aeolian dust outbreaks in East Asia because arid and/or semiarid regions distribute in relatively high latitude. These geographical characteristics make it difficult to understand the spatial and temporal distributions of

---

[¶] There is a description about a three-dimensional structure of aeolian dust caused by a synoptic disturbance in section 3.1.1 by citing this case as an example.

aeolian dust outbreaks in East Asia.

As described in previous sections, the distribution of aeolian dust sources has been investigated by use of surface meteorological data [*Littmann*, 1991; *Goudie and Middleton*, 1992; *Kurosaki and Mikami*, 2003] and satellite data [*Prospero et al.*, 2002]. In numerical models [e.g., *Tegen and Fung*, 1995], aeolian dust sources are given from land cover type data. However, anyone has not compared aeolian dust sources and land cover types. According to wind tunnel experiments and field experiments [*Bagnold*, 1941; *Gillette et al.*, 1980, 1982; *Shao and Raupach*, 1992; *Shao*, 2000; *Mikami et al.*, 2002], it is known that the threshold wind velocity of aeolian dust outbreak has various values according to land surface conditions (section 5.1). However, because their experiments are conducted in idealized conditions and/or the number of sites is limited, the spatial distribution of threshold velocities has not been plotted on a map. Furthermore, the effect of snow cover on aeolian dust outbreaks has not been studied except for *Kurosaki and Mikami* [2004].

The purpose of this study is to understand the aeolian dust outbreak in East Asia from the viewpoint of surface wind and land surface conditions. The author would like to improve the understanding of spatial and temporal distribution of aeolian dust in East Asia through this study. To achieve this objective, four goals are given as follows: (i) to clarify the relation between aeolian dust sources and land cover types, (ii) to clarify which largely control aeolian dust outbreaks, surface winds or land surface conditions, (iii) to clarify the spatial distribution of threshold wind velocities of aeolian dust outbreak, and (iv) to clarify the effect of snow cover on aeolian dust outbreak. To achieve these goals, this study conducted the following items of research by use of surface meteorological data (section 2.1), land cover type data (section 2.2.1) and snow cover data (section 2.2.2):

1. In Chapter 3, this study shows the distribution of dust sources in East Asia based on the definition of the potential dust source. Furthermore, the distributions of potential dust sources and land cover types are discussed;

2. In Chapter 4, this study shows seasonal, year-to-year and spatial variations of dust

outbreak frequencies around the Gobi Desert and in the Taklimakan Desert, which has already been known as major dust sources in East Asia [e.g., *Kurosaki and Mikami*, 2002, 2003]. These dust outbreak frequencies are discussed with reference to strong wind frequencies. The correlation between strong wind frequencies and dust outbreak frequencies is computed and the effects of surface wind and land surface condition on aeolian dust outbreaks are discussed. Furthermore, the characteristics of aeolian dusts in these two regions are compared:

3. In Chapter 5, two kinds of threshold wind velocities of aeolian dust outbreak are defined such as "*minimum threshold velocity* ($u_{t5\%}$)" and "*practical threshold velocity* ($u_{t50\%}$)", which are statistically obtained for each observatory from surface meteorological data. The former is the threshold velocity when the land surface is in nearly the most favorable condition for aeolian dust outbreaks at such observatory. The latter is the threshold wind velocity when the land surface is in a usual condition at such observatory. These threshold velocities ($u_{t5\%}$ and $u_{t50\%}$) and their difference ($\Delta u_t = u_{t50\%} - u_{t5\%}$) are plotted on maps for each observatory and their regional variations are discussed with reference to land cover types.

4. In Chapter 6, the effect of snow cover on aeolian dust outbreak is discussed. This study proposes parameters to measure this effect and they are validated, using statistics of snow cover, wind velocity and dust outbreaks. We will also discuss the effects of soil wetness, vegetation, and errors due to the subgrid heterogeneity of snow coverage.
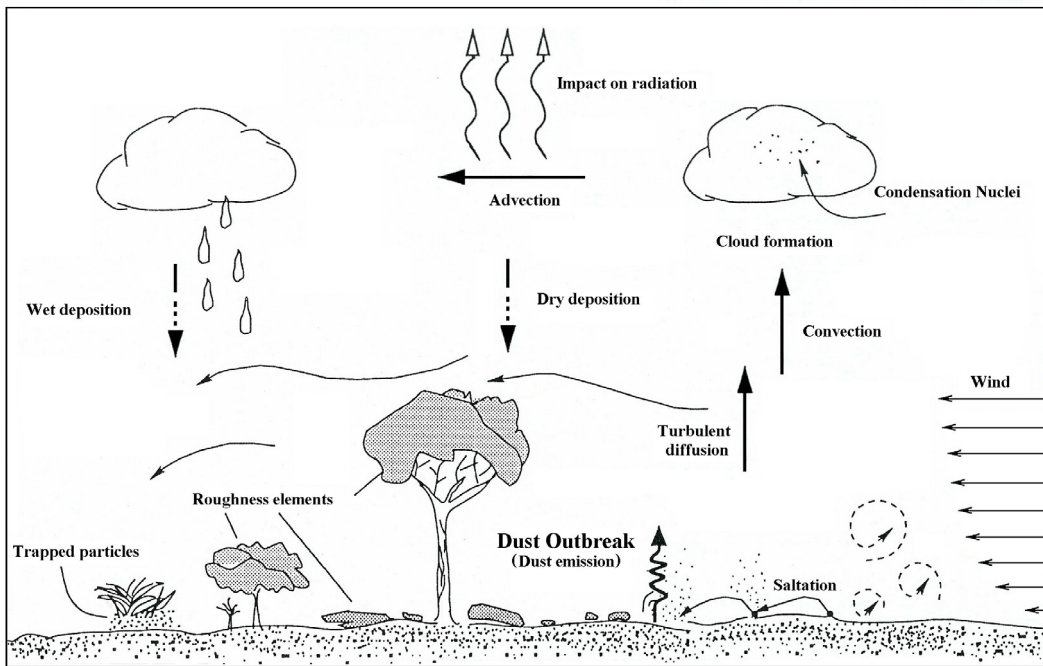
Fig. 1.1. A schematic illustration of the three distinct phases of aeolian dust: entrainment, transport and deposition. Atmospheric conditions (flow patterns, precipitation and turbulence), soil characteristics (texture, aggregation and moisture) and land-surface properties (roughness elements and vegetation) control the erosion process (modified from *Shao*, 2000).
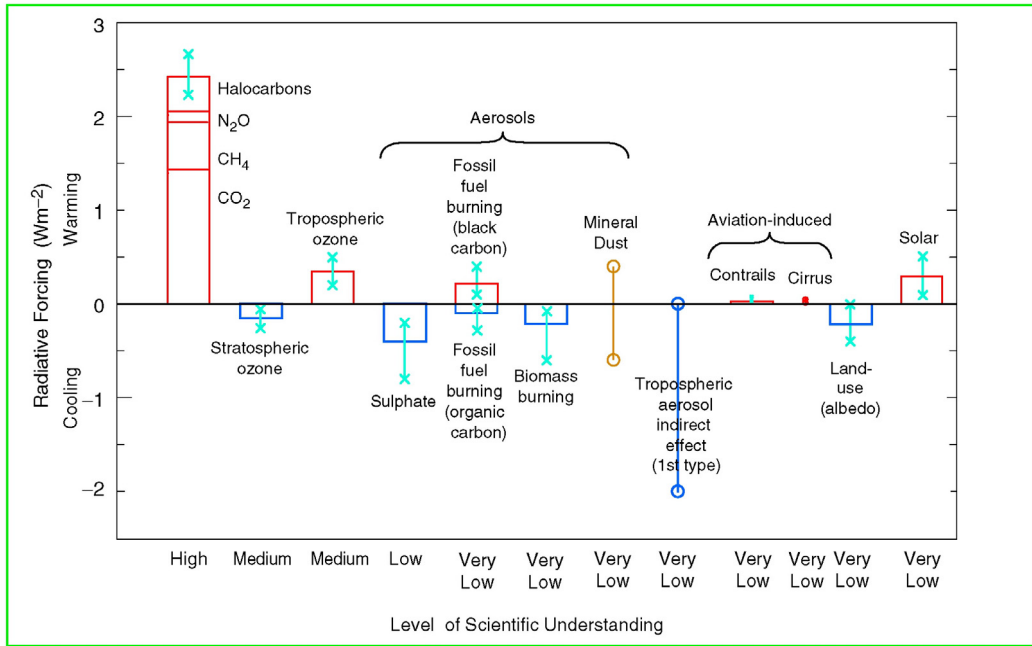
Fig. 1.2. Global, annual-mean radiative forcings (Wm⁻²) due to a number of agents for the period from pre-industrial (1750) to present (late 1990s; about 2000). The height of the rectangular bar denotes a central or best estimate value, while its absence denotes no best estimate is possible. The vertical line about the rectangular bar with "x" delimiters indicates an estimate of the uncertainty range, for the most part guided by the spread in the published values of the forcing. A vertical line without a rectangular bar and with "o" delimiters denotes a forcing for which no central estimate can be given owing to large uncertainties. The uncertainty range specified here has no statistical basis and therefore differs from the use of the term elsewhere in this document. A "level of scientific understanding" index is accorded to each forcing, with high, medium, low and very low levels, respectively. This represents the subjective judgment about the reliability of the forcing estimate, involving factors such as the assumptions necessary to evaluate the forcing, the degree of knowledge of the physical/chemical mechanisms determining the forcing, and the uncertainties surrounding the quantitative estimate of the forcing (after *IPCC*, 2001).
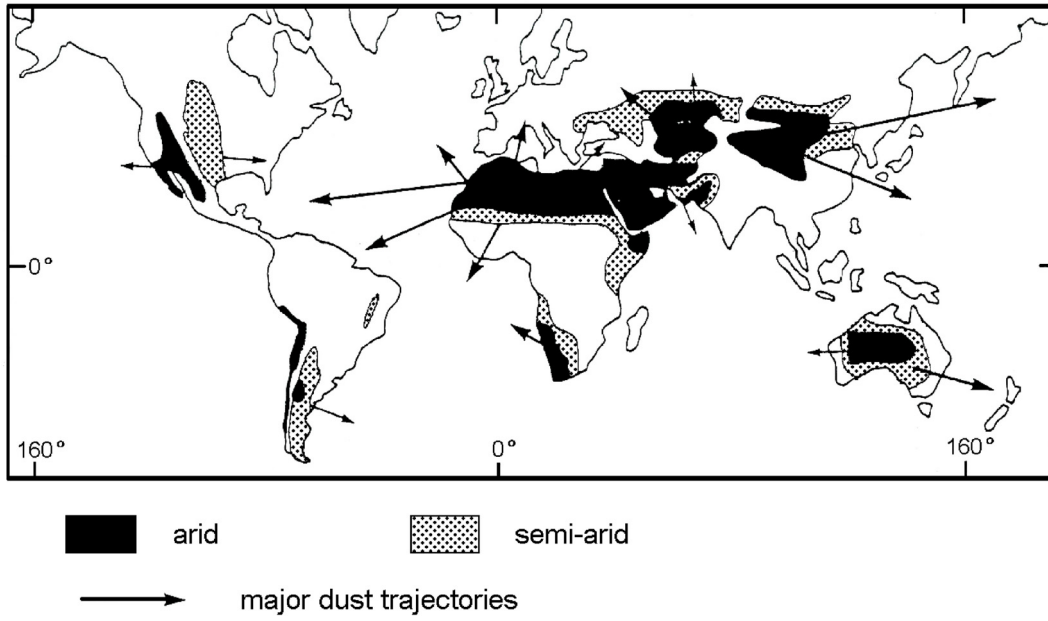
Fig. 1.3. Distribution of regions with high dust-storm activity and major dust trajectories (after *Pye*, 1987).
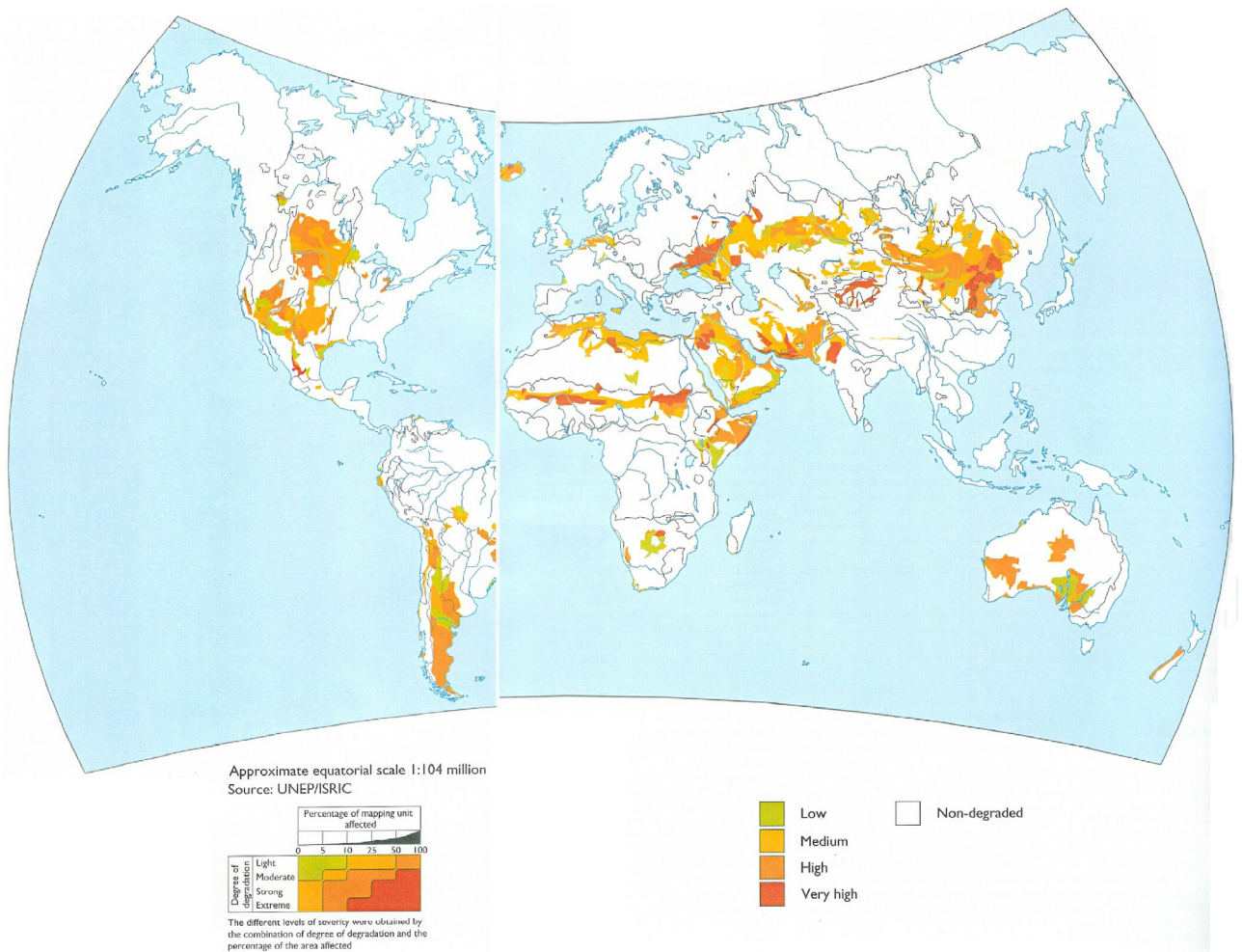
Fig. 1.4. Wind erosion severity. The different levels of severity were obtained by the combination of the degree of degradation and the percentage of the area affected (after *Middleton and Thomas*, 1997).

WIND EROSION SOURCE TYPES

LAND USE CHANGE:
CULTIVATION > DEFORESTATION

LAND USE CHANGE:
DEFORESTATION > CULTIVATION

EROSION, NO "OLD" AGRICULTURE
(OVERGRAZING)

EROSION + "OLD" AGRICULTURE

EROSION, NO "OLD" AGRICULTURE
+ LAND USE CHANGE

EROSION + "OLD" AGRICULTURE
+ LAND USE CHANGE

SAHARA BOUNDARY SHIFT
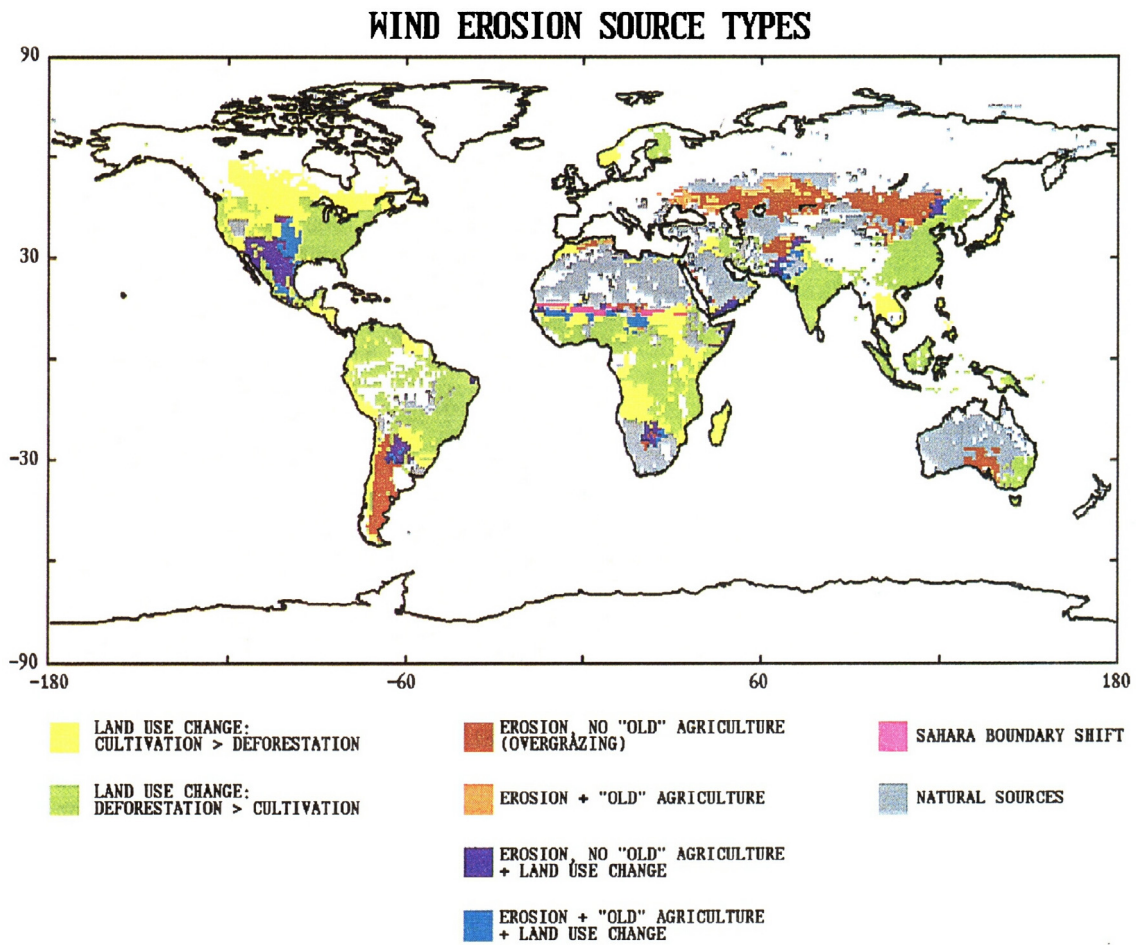
NATURAL SOURCES

Fig. 1.5. Geographical distribution of the different source types of aeolian dust, and a boundary condition of aeolian dust outbreaks in the numerical experiment of *Tegen and Fung* [1995].

14

ANNUAL DUST EMISSION FROM NATURAL SOILS
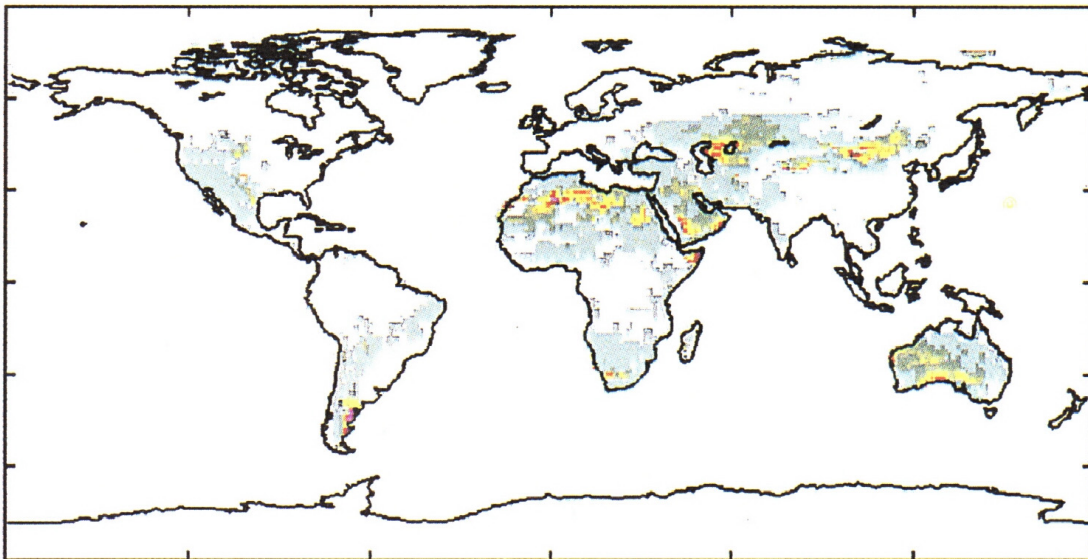
ANNUAL DUST EMISSION FROM DISTURBED SOILS
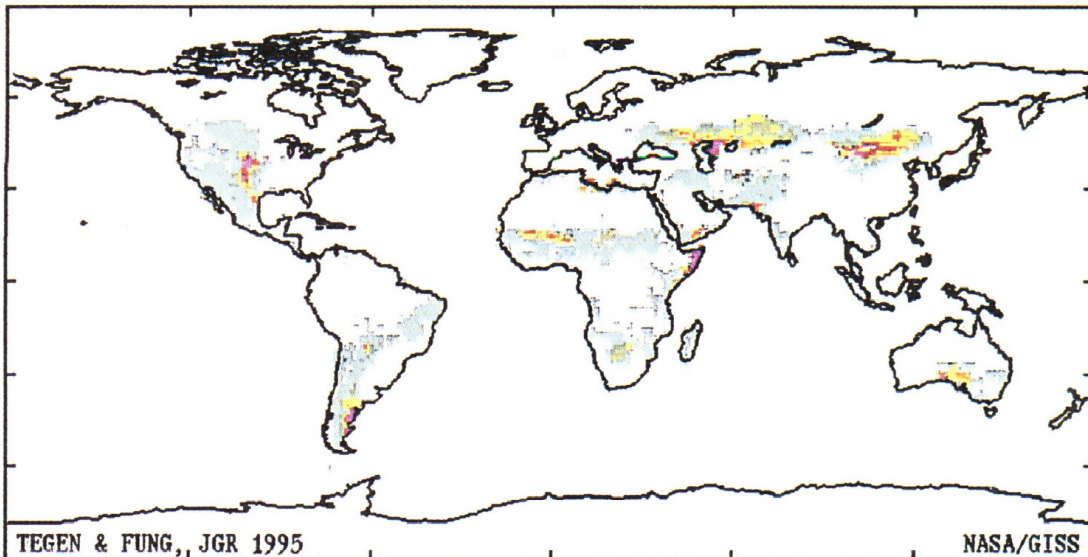
TEGEN & FUNG, JGR 1995   NASA/GISS

.00   .05   .10   .15   .20   .25   >0.25
(kg/m2/yr)
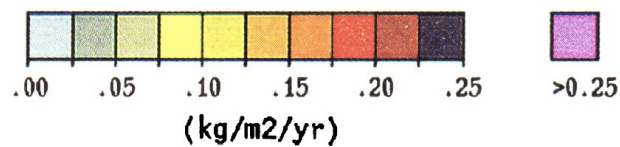
Fig. 1.6. Modeled annual dust emission simulated from natural (upper) and disturbed (lower) soils for the case of 50 % contribution from disturbed soils to the total dust load. The global annual dust emission for each of both source types is 1500 Mt yr^{-1}. Results of numerical simulation in *Tegen and Fung* [1995].
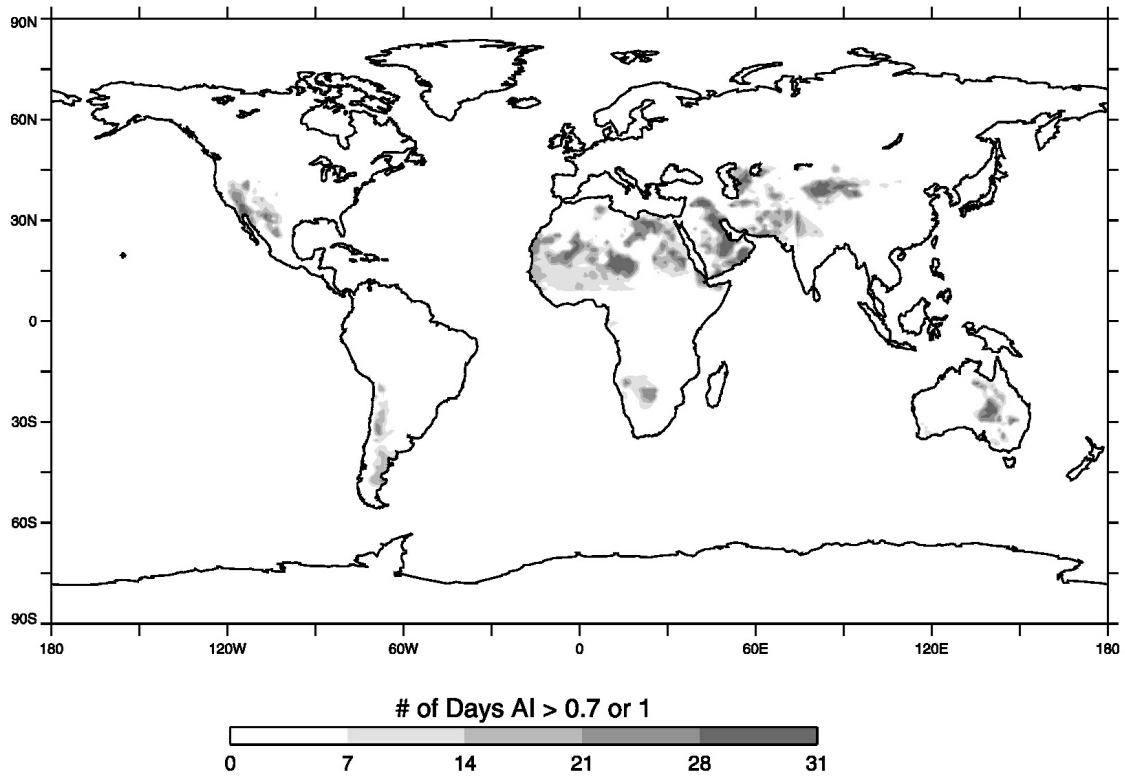
Fig. 1.7. The global distribution of TOMS dust sources. This figure is a composite of selected monthly mean TOMS AI frequency of occurrence distributions for specific regions using those months which best illustrate the configuration of specific dust sources. The distributions were computed using a threshold of 1.0 in the dust belt (see section 1.4.2) and 0.7 everywhere else (after *Prospero et al.*, 2002).
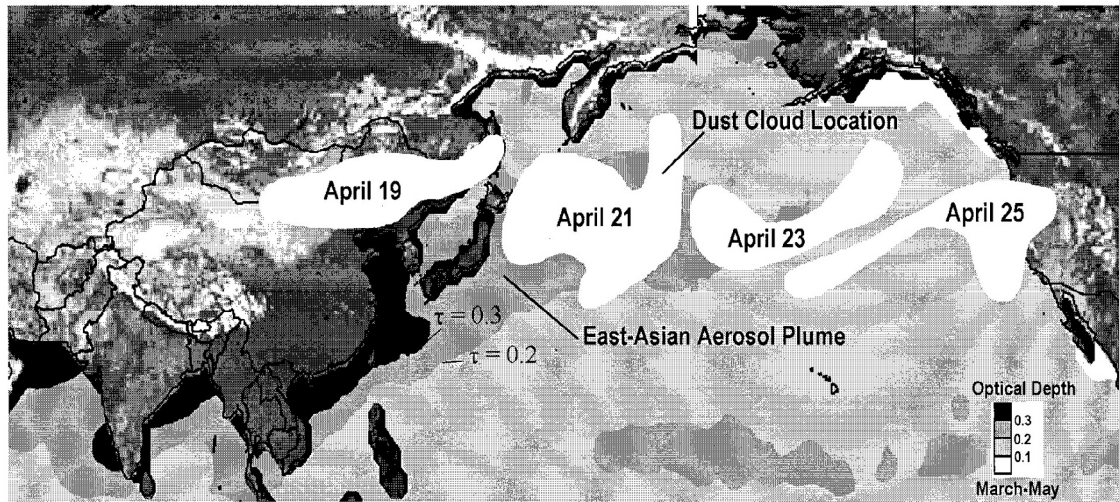
Fig. 1.8. Approximate location of the April 19 dust cloud over the Pacific Ocean between April 21 and 25. The daily dust pattern was derived from the SeaWiFS images, GOES 9 and GOES 10 images, and TOMS absorbing aerosol index data. Over the Pacific Ocean the dust cloud followed the path of the springtime East Asian aerosol plume shown by the contours of optical thickness derived from AVHRR data (after *Husar et al.*, 2001).

April 20, 1998

April 23, 1998

April 21, 1998

April 24, 1998

April 22, 1998
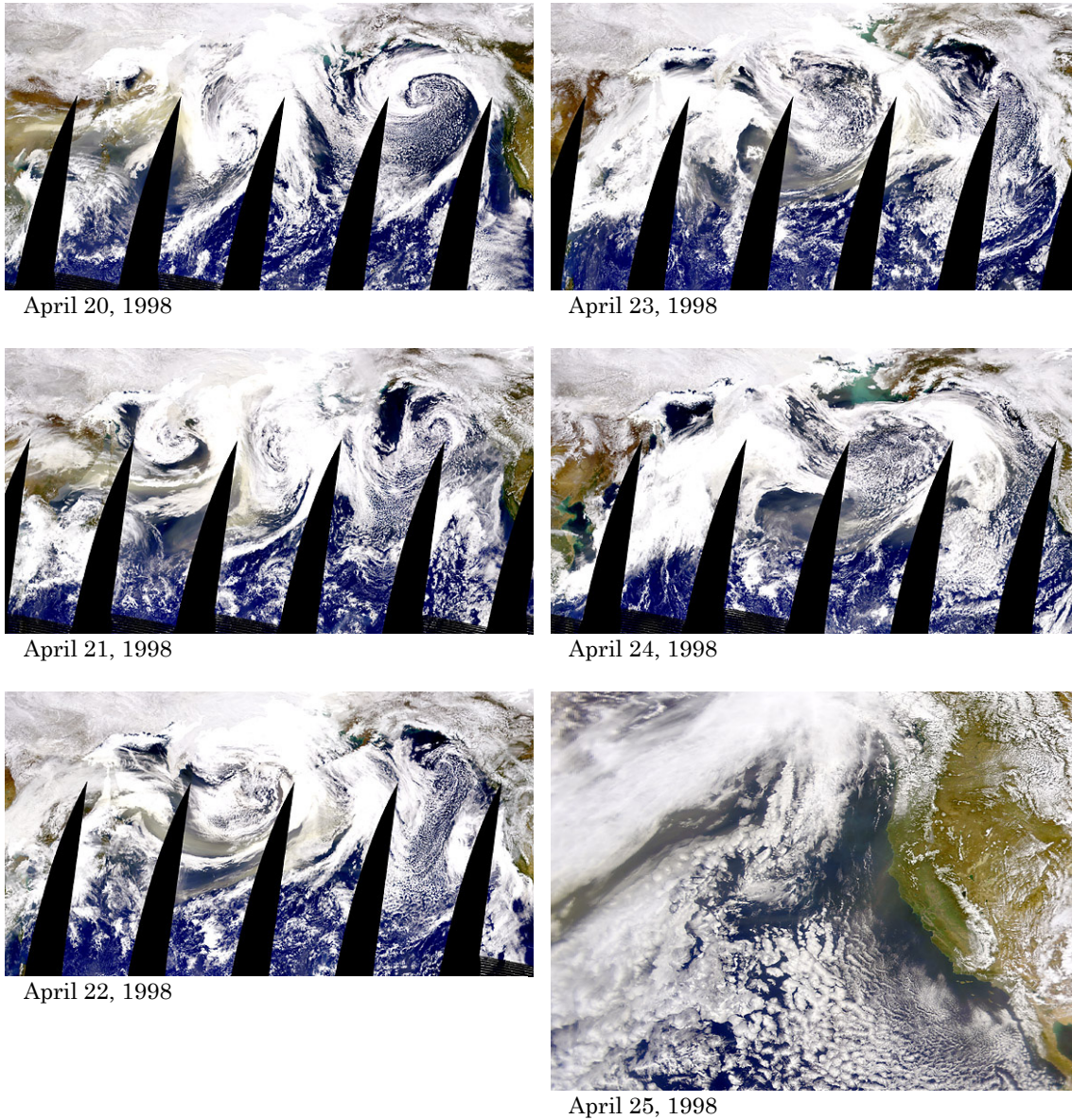
April 25, 1998

Fig. 1.9. SeaWiFS true color images of the trans-Pacific dust transport from April 20 – 25, 1998. These images are obtained from http://daac.gsfc.nasa.gov/CAMPAIGN_DOCS/OCDST/asian_dust.html. Detail explanations about this episode are also indicated in this homepage.
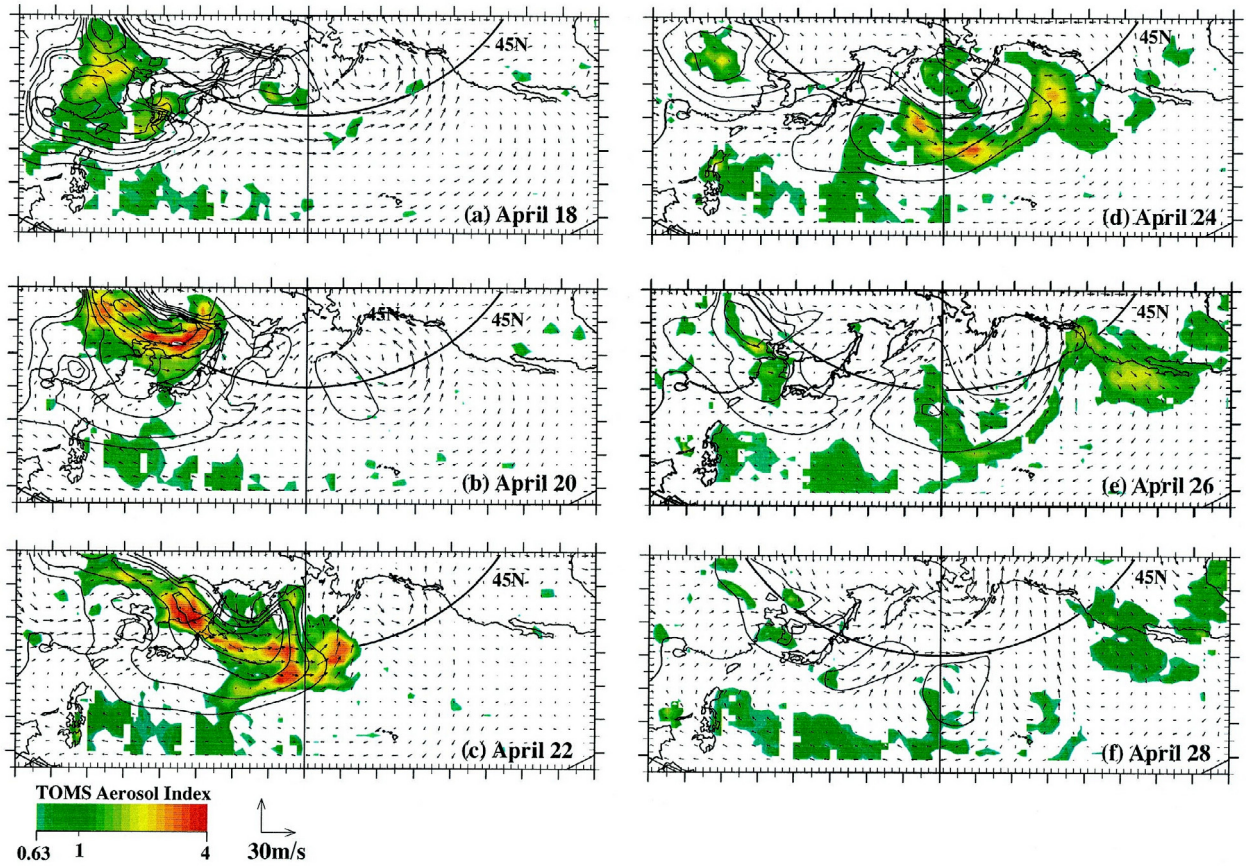
Fig. 1.10. Wind vector at z* = 1500 m (model output), horizontal distribution of column-averaged concentration of dusts shown by contours (model output), and TOMS aerosol index shown by color hatches (satellite observations) for April 18 – 28, 1998, over the North Pacific basin. Dust concentration levels of 1, 2.5, 6.3, 10, 16, 25, 40, and 100μg/m^3 are shown by contour lines (after *Uno et al.*, 2001). z* is the terrain-following vertical coordinate and this is defined as $z_t(z - z_g) / (z_t - z_g)$, where z_t and z_g are the levels of the top and the ground surface of the model atmosphere, respectively.

Chapter 2

Data and Methods

2.1 Surface meteorological data

2.1.1 SYNOP

This study used meteorological information, which is obtained from SYNOP reports [*World Meteorological Organization (WMO)*, 1974]. "*SYNOP*" is a name of meteorological report, which is sent from WMO synoptic observatories located around the world via the global telecommunication system (GTS). A meaning of the term "*synoptic*" is "*relating to or displaying atmospheric or weather conditions as they exist simultaneously over a broad area*" [*Gove et al.*, 1981; Webster's Third New International Dictionary]. Literally synoptic observations are conducted 3 hourly at the same time (00, 03, 06, ⋯, and 21 UTC) at all observatories in the world. There are exceptional observations (e.g., 6 hourly, 12 hourly, daily, and so on), while observations are conducted at 00, 03, 06, ⋯, or 21 UTC.

2.1.2 Phenomena of aeolian dust (floating dust, dust outbreak, dust storm and dust event)

This study used present weathers in a SYNOP report in order to detect phenomena of aeolian dust in the analysis region (30°N – 60°N, 75°E – 145°E) (Fig. 2.1) for the period from March 1988 to June 2003. There are 100 kinds of present weathers such as ww = 00, 01, 02, ⋯, and 99 (see Appendix 1). Symbolic letters "ww" identifies the

present weather in a SYNOP report. Present weathers related with dust phenomena are ww = 06, 07, 08, 09, 30, ···, 35, and 98 (Table 2.1). This study makes four categories of dust phenomena such as floating dust, dust storm, dust outbreak, and dust event. Each of dust phenomena is defined as follows: (1) when ww is 06, a floating dust occurs; (2) when ww is 09, 30, ···, 35, or 98, a dust storm occurs; (3) when ww is 07, 08, 09, 30, ···, 35, or 98, a dust outbreak occurs; (4) when ww is any number of codes related with dust phenomena (i.e., ww=06, 07, 08, 09, 30, ···, 35, or 98), a dust event occurs (Table 2.2).

2.1.3 Wind velocity and strong wind

A SYNOP report includes information about surface wind. A wind velocity in a SYNOP report is an average during ten-minute period immediately preceding the time of synoptic observation [*WMO*, 1974].

The strong wind should be defined in order to discuss relation between frequencies of dust outbreaks and strong winds. This study presents two definitions of strong wind. In one definition, a strong wind must have a velocity of at least 6.5 m/sec. This value, 6.5 m/sec, is the threshold for a dust outbreak in many numerical models [e.g., *Tegen and Fung*, 1994; *Takemura et al.*, 2000; *Uno et al.*, 2001] (see section 5.1). Threshold velocities of dust outbreaks actually exhibit various values with differing land surface conditions. However, a constant value was used to define a strong wind in their models, because land surface conditions and the threshold velocity for each land surface condition have not yet been clarified. For the same reason, this definition is used in Chapters 4 and 6 of this study. In another definition, a threshold velocity of strong wind varies with snow cover. Details will be shown in the sections 6.3.2 and 6.3.3.

2.1.4 Dust outbreak frequency and strong wind frequency

The total numbers of synoptic observations for a given period are different site-by-site because of disuses and/or establishments of observatories, different numbers of observations in a day, cancellations of observations, and so on. This makes it impossible to compare frequencies of objective phenomenon (e.g., dust outbreak and

strong wind) by using simply accumulated number of objective phenomenon. For this reason, the frequency of dust outbreaks (hereafter, dust outbreak frequency) is defined as the percentage of the number of dust outbreaks to the total number of observations within a given period at each observatory and/or given region. Similarly, the frequency of strong winds (hereafter, strong wind frequency) is defined as the percentage of the number of strong winds to the total number of observations. However, when the total number of synoptic observations is small for a given period at a site, data at this site is invalid. If the total number of observations is smaller than the total number of days for a given period, data was not used. Similarly, dust event frequency, floating dust frequency and dust storm frequency can be defined.

2.2 Data of land surface conditions

2.2.1 Land cover type

In order to identify the land cover types in dust source regions, land cover information was extracted from Global Land Cover Characteristics Data Base Version 2.0 with the Global Ecosystem classification [*Loveland et al.*, 2000] (http://edcdaac.usgs.gov/glcc/globdoc2_0.html), which is distributed by U.S. Geological Survey (USGS). This data set is derived from 1 km monthly composites of Advanced Very High Resolution Radiometer (AVHRR) – Normalized Difference Vegetation Index (NDVI) spanning a 12-month period (April 1992 – March 1993) and other key geographic data: digital elevation data, ecoregions interpretations, country or regional-level vegetation, land cover maps, and so on. In the classification of land cover types, analyses of vegetation phenology (i.e., onset, peak, and seasonal duration of greenness) are conducted by use of a 12-month period NDVI data. This means that there are not seasonal and year-to-year variations of land cover types in this data set.

While there are 96 kinds of land cover types in this data set referring to the Global Ecosystem Legend [*Olson*, 1994a, 1994b] (see Appendix 2), these were classified into 9 types in this study: Bare Desert, Semi Desert, Semi Desert Shrubs, Grass/Shrub,

Cultivation, Savanna, Forest, Tundra and others (Table 2.3).

2.2.2 Snow cover

Snow cover data used in this study (Chapter 6) is derived from the Special Sensor Microwave/Imager (SSM/I). This data set is distributed by the National Climatic Data Center (NCDC) as monthly and weekly snow cover fractions (hereafter, SCFs) [*Grody and Basist*, 1996; *Basist et al.*, 1996] (http://lwf.ncdc.noaa.gov/servlets/SSMIBrowser). Monthly and weekly SCFs refer to fractions of days with snow cover for a month and for a week, respectively.

ww	Contents
06	Widespread dust in suspension in the air, not raised by wind at or near the station at the time of observation
07	Dust or sand raised by wind at or near the station at the time of observation, but no well-developed dust whirl(s) or sand whirl(s), and no duststorm or sandstorm seen; or, in the case of ships, blowing spray at the station
08	Well-developed dust whirl(s) or sand whirl(s) seen at or near the station during the preceding hour or at the time of observation, but no duststorm or sandstorm
09	Duststorm or sandstorm within sight at the time of observation, or at the station during the preceding hour
30	Slight or moderate duststorm or sandstorm - has decreased during the preceding hour
31	Slight or moderate duststorm or sandstorm - no appreciable change during the preceding hour
32	Slight or moderate duststorm or sandstorm - has begun or has increased during the preceding hour
33	Severe duststorm or sandstorm - has decreased during the preceding hour
34	Severe duststorm or sandstorm - no appreciable change during the preceding hour
35	Severe duststorm or sandstorm - has begun or has increased during the preceding hour
98	Thunderstorm combined with duststorm or sandstorm at time of observation

Table 2.1. Present weathers in SYNOP associated with aeolian dust phenomena. All kinds of present weathers are presented in Appendix 1.

dust event		
suspending phase **floating dust**	**generating phase** **dust outbreak**	
	weak or moderate dust outbreak	severe dust outbreak **dust storm**
ww=06	ww=07 and 08	ww=09, 30–35 and 98

Table 2.2. Definitions about phenomena of aeolian dust. Symbolic letters "ww" identifies the present weather in a SYNOP report.

Legend of Land Cover Types in this study	Numbers of Global Ecosystems Legend (See Appendix 2)
Bare Desert	08
Semi Desert	11
Semi Desert Shrubs	51
Grass/Shrub	02, 07, 10, 16, 17, 40, 41, 42 and 87
Cultivation	30, 31, 35, ···, 39, 92, 93 and 94
Savanna	43, 58 and 91
Forest	03, ···, 06, 18, ···, 29, 32, 33, 34, 48, 54, 56, 57, 60, 61, 78, 79 and 90
Tundra	09, 53 and 63
others	others of the above

Table 2.3. Legend of land cover types in this study (left column) and their corresponding to numbers of the Global Ecosystem Legend (right column). The Global Ecosystem Legend is presented in Appendix 2.
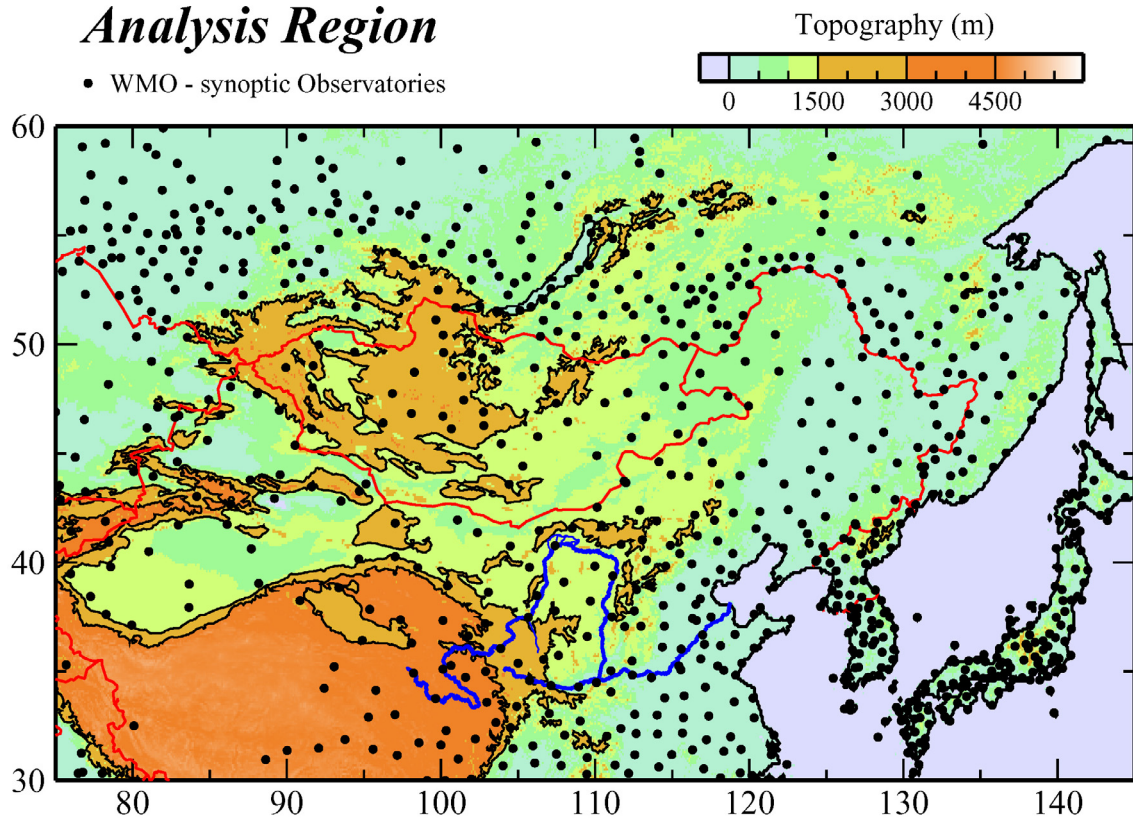
Fig. 2.1. The analysis region. Both color hatches and black contour lines indicate topography. Contour lines indicate coastlines and elevations of 1500 m and 3000 m. Dots show WMO synoptic observatories. Blue lines indicate Huang He River. Red lines indicate national borders.

Chapter 3

Potential Dust Sources

3.1 Geographical characteristics of East Asia

A conspicuous characteristic of East Asian geography is its massive topography. Figure 3.1 shows topography around the global dust belt shown by *Prospero et al.* [2002] (section 1.4.2) (a) and around East Asia (b). Topography affects atmospheric and land surface environments. As a result, three following geographical characteristics are essential for the aeolian dust outbreak in East Asia: (1) frequent synoptic disturbances in spring, (2) complicated distribution of land cover types, and (3) frequent snow covers in early spring. In this section, the relations among the aeolian dust outbreak, these three geographical characteristics and massive topography in East Asia are described.

3.1.1 Frequent synoptic disturbances in spring

It is well known that strong winds cause aeolian dust outbreaks when synoptic disturbances pass over the regions around the Gobi Desert (Fig. 3.2) [*Watts*, 1969; *Pye*, 1987; *Littmann*, 1991; *Goudie and Middleton*, 1992; *Sun et al.*, 2001; *Youlin*, 2001; *Gao et al, 2002; Qian et al.*, 2002]. These synoptic disturbances derive from Altai-Sayan lee cyclogeneses indicated by *Chen et al.* [1991]. *Chen et al.* [1991] show frequent cyclogeneses around the lee sides of the Altai-Sayan Mountains in spring (Fig. 3.3) and indicate that these cyclogenetic events occur by the effect of lee low.

For example, a huge aeolian dust event occurred as a cause of synoptic disturbance in April 1998. This event is famous as a trans-Pacific dust transport (see section 1.4.2).

Figure 3.4 is a SeaWiFS true color image of April 16, 1998, which shows yellow (or brown) cloud of aeolian dusts and white cloud due to a synoptic disturbance in the beginning stage of the trans-Pacific dust transport. Figure 3.5 shows surface meteorological sites where aeolian dusts were observed near the same time of the SeaWiFS image (03 UTC, April 16). The cloud image by GMS IR1 channel is illustrated in the same figure. According to Fig. 3.5, aeolian dusts near the land surface can be found in the back of a cold front. *Uno et al.* [2001] simulated this event and they indicated three-dimensional structures (Fig. 3.6) and time-height cross sections (Fig. 3.7) of these aeolian dusts. Aeolian dusts are horizontally and vertically transported by this synoptic disturbance (Fig. 3.6). As a result, aeolian dusts reach earlier in the higher level than in the lower level (Fig. 3.7). There are some regions where yellow aeolian dust clouds can be found in the SeaWiFS image (Fig. 3.4) but aeolian dusts were not observed at land surface (Fig. 3.5). Furthermore, there are other regions where white and yellow clouds are mixed in Fig. 3.4. It is practically certain that these indicate the transport of aeolian dusts into the upper level by this synoptic disturbance.

3.1.2 Complicated distribution of land cover types

Figure 3.8 shows the distribution of land cover types around the global dust belt (a) and around East Asia (b). Regions of each land cover type are distributed as an east-west belt in north part of Africa (Fig. 3.8a). East-west belts of Bare Desert, Semi Desert Shrubs, Grass/Shrub, Savanna and Forest range from north to south. On the other hand, land cover types are complicatedly distributed in East Asia (Fig. 3.8b). Bare Desert regions are distributed in the Taklimakan Desert and its eastern neighborhood. Semi Desert and Semi Desert Shrubs regions are distributed on the south and on the northeast of Bare Desert regions, respectively. Grass/Shrub regions are distributed on the east of Semi Desert regions and on the north and east of Semi Desert Shrubs regions. Cultivation regions are distributed on the east of Grass/Shrub regions. Forest regions are distributed on the north of Grass/Shrub and Cultivation regions. Regions of Bare Desert and Semi Desert Shrubs are distributed beside the Tibetan Plateau, Tian

Shan Mountains, Altai Mountains. These topographies complicate the distribution of land cover types. *Rodwell and Hoskins* [1996], *Sasaki* [2002] and *Sato and Kimura* [2004] discussed why arid and semiarid regions distribute in relatively high latitude in East Asia with reference to the massive topography (see next section). These complicated distribution of land cover types suggest that aeolian dust sources also complicatedly distribute in East Asia.

3.1.3 Frequent snow covers in early spring

Regions of Bare Desert and Semi Desert Shrubs in East Asia and Central Asia are located in higher latitude in comparison with Africa and the Middle East (Fig. 3.8a). Therefore, snow frequently covers dust sources in East Asia and Central Asia in early spring (Fig. 3.9), and this snow cover condition largely affects aeolian dust outbreaks. Past studies have indicated that the topographies make arid conditions in East Asia and Central Asia. *Rodwell and Hoskins* [1996] explain the arid condition around the Aral Sea by their theory of monsoon-desert mechanism, which is that a diabatic heating in the Asian monsoon induces a decent flow around the Aral Sea. *Sasaki* [2002] obtains a result that the Altai-Sayan Mountains reduce inflow of water vapor into the Gobi Desert in spring and most of synoptic disturbances are not accompanied by precipitation in this season. According to *Sato and Kimura* [2004], the effect of heating by the Tibetan Plateau induces a descent flow above the Gobi Desert in summer. The super arid condition in the Taklimakan Desert is induced by the obstruction of inflow of water vapor from the surrounding mountains.

3.2 Potential dust sources in the global dust belt

Figures 3.10 (a) and (b) show the maximum monthly dust outbreak frequency (hereafter, maximum frequency in this chapter) during about 15 years (March 1988 – June 2003) at WMO synoptic observatories in the global dust belt. Sites, whose maximum frequency is greater than 2 % and 4 %, are plotted by open circles in Figs. 3.10 (a) and (b), respectively. Other sites are plotted by dots. The 4 % of monthly

frequency corresponds to about 10 dust outbreaks for a month at a site where eight observations are conducted for a day (i.e., 3-hourly observation). A WMO synoptic observatory is considered to be a potential dust source when the maximum frequency is high. A potential source is assumed to be a site whose maximum frequency exceeds 2 %. Under this assumption, potential dust sources (i.e., open circles in Fig. 3.10a) are distributed more widely in comparison with dust source regions shown by previous studies (Figs. 1.3, 1.4, 1.6 and 1.7). For example, dust sources in Fig. 3.10a are distributed in tropical rain forests of the Indochina Peninsula, Indonesia and Africa, although these regions are not dust sources in previous studies. Rather than Fig. 3.10a, the distribution of potential dust sources in Fig. 3.10b fits dust sources shown by previous studies. From these results, we define a potential dust source as an observatory, whose maximum frequency exceeds 4 %. On the contrary, we define a non-dust-source as an observatory, whose maximum frequency does not reach 4 %. According to Fig. 3.10b, potential dust sources are distributed mainly in regions of Bare Desert, Semi Desert Shrubs, Grass/Shrub, Cultivation, and Savanna. These are distributed along the global dust belt indicated by *Prospero et al.* [2002]. Most of sites in regions of Bare Desert and Semi Desert Shrubs are potential dust sources. Many potential dust sources are found in regions of Grass/Shrub, Savanna and Cultivation, although most of sites are non-dust-sources in these regions. It cannot be judged whether Semi Desert regions, which are distributed in high lands as the Tibetan Plateau and the Ethiopian Plateau, possess potential of dust source or not, because there are a small number of sites in this land cover type.

3.3 Potential dust sources in East Asia

It has been well known that East Asia possesses two major dust source regions; one is the Gobi Desert and the other is the Taklimakan Desert. Figure 3.11 indicates that these two deserts, regions of Bare Desert and Semi Desert Shrubs, possess large potential of dust source. Furthermore, potential dust sources are distributed outside of the Gobi Desert. These potential dust sources are distributed in regions of Grass/Shrub,

Cultivation and Savanna. The northern boundary of the potential dust sources almost corresponds to the southern boundary of the Forest. The potential dust sources in their southern boundary are distributed around the Huang He River. The southern boundary of the potential dust sources almost corresponds to the southern boundaries of the Semi Desert Shrubs and Bare Desert in the middle and upper reaches of this river. This result suggests that deforestation and desertification will cause an expansion of dust source.
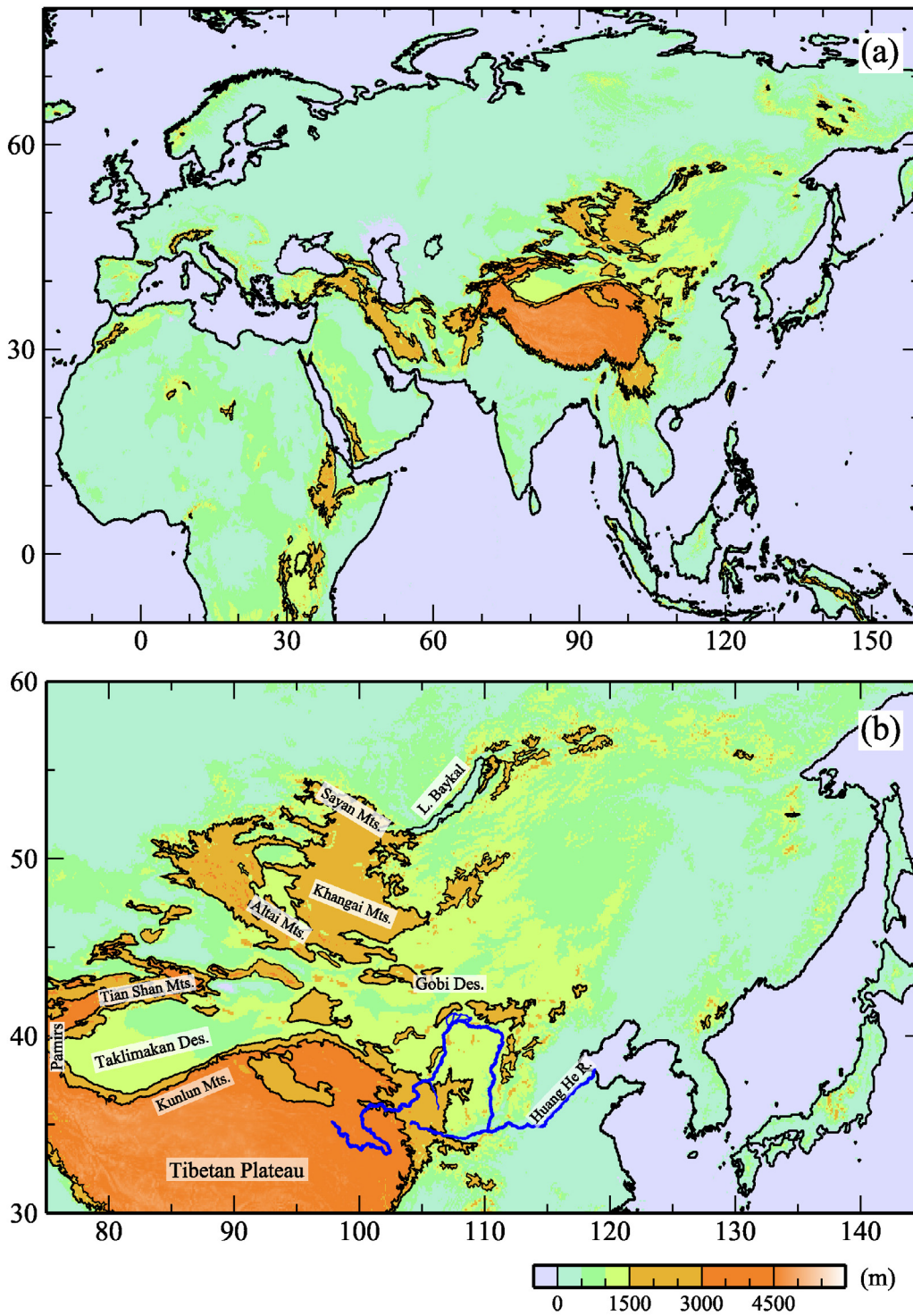
Fig. 3.1. Topography around the global dust belt (a) and East Asia (b). Black solid contours indicate coast and elevations of 1500 m A.S.L. and 3000 m A.S.L.
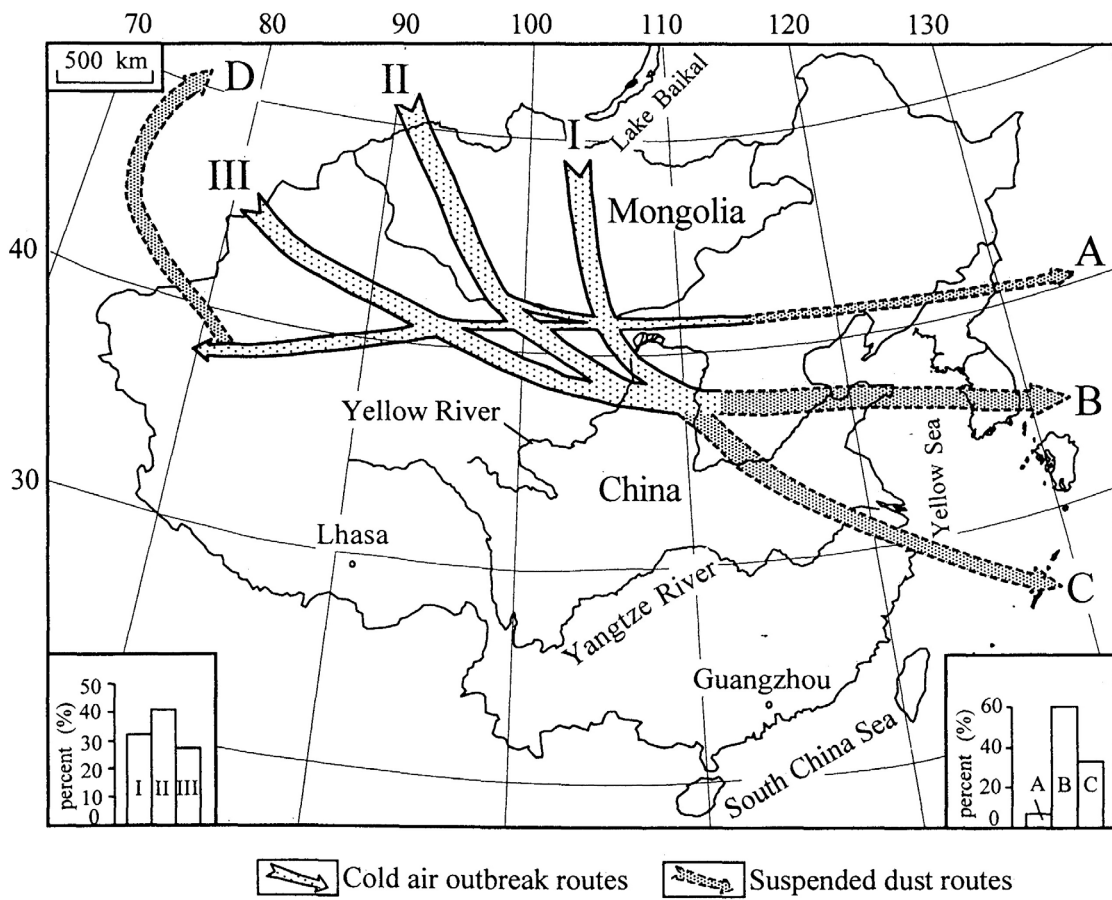
Fig. 3.2. Routes of the cold air outbreaks and the dust transport patterns in China (after *Sun et al.*, 2001).
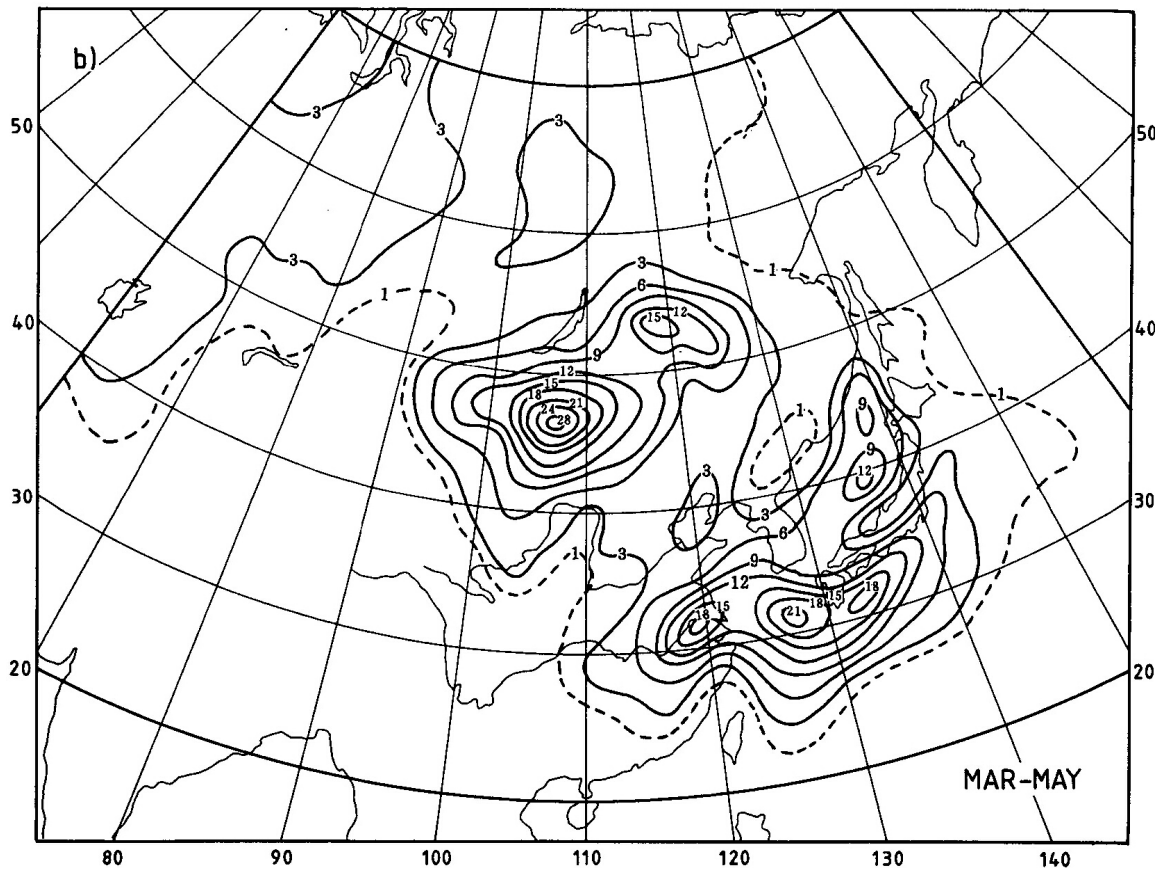
Fig. 3.3. Number of cyclogenetic events (10^{-2}) per 2.5° quadrangle per month for spring (March to May) for the period 1958 – 1987 (after *Chen et al.*, 1991).
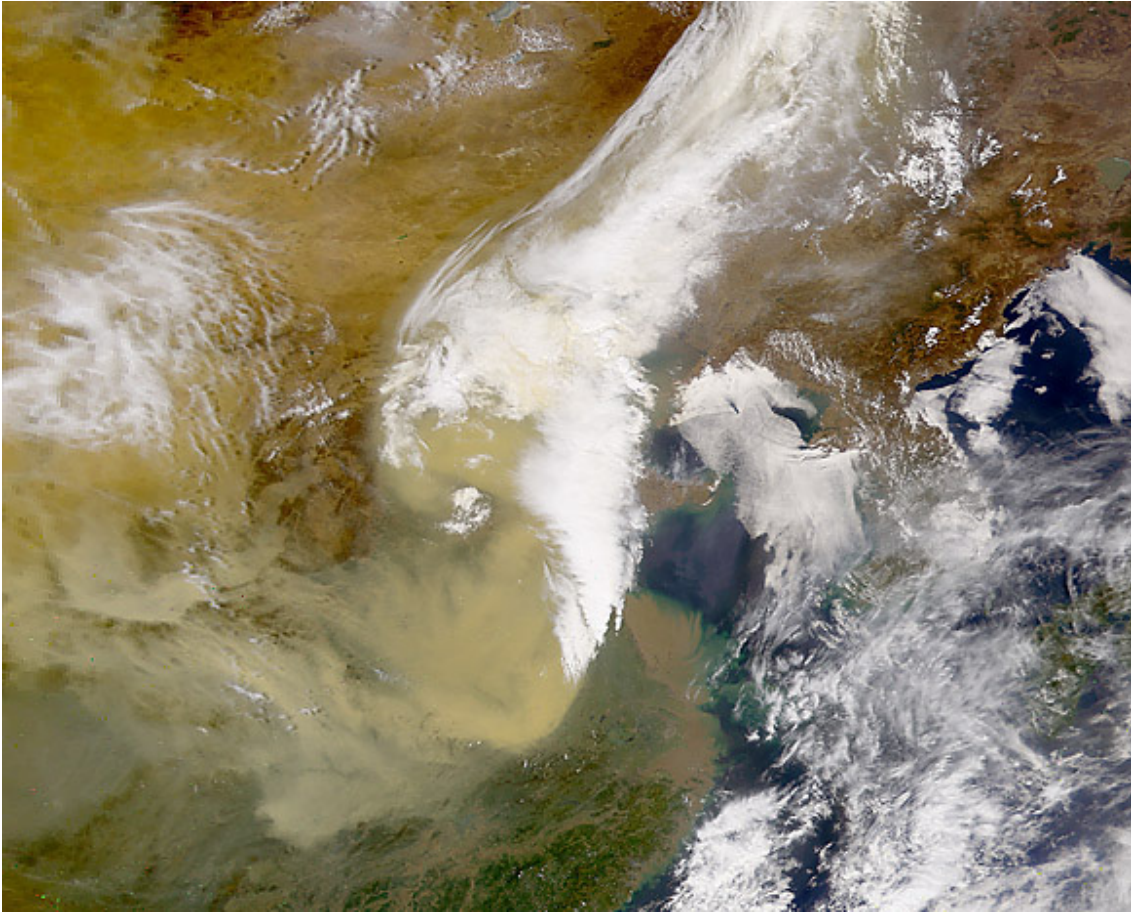
Fig. 3.4. The SeaWiFS true color image of April 16, 1998. White cloud due to a synoptic disturbance and yellow (or brown) cloud of aeolian dusts can be seen from this image. This image is obtained from the following homepage, http://daac.gsfc.nasa.gov/CAMPAIGN_DOCS/OCDST/asian_dust.html.
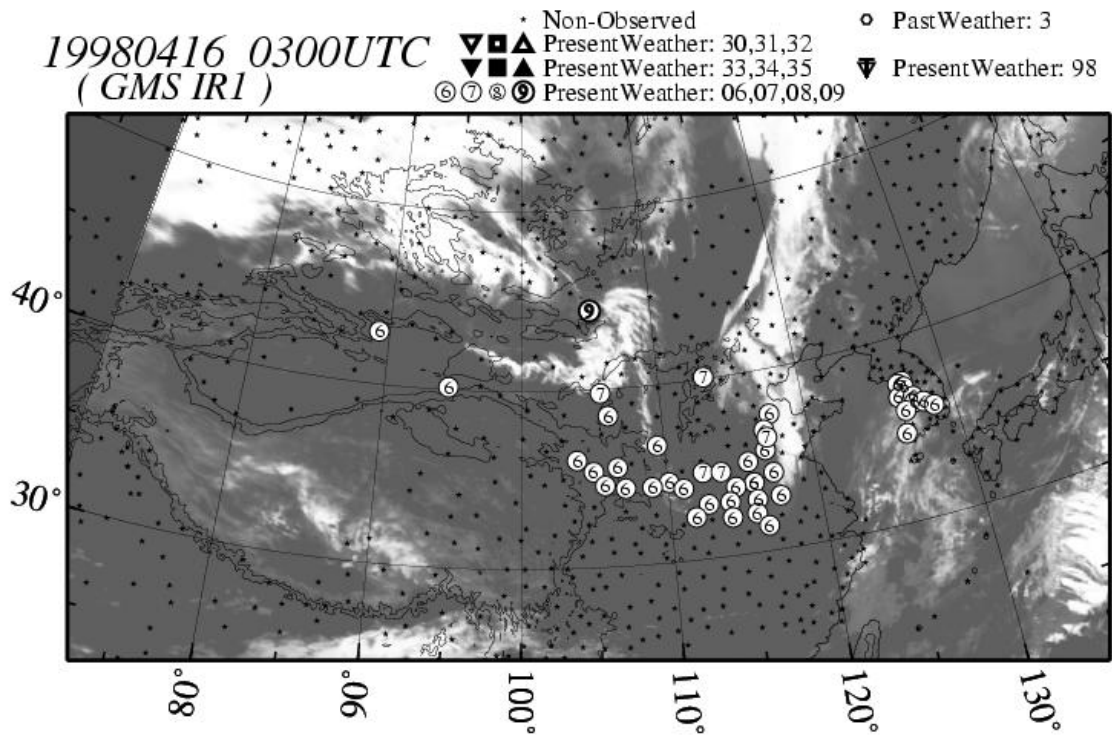
Fig. 3.5. Surface meteorological sites where aeolian dusts were observed at 03 UTC in April 16, 1998 (shown by symbols) and a cloud image by GMS IR1 channel at the same time. Symbols indicate present weather of SYNOP report (see section 2.1.2).
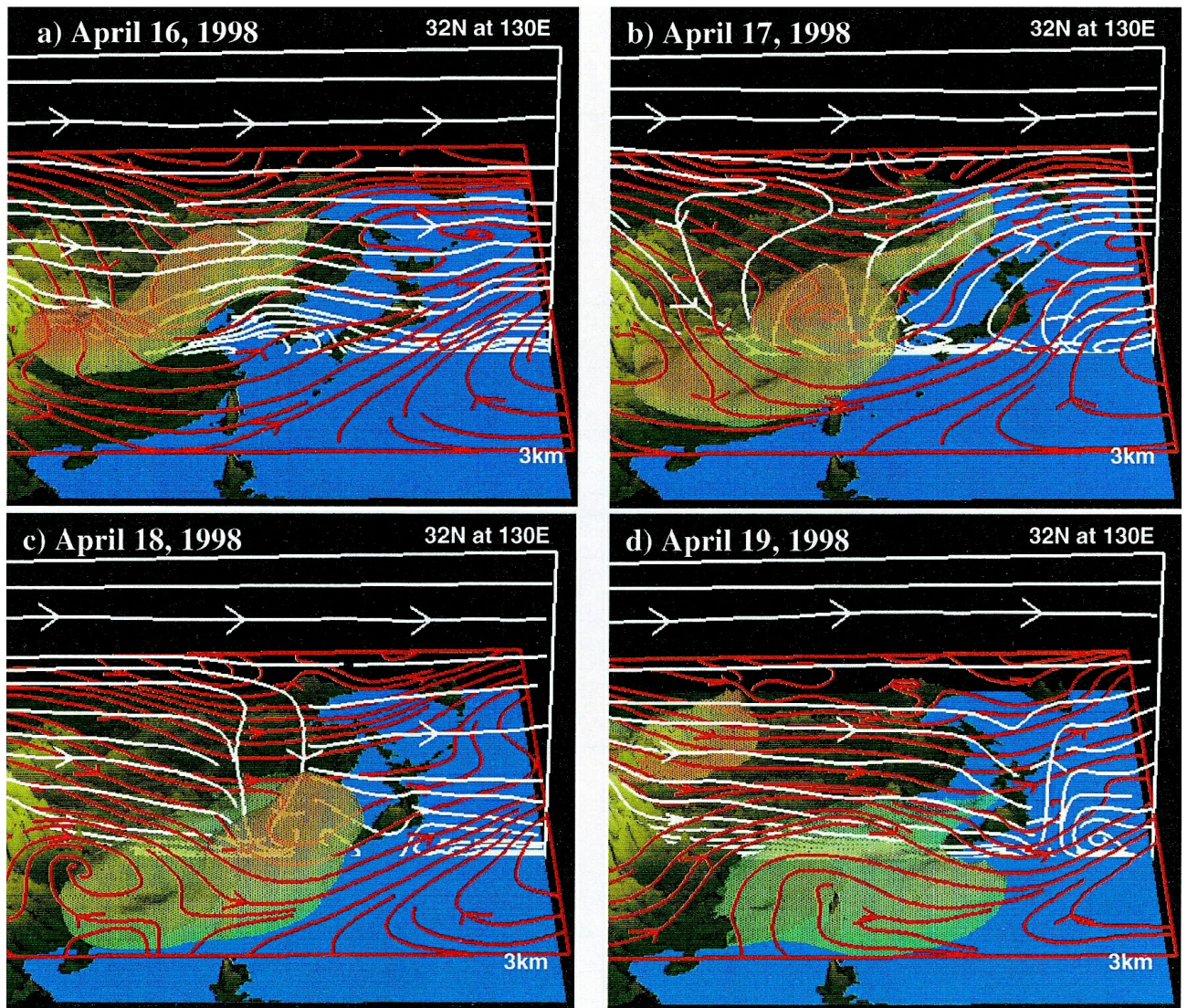
Fig. 3.6. Three-dimensional structure of the dust cloud around the cutoff vortex from April 16 to 19 over China and Japan. Streamlines on a horizontal plane at 3 km level are plotted in orange, and those on a vertical plane passing through at 32°N and 130°E (from surface to 18 km level) are plotted in white. Dust concentration of 100 μg/m³ is shown by isosurfaces, and its surface is colored by the value of potential temperature (after *Uno et al.*, 2001). These are model outputs of *Uno et al.* [2001].
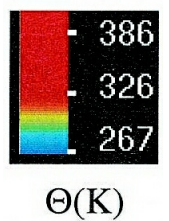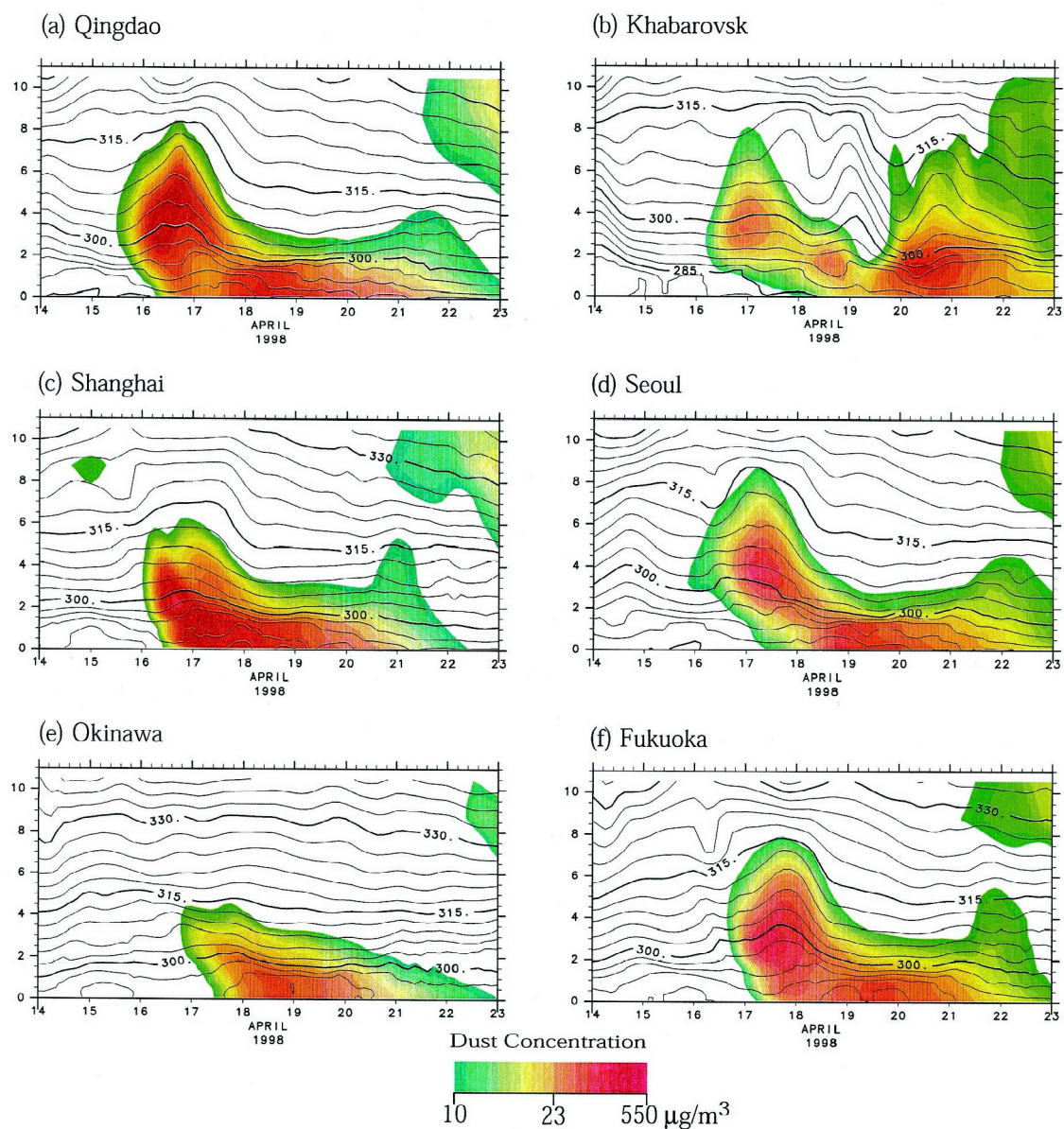
Fig. 3.7. Time-height cross section of potential temperature (contour, 3° interval) and dust concentration (color) at several sites: (a) Qingdao, (b) Khabarovsk, (c) Shanghai, (d) Seoul, (e) Okinawa, and (f) Fukuoka (after *Uno et al.*, 2001). These are model outputs of *Uno et al.* [2001].
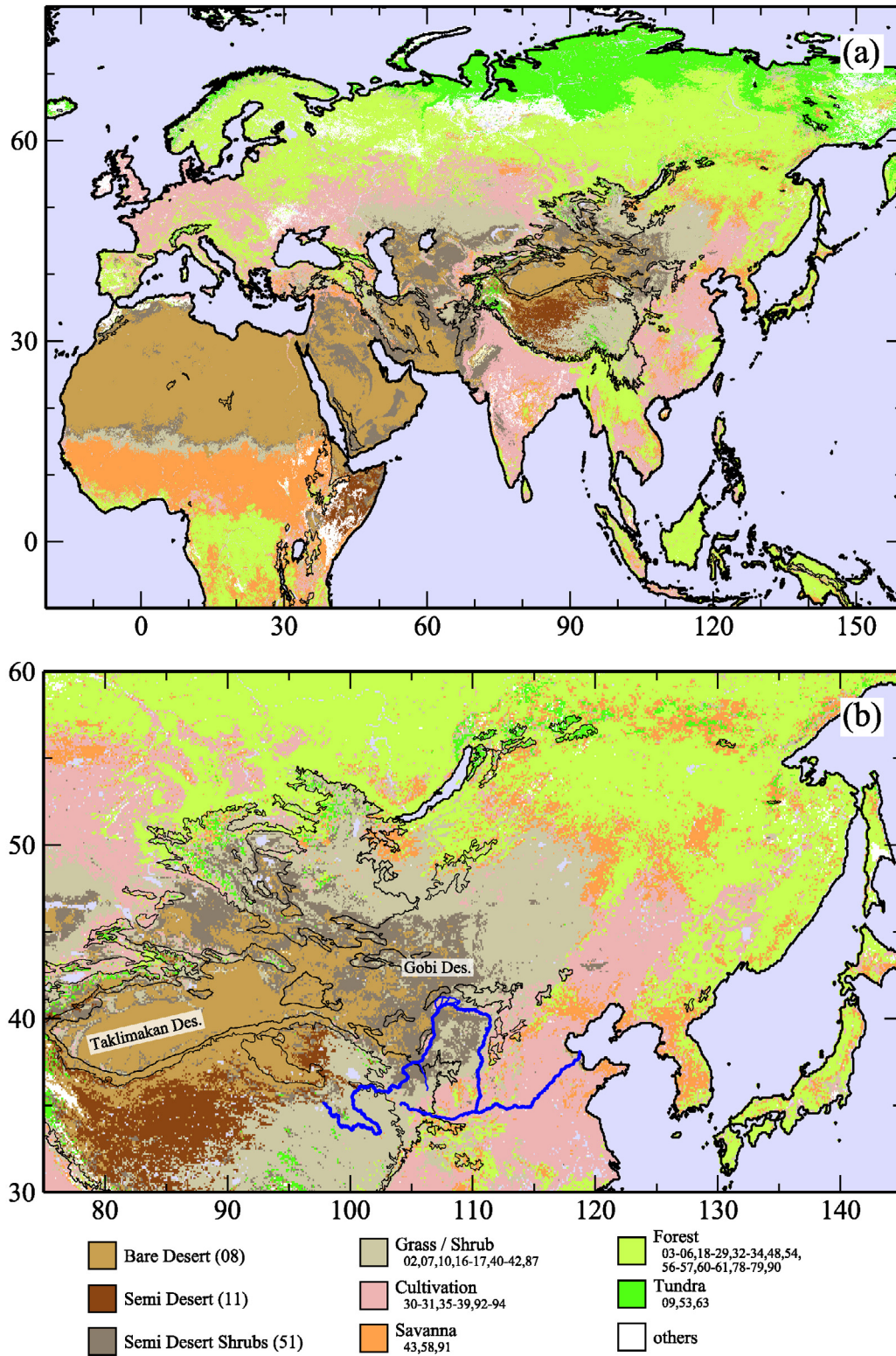
Fig. 3.8. Land cover types around the global dust belt (a) and East Asia (b). Black solid contours indicate coast and elevations of 1500 m A.S.L. and 3000 m A.S.L. same as Fig. 3.1. Legends should be referred to section 2.2.1.

40
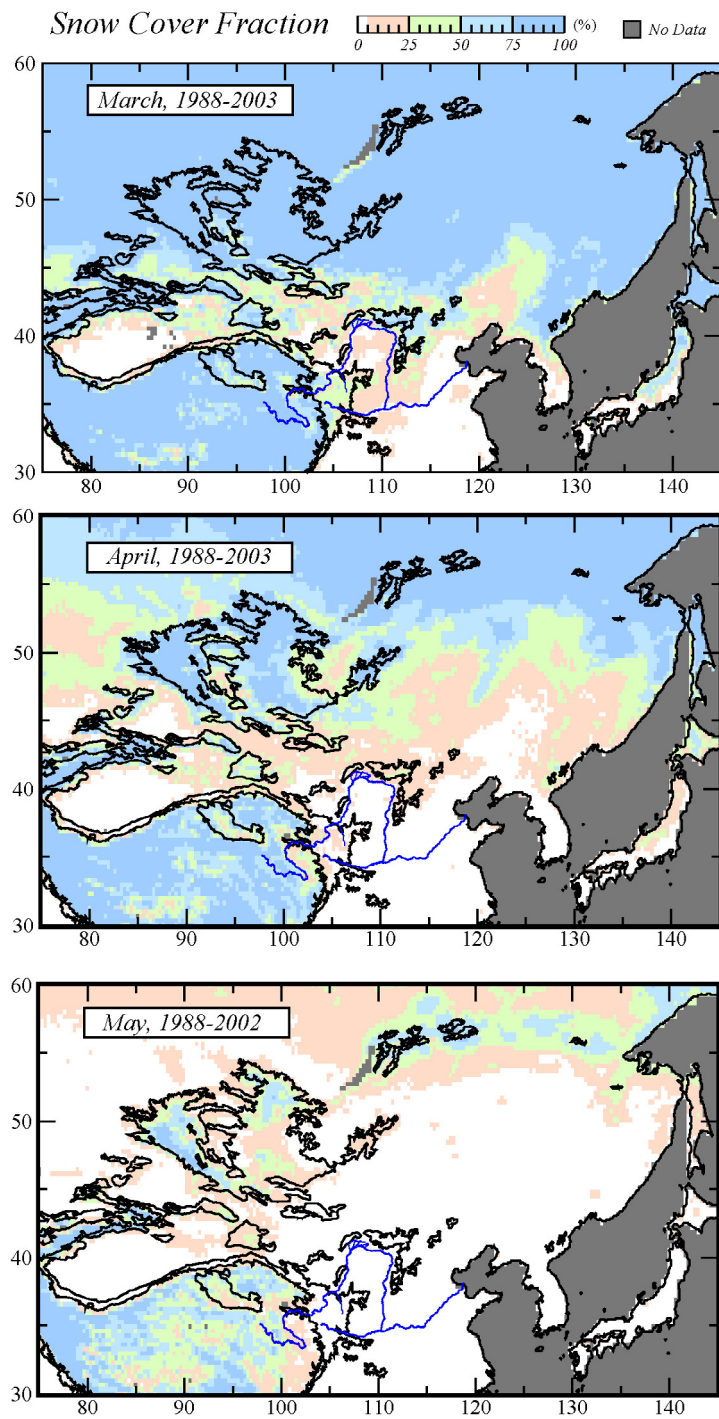
Fig. 3.9. Distributions of snow cover in March for 1988 – 2003 (upper panel), in April for 1988 – 2003 (middle panel) and in May for 1988 – 2002 (lower panel). Snow cover data used for these figures is the same as that described in section 2.2.2.
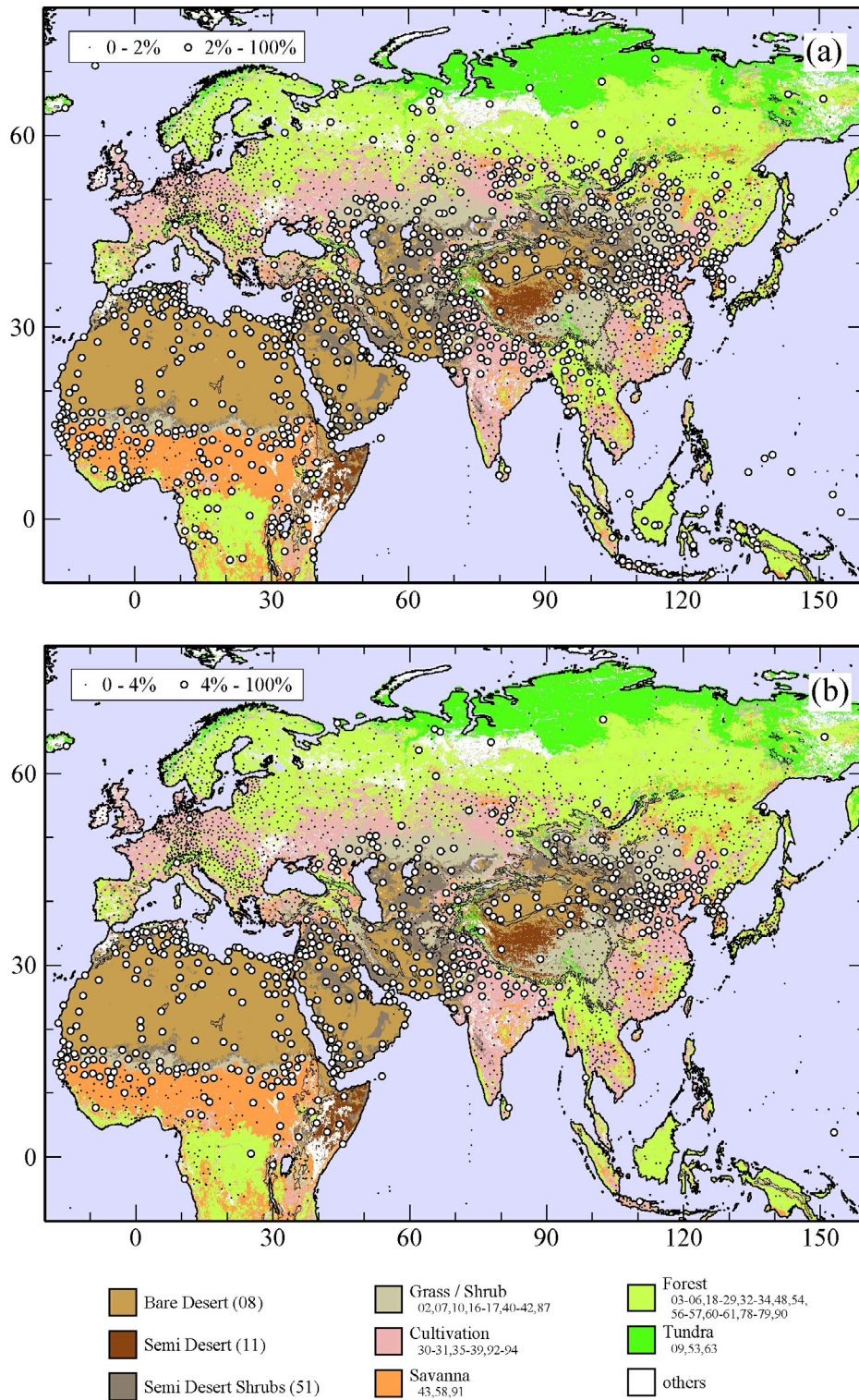
Fig. 3.10. Distributions of potential dust sources around the global dust belt when threshold of maximum monthly dust outbreak frequency is selected 2 % (a) and 4% (b). Potential dust sources are plotted by open circles and non-dust-sources are plotted by dots.
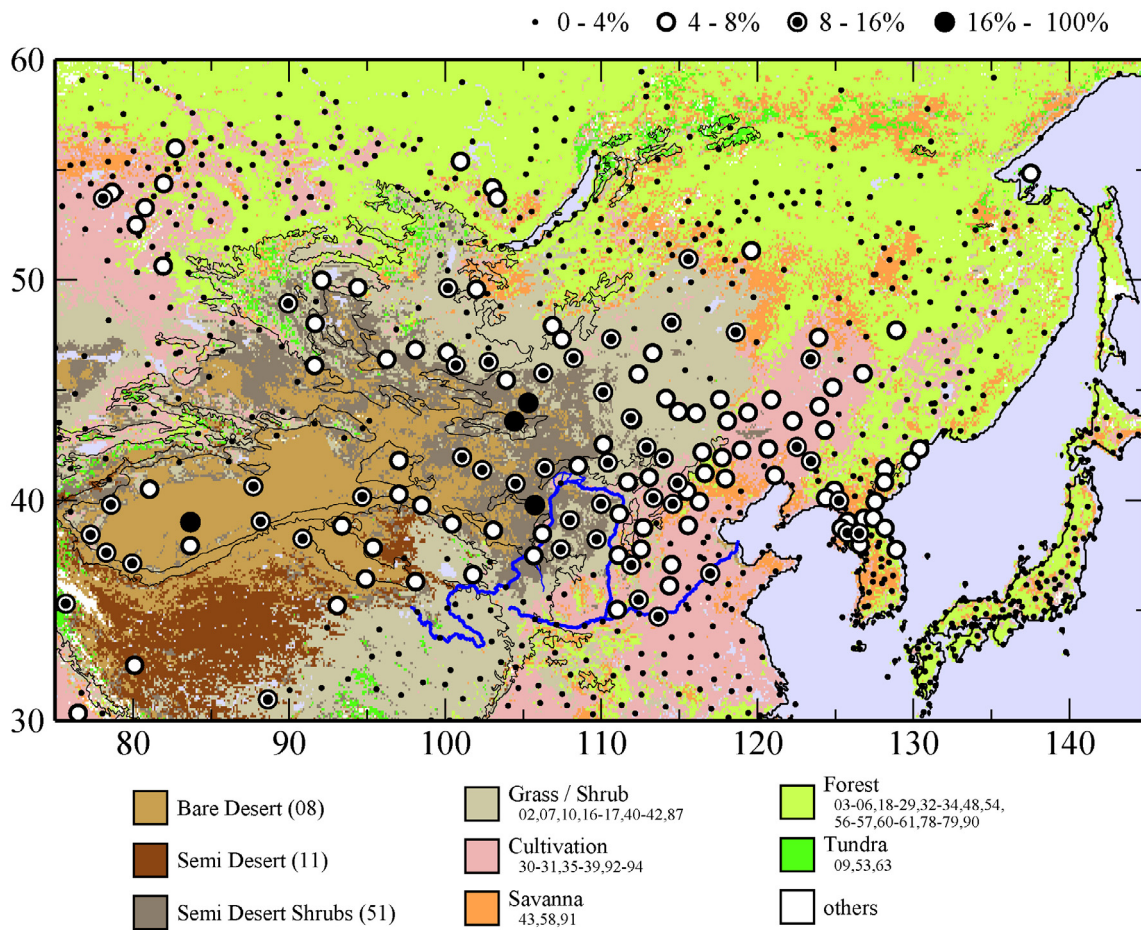
Fig. 3.11. Distributions of potential dust sources in East Asia. WMO synoptic observatories plotted by dots are non-dust-sources. Observatories plotted by other large symbols are potential dust sources, where the maximum monthly dust outbreak frequencies are more than 4 %.

Chapter 4

Characteristics of Aeolian Dust in East Asia

It has been well known that East Asia possesses two major dust source regions; one is the Gobi Desert and the other is the Taklimakan Desert. Although these two dust sources adjoin, different weather systems cause aeolian dust outbreaks. As described in section 3.1, when a synoptic disturbance passes over the Gobi Desert, strong winds accompanied by this disturbance cause dust outbreaks. On the other hand, most of synoptic disturbances cannot directly pass over the Taklimakan Desert because this desert is surrounded by steep topography such as the Tian Shan Mountains, the Pamirs and the Kunlun Mountains. According to *Sun et al.* [2001], dust outbreaks occur by easterly cold airflows in a branch of a major route of synoptic disturbance (Fig. 3.2). *Aoki* [2003] indicates that there are three major routes of synoptic disturbance causing dust outbreaks: they are easterly cold airflow same as *Sun et al.* [2001], northerly one beyond the Tian Shan Mountains, and westerly one beyond the Pamirs.

Referring to the above, we provide two analysis regions in this chapter: one is the region "*around the Gobi Desert*" (Region I) and the other is "*the Taklimakan Desert*" (Region II) (Fig. 4.1). The region around the Gobi Desert includes potential dust sources in regions of Grass/Shrub, Cultivation and Savanna surrounding the Gobi Desert (section 3.3). In this chapter, characteristics of aeolian dust in Regions I and II are studied in sections 4.1 and 4.2, respectively. Aeolian dusts in these two regions are compared in section 4.3.

4.1 Aeolian dust around the Gobi Desert

4.1.1 Introduction

The long-term variations of dust event frequencies have exhibited a negative trend over the last 40 years in China [*Qian et al.*, 2002; *Parungo et al.*, 1994; *Sun et al.*, 2000; *Yoshino*, 2002]. However, East Asian dust events have become uncommonly active in recent years. A report for the press of Japan Meteorological Agency (http://www.jma.go.jp/JMA_HP/jma/press/0204/15a/kosa.pdf) stated that it is remarkable that Kosa (i.e., yellow sand) events were frequently observed in Japan in the last three years (2000 – 2002) (Fig. 4.2). Dust phenomena also frequently occurred after 2000 in Korea. Dust phenomena were observed over 10 days in Seoul City in every year after 2000, although the average number of days of dust phenomena was 5.2 from 1915 – 2002 [*Chun et al.*, 2002; *Chun et al.*, 2001]. In addition, large-scale dust events that transported mineral dust particles across the Pacific Ocean occurred in 1998 and 2001 [e.g., *Husar et al.*, 2001]. The reasons for the recent trend of active dust events and any relation to the dust outbreaks in East Asia have not been clarified.

Aeolian dust is usually generated by strong surface wind on arid and/or semi-arid regions with low vegetation cover. East Asian cyclone activity is strong around the Gobi Desert in spring [*Chen et al.*, 1991], and the Gobi Desert is a major dust source region in East Asia.

The relationship between dust outbreaks and strong winds was investigated in section 4.1 to clarify the recent active dust events around the Gobi Desert. We conducted statistical analyses of dust outbreaks and strong surface winds around the Gobi Desert during the past ten years (1993 – 2002), using the present weather code and the surface wind velocity obtained from the SYNOP report [*WMO*, 1974].

4.1.2 Data and methods

The data used in section 4.1 were the present weather code and surface wind velocity at a 10 m height over the analysis region given in section 4.1.3. They were obtained

from SYNOP reports. The analysis period was from January 1993 to June 2002. The code numbers of the present weather, ww=07, 08, 09, 30-35, and 98, were classified as the dust outbreaks as defined in section 2.1.2. A strong surface wind was defined as one with a velocity exceeding 6.5 m/s, which is the threshold for a dust outbreak in many numerical models (see section 2.1.3). Threshold velocities actually exhibit various values with differing land surface conditions. However, a constant value was used to define a strong wind in this study, because land surface conditions and the threshold velocity for each land surface condition have not yet been clarified.

As defined in section 2.1.4, the dust outbreak frequency is the percentage of the number of dust outbreaks to the total number of observations within a given period at each observatory and/or given region. Similarly, the strong wind frequency is the percentage of the number of strong winds to the total number of observations.

4.1.3 Analysis region

Figure 4.3 illustrates the maximum monthly dust outbreak frequency (hereafter, maximum frequency) from January 1993 to June 2002 at each observatory. As defined in section 3.2, a site is a potential dust source during this period when the maximum frequency exceeds 4 % at such a site. We represent the analysis region in section 4.1 by a box in Fig. 4.3 ($33.5°N - 52.0°N$, $88.5°E - 131.5°E$); this box indicates the north, east, and south boundaries of the potential dust source region around the Gobi Desert. Thus, a total of 105 potential dust source observatories are included within the analysis region. The data at these observatories were used in the statistical analyses in sections 4.1.4.1, 4.1.4.2, and 4.1.4.3.

4.1.4 Results

4.1.4.1 Seasonal variations

The white bar chart and line graph with white circles in Fig. 4.4 indicate the frequencies of monthly dust outbreaks and strong winds from January 1993 to June 2002. Dust outbreaks occur most frequently in spring. This result agrees with previous

studies [*Littmann*, 1991; *Parungo et al.,* 1994]. Two-thirds of the dust outbreaks can be observed in March, April, and May. In contrast, dust outbreaks are the least frequent in summer (July, August, and September). Strong winds also occur most frequently in spring and least frequently in summer. A weak secondary peak of strong wind frequency occurs around November; however, the dust outbreak frequency has no peak in this season.

4.1.4.2 Year-to-year variation

The dust outbreak frequency in spring has been greater in the last three years (2000 − 2002) than in the preceding seven years (1993 − 1999) (Fig. 4.5). The last three years (2000 − 2002) will hereafter be referred to as the dust-frequent years (DFY), and the previous seven years (1993 − 1999) as the dust-normal years (DNY). The year-to-year variation of Kosa events (Fig. 4.2) is similar to that of dust outbreaks in East Asia (Fig. 4.5); i.e., Kosa is frequently observed in DFY. The strong wind frequency is also high in DFY and low in DNY.

A clear positive correlation was found between dust outbreak frequencies and strong wind frequencies in year-to-year variations. However, the month of April was an exception in both 1995 and 1998. The strong wind frequency was as high as in DFY in 1995; nevertheless, the dust outbreak frequency was almost equal to the average of the DNY. In contrast, the dust outbreak frequency was somewhat high in 1998, although the strong wind frequency was almost equal to the average of the DNY. The dust phenomena in exceptional years will be discussed in section 6.3.1.

4.1.4.3 Months that dust outbreaks increased

The black bar chart and line graph with black dots in Fig. 4.4 indicate the frequencies of monthly dust outbreaks and strong winds for DFY (2000 − 2002). Although the most frequent months for dust outbreaks are March, April, and May in a 10-year average (white bar chart), remarkable increases of dust outbreak frequencies occurred in March and April, while no increase was observed in May. The strong wind frequencies also exhibit the same tendency as the dust outbreak, i.e., increases only in

March and April.

4.1.4.4 Spatial distribution of dust outbreaks

Figures 4.6 (a) and (b) illustrate the spatial distribution of the dust outbreak frequencies for March and April in DNY (1993 − 1999) and DFY (2000 − 2002). Areas of frequent dust outbreaks can be seen in the western part of the analysis region in DNY (Fig. 4.6a), i.e., around southern Mongolia (about 44°N, 105°E), the Badain Jaran Desert (about 42°N, 102°E), and the western Loess Plateau (about 40°N, 105°E). The dust outbreak frequencies were low at most observatories in the eastern part of the analysis region, i.e., around the North China Plain (about 40°N, 115°E), northeastern China (about 45°N, 125°E), and the Korean Peninsula (about 38°N, 127°E). In contrast, the region of frequent dust outbreaks expanded to the east in DFY (Fig. 4.6b), and dust outbreaks frequently occurred at many observatories in the eastern region. Although the area of frequent dust outbreaks expanded little into the western region, dust outbreak frequency increased at each observatory.

4.1.4.5 Spatial difference in dust outbreaks with strong winds

Section 4.1.4.2 described the correlation between dust outbreaks and strong winds in the year-to-year variations; the spatial differences in dust outbreaks with strong winds are shown in Fig. 4.7. This figure is a scatter diagram of increases in the frequency of strong winds (abscissa) and dust outbreaks (ordinate) from DNY (1993 − 1999) to DFY (2000 − 2002). The frequencies were calculated for the period from March to April at each observatory. Each symbol in this figure indicates the dust outbreak frequency in DFY.

Most of the plots are in the first quadrant. This indicates that the dust outbreak frequencies increased at observatories where the strong wind frequencies increased. Dust outbreak frequencies increased remarkably at sites of frequent dust outbreaks (black circle plots). This signifies that an increase of strong winds is always accompanied by an increase of dust outbreaks in these regions. No dust outbreaks were noted at observatories indicated by dot plots in DNY and DFY.

4.1.5 Discussion and summary

In section 4.1, it was clarified that dust outbreaks remarkably increased around the Gobi Desert during the last three years (2000 – 2002) compared with the previous seven years (1993 – 1999). The findings suggest that frequent Kosa events in Japan during DFY (2000 – 2002) followed frequent dust outbreaks in East Asia. Although March, April, and May are the most active months for dust outbreaks, remarkable increases of dust outbreaks occurred only in March and April. The spatial distribution of dust outbreaks in March and April (Fig. 4.6) indicates that regions of frequent dust outbreaks expanded extensively to the east from DNY (1993 – 1999) to DFY (2000 – 2002).

We found good correlation between the frequencies of strong winds and dust outbreaks with respect to their year-to-year variations and their spatial distributions. This implies that increases of strong winds caused frequent dust outbreaks in DFY. An increase in strong winds effectively increases dust outbreaks in the regions of frequent dust outbreaks, as shown in Fig. 4.7. The greatest increases in the frequency of dust outbreaks occurred around southern Mongolia, the Badain Jaran Desert, and the western Loess Plateau, in which dust outbreak frequencies were already high in DNY (Fig. 4.6). In section 4.1, it was clarified that frequent strong winds are the primary cause of frequent dust outbreaks; however, the cause for the recent frequent strong winds was not determined.

There was no positive correlation between the strong wind frequency and the dust outbreak frequency with respect to the year-to-year variations in 1995 and 1998. There was also no positive correlation at some observatories between the strong wind frequencies and dust outbreak frequencies, particularly in the second and fourth quadrants in Fig. 4.7. These temporal and spatial exceptions suggest that dust outbreaks do not always depend exclusively on wind. The impact of other factors (e.g., land surface conditions) on dust outbreaks should be considered in their explanation.

4.2 Aeolian dust in the Taklimakan Desert

4.2.1 Introduction

Radiative forcing caused by aerosols is the major factor of the radiation balance of the atmosphere. Mineral dust is the major component of aerosols; nevertheless, the radiative forcing owing to mineral dust is not understood because it is difficult to evaluate spatial and temporal information of mineral dust particles at present [*IPCC*, 2001] (see section 1.3). For these reasons, the Japan-China joint project on Aeolian Dust Experiment on Climate impact (ADEC) was proposed and started in April 2000. The Taklimakan Desert is one of the research fields of the project. The aim of the observation in this region is to understand the wind erosion process [*Mikami et al.*, 2002]. The Taklimakan Desert is surrounded by mountains, including the Tibetan Plateau and the Tian Shan Mountains (see Fig. 4.8). Process studies have been conducted since March 2001 at a gobi desert¶ in the southern part of the Taklimakan Desert using the Automatic Weather Station (AWS). However, to understand the characteristics of the dust outbreak in this region, the basic statistical features of dust events around this region should be well understood.

He and Zhao [1999] and *He et al.* [1996] indicated the annual number of days with floating dust and dust storm for each WMO synoptic observatory in the Taklimakan Desert, respectively. *Yoshino* [1997] discussed the monthly variation of dust storms from the viewpoint of atmospheric circulation. Severe dust outbreak (i.e., dust storm) has been the main focus of past studies, although *He and Zhao* [1999] include a figure showing the spatial distribution of floating dust. Floating dust and dust storm were separately investigated in different studies, but their relationship was not investigated. Weak or moderate dust outbreak, which is called as "*blowing dust*" in section 4.2, has

---

¶ A stony desert is called as "*a gobi desert*" in China. According to *Aoki et al.* [2002], a gobi desert is composed of various particle-size soil (i.e., clay, silt, sand) and stones with a size of a few centimeters at most in the south of the Taklimakan Desert and it is known that the ratio of fine soil particles (i.e., clay and silt) is larger in a gobi desert than that in a sand desert through researches of ADEC. "*A gobi desert*" differs from "*the Gobi Desert*".

not been analyzed yet.

In section 4.2, dust phenomena in the suspending phase and the generating phase are investigated, and their regional difference in the Taklimakan Desert is compared with their seasonal variation through the analysis of present weather data of SYNOP report (section 2.1.2). Statistics in the whole Taklimakan Desert region are conducted, and year-to-year and seasonal variations of dust events are given in sections 4.2.3.1 and 4.2.3.2, respectively. Statistics for each WMO synoptic observatory is conducted, and spatial distribution of dust events is discussed in section 4.2.3.3.

4.2.2 Data and methods

The data used in this study are three hourly present weather data of SYNOP report [*WMO*, 1974] (see section 2.1.2) at twelve meteorological observatories, as shown in Fig. 4.8. The data from March 1996 to July 2001 are used for the analysis. For the annual statistics, however, the data until February 2001 are used and the beginning of a year is defined as March. The name and location of each station are shown in Table 4.1. Data from the Andir station (51848) are available until December 1998; after January 1999, data from the Tazhong station (51747) are presented.

In section 4.2, we separately analyze two phases of dust in the Taklimakan Desert such as the suspending phase (i.e., floating dust) and the generating phase (i.e., dust outbreak). Furthermore, the generating phase is separated into weak or moderate dust outbreak (i.e., blowing dust) and severe dust outbreak (i.e., dust storm). As a result, in section 4.2, five categories of dust phenomena are given such as floating dust, blowing dust, dust storm, dust outbreak, and dust event. While symbolic letters "ww" identifies the present weather in SYNOP report (section 2.1.2), each category is defined as follows: (1) when ww is 06, a floating dust occurs; (2) when ww is 07, a blowing dust occurs; (3) when ww is 09, 30, ···, 35, or 98, a dust storm occurs; (4) when ww is 07, 09, 30, ···, 35, or 98, a dust outbreak occurs; (5) when ww is 06, 08, 09, 30, ···, 35, or 98, a dust event occurs (Table 4.2). In section 4.2, ww=08 is a member of neither dust outbreak nor dust storm although it is a member of both categories in other sections.

For the purpose of discussing the temporal and spatial density of a dust event, the dust event frequency is defined as the percentage of dust events to all observations. Similarly, the floating dust frequency, the blowing dust frequency, the dust storm frequency and the dust outbreak frequency is also defined. These definitions are the same as in section 2.1.4.

4.2.3 Results

Figure 4.9 shows the time sequence of the monthly dust event frequency in the Taklimakan Desert from March 1996 to July 2001. Floating dust is observed quite more frequently than blowing dust or dust storm.

4.2.3.1 Annual change of the dust event

Figure 4.10a shows the annual dust event frequency during twelve months from March to the following February in the Taklimakan Desert. Figure 4.10b shows the annual frequency during three months, March, April, and May (hereafter, MAM). The difference of the dust event frequency within each year shown in Fig. 4.10a is quite less than that shown in Fig. 4.10b because the dust event frequency during MAM is quite larger than that during the other nine months (see also Fig. 4.11). Fig. 4.10c shows the KOSA-event days for each year (data from Japan Meteorological Agency). This means the total number of days which floating dust was observed at meteorological stations in Japan. KOSA means floating dust observed in Japan, especially during MAM [*Murayama*, 1991]. A certain correspondence can be seen between the annual change of dust event frequency during MAM (Fig. 4.10b) and that of KOSA-event days (Fig. 4.10c) except for the year 2000, although their relationship cannot be clarified from these two figures alone.

4.2.3.2 Monthly change of the dust event

Figure 4.11 shows the time sequence of monthly dust event frequency during the last five years from March 1996 to February 2001. The dust event in the Taklimakan Desert has two characteristics. One is that it shows two maximums of dust event frequency.

The primary peak appears in April, and the frequency is high in March and May as well. This shows good agreement with the seasonal characteristics of strong wind in the southern part of the Taklimakan desert [*Mikami et al.*, 1995]. The secondary peak occurs in September. The other characteristic is that it shows one maximum of dust outbreak frequency, which appears in May.

4.2.3.3 Spatial distribution of the dust event

The central part of Fig. 4.12 shows the dust event frequency during the last five years, from March 1996 to February 2001. Frequency is shown by six kinds of symbols as well as by numerical values. Bar charts located in the surrounding parts of Fig. 4.12 show the monthly dust event frequency for each station. Figure 4.13 is the same as Fig. 4.12 but for the dust outbreak. The numerical value in parenthesis is the frequency of dust storms.

According to these two figures, the Taklimakan Desert can be divided into the six regions shown in Table 4.1, which are the east, north, west, southwest, southeast, and central regions.

The spatial distribution of the dust event is examined by the central part of Fig. 4.12. The dust event is observed frequently in the southwest, southeast, and central regions, especially at Hotan (51828). The dust event frequency is relatively high in the west region; a dust event is seldom observed in the north and east regions. Subsequently, the spatial distribution of the dust outbreak is considered by the central part of Fig. 4.13. The dust outbreak frequently occurs in the east region, but a dust event seldom occurs. On the other hand, the dust outbreak frequency is relatively low in the southwest region except for Pishan (51818), although the dust event is observed with the highest frequency in the Taklimakan Desert. The dust outbreak frequency is remarkably high at Tazhong (51747), which is located in the central region. Dust outbreak, as well as dust event, occurs rarely in the north region. The above results of the dust event and the dust outbreak show good agreement with the spatial distributions of floating dust and dust storms given by *He and Zhao* [1999] and *He et al.* [1996], respectively, although the east-west distribution of sand storms reported by *He and Zhao* [1999] differs from this

study.

Monthly changes of the dust event and dust outbreak are examined in the bar charts of Fig. 4.12 and Fig. 4.13, respectively. The single maximum of the dust event appears in some stations, although two maximums appeared in the statistics of the whole Taklimakan Desert region (Fig. 4.11). Two maximums of the dust outbreak, on the contrary, appear in some stations, although only single maximum appeared in Fig. 4.11. Although the secondary peak of the dust event does not appear around the east region, the dust outbreak has the secondary peak in August. Only the single maximum of the dust outbreak, on the other hand, appears in the southwest region, where the secondary peak of the dust event appears clearly in September. These results of the dust outbreak are almost consistent with the monthly changes of dust storms for each station reported by *He et al.* [1996]. Especially, the primary peak of the dust outbreak in this study corresponds well with that of dust storms given by *He et al.* [1996].

The month of the maximum is listed for the dust event and dust outbreak in Table 4.3. The primary peak of the dust event appears in different months at different stations. The primary peak of the dust event appears around March in the east and north regions. In the west and southwest regions, on the other hand, the primary peak of the dust event appears around April. This difference concerning the month of occurrence of the primary peak is also observed with regard to the dust outbreak, whose primary peak appears about one month later than that of dust event at all stations except for Andir (51848) and Tazhong (51747).

The secondary peak of the dust event appears around September. However, that of the dust outbreak appears in any month from June to November.

4.2.4 Discussion

The annual tendency of dust event frequency during MAM (March, April, and May) and that of KOSA-event days show rough correspondence. *Iwasaka et al.* [1983] and *Sun et al.* [2001] observed that dust originating from the Taklimakan Desert is blown up to higher elevation than the surrounding mountains and it is transported over long

distance. However, the mechanism and the amount of discharging dust have not been clarified. Furthermore, it could not be determined in our study whether dust generated in the Taklimakan Desert is transported to Japan or not, although the source regions of KOSA are the Gobi Desert and the Taklimakan Desert, according to a case study by *Iwasaka et al.* [1983].

Two maximums of the dust event (i.e., April and September) and a single maximum of the dust outbreak (i.e., May) are clarified after the analysis of monthly frequency in the whole Taklimakan Desert region in section 4.2.3.2. The minimum of the dust event between April and September can be explained by weak upper westerlies and the lower circulation suitable for precipitation in the summer season [*Yoshino*, 1997]. However, two questions remain: (1) why the former peak of the dust event (i.e., April) is one month earlier than the peak of the dust outbreak (i.e., May), and (2) why the dust event has the second peak in September and the dust outbreak does not. This means that floating dust occurs before or without the occurrence of a dust outbreak.

All stations are located in an oasis except Tazhong (51747). An oasis is generally an unfavorable environment for a dust outbreak; however, floating dust can advect into an oasis. This can explain the floating dust without the occurrence of a dust outbreak; however, the other question, which is floating dust before the occurrence of a dust outbreak, still remains unanswered.

The dust events investigated in this study must be brought by several-scale disturbances (e.g., synoptic scale, meso scale, and diurnal scale disturbances). Different meteorological conditions such as wind or precipitation cause different-scale dust events. Consideration, however, was not given separately to each scale in this study.

This study raised the question of why floating dust is observed before or without the occurrence of a dust outbreak. Other subjects also remain, namely, how long dust stay suspended and how dust is discharged from the Taklimakan Desert. To resolve these problems, the dust event should be studied for each scale by the use of objective analysis data and upper air data as well as surface wind and precipitation, and numerical experiments should also be conducted.

4.2.5 Summary

Seasonal changes and regional differences of the dust event and dust outbreak in the Taklimakan Desert were investigated by the analysis of three hourly present weather data of SYNOP report from March 1996 to July 2001. The results are summarized as follows:

1. The annual change of the dust event during three months, March, April, and May, in the Taklimakan Desert corresponds in some degree to that of the KOSA-event in Japan except for the year 2000. From this study, however, it could not be determined whether the origin of KOSA is the Taklimakan Desert or not.

2. The dust event frequency has two maximums in the statistics of the whole Taklimakan Desert region. The primary peak appears in April, and the secondary peak appears in September. The dust outbreak frequency, however, only has a single maximum in May.

3. The dust event occurs in the southwest, south, and central regions with the highest frequency, especially at Hotan (51828). On the other hand, a dust event rarely occurs in the north and east regions.

4. The dust outbreak frequency is relatively high in the east region; however, a dust event rarely occurs there. On the contrary, the dust outbreak frequency in the southwest region is relatively low, but the dust event is frequent. The dust outbreak occurs with remarkable frequency at Tazhong (51747), which is located in the central region.

5. One maximum of the dust event frequency and two maximums of the dust outbreak frequency are found in the statistics of some stations, although the reverse is true in the statistics of the whole Taklimakan Desert region.

6. The primary peak of the dust event appears in March in the east and north regions and appears in April in the west and southwest regions. In the case of the dust outbreak as well, the primary peak appears in a different month region by region, but the month of the primary peak is about one month later than that of the dust event.

4.3 Comparison between aeolian dust outbreaks around the Gobi Desert and in the Taklimakan Desert

In section 4.3, we compare aeolian dust outbreaks between around the Gobi Desert (Region I indicated by Fig. 4.1) and in the Taklimakan Desert (Region II) in the dust season (i.e., March, April and May) from 1988 to 2003. The data are present weathers and wind velocities in SYNOP reports. The definitions such as dust outbreak, strong wind, dust outbreak frequency and strong wind frequency are the same as those in Chapter 2. The threshold for the definition of strong wind is 6.5 m/sec. Relations between strong wind and dust outbreak are discussed for each region in sections 4.3.1.1 and 4.3.1.2. In these sections, the data at potential dust sources (section 3.2) are available while the data at non-dust-sources are not used for analyses. The dust outbreak frequency is plotted for each WMO synoptic observatory on a map in section 4.3.1.3 and major dust sources in East Asia are discussed.

4.3.1 Results and discussion

4.3.1.1 Seasonal variations

Figures 4.14 shows seasonal variations of dust outbreak frequency and strong wind frequency for the region around the Gobi Desert (Region I) (a) and for the region in the Taklimakan Desert (Region II) (b). Dust outbreak frequency and strong wind frequency are indicated by bar chart (left axis) and by line graph (right axis), respectively.

In both regions, dust outbreaks frequently occur in months of frequent strong winds and these are most frequent in spring. Major months of frequent dust outbreaks are March, April and May around the Gobi Desert (Fig. 4.14a). The contrast of dust outbreak frequency is clear between in these months and in other months around the Gobi Desert. However, dust outbreaks frequently occur in June, July and/or August as well as in March, April and May in the Taklimakan Desert (Fig. 4.14b).

The ratio of dust outbreaks to strong winds is much smaller around the Gobi Desert than that in the Taklimakan Desert. This tendency is remarkable in April that both dust outbreaks and strong winds occur most frequently in both regions. The dust

outbreak frequency (4.1 %) is almost the same as the strong wind frequency (3.9 %) in April in the Taklimakan Desert. On the other hand, the dust outbreak frequency (2.3 %) is much less than the strong wind frequency (16.4 %) in April around the Gobi Desert. In other words, the probability of dust outbreak is about one seventh when a strong wind (over 6.5 m/sec) occurs. This result suggests that the threshold velocity of dust outbreak should be around 6.5 m/sec in the Taklimakan Desert while it should be larger than 6.5 m/sec around the Gobi Desert.

4.3.1.2 Correlation between strong winds and dust outbreaks

Figure 4.15 shows relations between the strong wind frequency and the dust outbreak frequency in March (upper panel), April (middle panel) and May (lower panel) of each year from 1988 to 2003. White and black circles indicate results for the regions around the Gobi Desert and in the Taklimakan Desert, respectively. Regression equations and correlation coefficients between these frequencies are indicated as well.

The correlation is higher in the Taklimakan Desert than that around the Gobi Desert in each month. This means that the wind condition more largely control the occurrence of dust outbreak in the Taklimakan Desert than around the Gobi Desert. This suggests that the land surface condition varies less in the Taklimakan Desert than around the Gobi Desert.

For both regions, the correlations are large in March and April while they are small in May. Especially, it is small around the Gobi Desert in May. This means that the wind condition more largely controls the occurrence of dust outbreak in March and April than in May. On the other hand, land surface conditions such as soil wetness, vegetation activity largely affect dust outbreaks in May, especially around the Gobi Desert.

As described in section 4.1, Fig. 4.15 indicates that dust outbreaks are frequent in March and April during dust frequent years (2000 – 2002) around the Gobi Desert. In the Taklimakan Desert, on the other hand, although dust outbreaks are frequent in April during dust frequent years (2000 – 2002), they are not frequent in March as well as in May.

4.3.1.3 Spatial distribution of dust outbreak frequency

Figure 4.16 shows the spatial distribution of dust outbreak frequencies for March, April and May from 1988 to 2003. In the Region I (i.e., around the Gobi Desert), dust outbreaks frequently occur around the southern Mongolia (about 44°N, 105°E), the Badain Jaran Desert (about 42°N, 102°E), and the western Loess Plateau (about 40°N, 105°E). According to section 4.1, dust outbreaks frequently occur in the same regions for March and April from 1993 to 1999 (Fig. 4.6a) although the analysis periods are different. The dust outbreaks frequently occur in the Taklimakan Desert (Region II) in almost the same degree as in these three regions.

4.3.2 Summary

In section 4.3, aeolian dust outbreaks are compared between around the Gobi Desert (Region I) and in the Taklimakan Desert (Region II) in the dust season (i.e., March, April and May) from 1988 to 2003. The results are summarized as follows:

1. Dust outbreaks frequently occur in months of frequent strong winds in both regions. However, although the months of frequent dust outbreaks are limited in March, April and May around the Gobi Desert, dust outbreaks frequently occur from March to July and/or August in the Taklimakan Desert.

2. The ratio of dust outbreaks to strong winds (over 6.5 m/sec) is small around the Gobi Desert. This tendency is remarkable in April that both dust outbreaks and strong winds occur most frequently in both regions. The probability of dust outbreak is about one seventh when a strong wind (over 6.5 m/sec) occurs in April around the Gobi Desert, although these frequencies are almost the same in the Taklimakan Desert. This suggests that the threshold velocity of dust outbreak should be around 6.5 m/sec in the Taklimakan Desert while it should be larger than 6.5 m/sec around the Gobi Desert.

3. The correlation between the strong wind frequency and the dust outbreak frequency is always higher in the Taklimakan Desert than that around the Gobi Desert from March to May. This means that the wind condition largely controls the occurrence of

dust outbreak in the Taklimakan Desert because of small variations of land surface conditions.

4. The correlations between the strong wind frequency and the dust outbreak frequency are large in March and April in both regions while it is small in May, especially around the Gobi Desert. This result suggests that land surface conditions such as soil wetness and vegetation activity largely affect dust outbreaks in May.

5. Major dust frequent regions are the southern Mongolia (about 44°N, 105°E), the Badain Jaran Desert (about 42°N, 102°E), the western Loess Plateau (about 40°N, 105°E) and the Taklimakan Desert.

Station No.	Station Name	Latitude	Longitude	Altitude	Region Name
51777	Ruoqiang	39°02' N	88°10' E	889 m	East
51765	Tikanlik	40°38' N	87°42' E	847 m	East
51656	Korla	41°45' N	86°08' E	933 m	North
51644	Kuqa	41°43' N	82°57' E	1100 m	North
51730	Alar	40°30' N	81°03' E	1013 m	North
51716	Bachu	39°48' N	78°34' E	1117 m	West
51709	Kashi	39°28' N	75°59' E	1291 m	West
51811	Shache	38°26' N	77°16' E	1232 m	Southwest
51818	Pishan	37°37' N	78°17' E	1376 m	Southwest
51828	Hotan	37°08' N	79°56' E	1375 m	Southwest
51848*	Andir	37°56' N	83°39' E	1264 m	Southwest
51747*	Tazhong	39°00' N	83°40' E	1099 m	Central

*Data at Andir (51848) and at Tazhong (51747) are available until December 1998 and as from January 1999, respectively.

Table 4.1. Selected stations in the Taklimakan Desert and region names defined in this study.

	dust event	
suspending phase floating dust	**generating phase** dust outbreak	
	weak or moderate dust outbreak blowing dust	severe dust outbreak dust storm
ww=06	ww=07	ww=09, 30–35 and 98

Table 4.2. Definitions about phenomena of aeolian dust in section 4.2. Symbolic letters "ww" identifies the present weather in a SYNOP report (see section 2.1.2). Although dust outbreak corresponds to ww=07, 09, 30-35 and 98 in section 4.2, ww=08 is a member of dust outbreak in other sections (i.e., ww=07, 08, 09, 30-35 and 98). In other words, ww=08 is excluded from the group of dust outbreak in section 4.2. Similar to dust outbreak, ww=08 is not a member of dust event in section 4.2 (see also Table 2.2).

Station	Region	Primary Peak		Secondary Peak	
		Dust Event	Dust Outbreak	Dust Event	Dust Outbreak
51777	East	Mar.	Apr.	—	Aug
51765	East	Mar.*	Mar., Apr. or May	—	Aug
51656	North	Mar.*	Mar. or Apr.*	—	—*
51644	North	Mar.*	Apr. or May*	Sep.	—*
51730	North	Mar. or Apr.	Apr.	Aug.	Aug.
51716	West	Mar. or Apr.	May	Sep.	Oct.
51709	West	Apr.	May*	Sep.	Nov.*
51811	Southwest	Apr.	May	Sep.	—
51818	Southwest	Apr.	May	Sep.	—
51828	Southwest	Apr. or May	May	Sep.	—
51848	Southeast	Jun.	Apr.	Aug. or Sep.	Jun.
51747	Central	Apr.	Apr.	—	Sep.

Note1: The asterisk (*) means low frequency of the dust event or dust outbreak

Note2: The bar (—) means no peak

Table 4.3. Month of peak for the dust event and the dust outbreak.
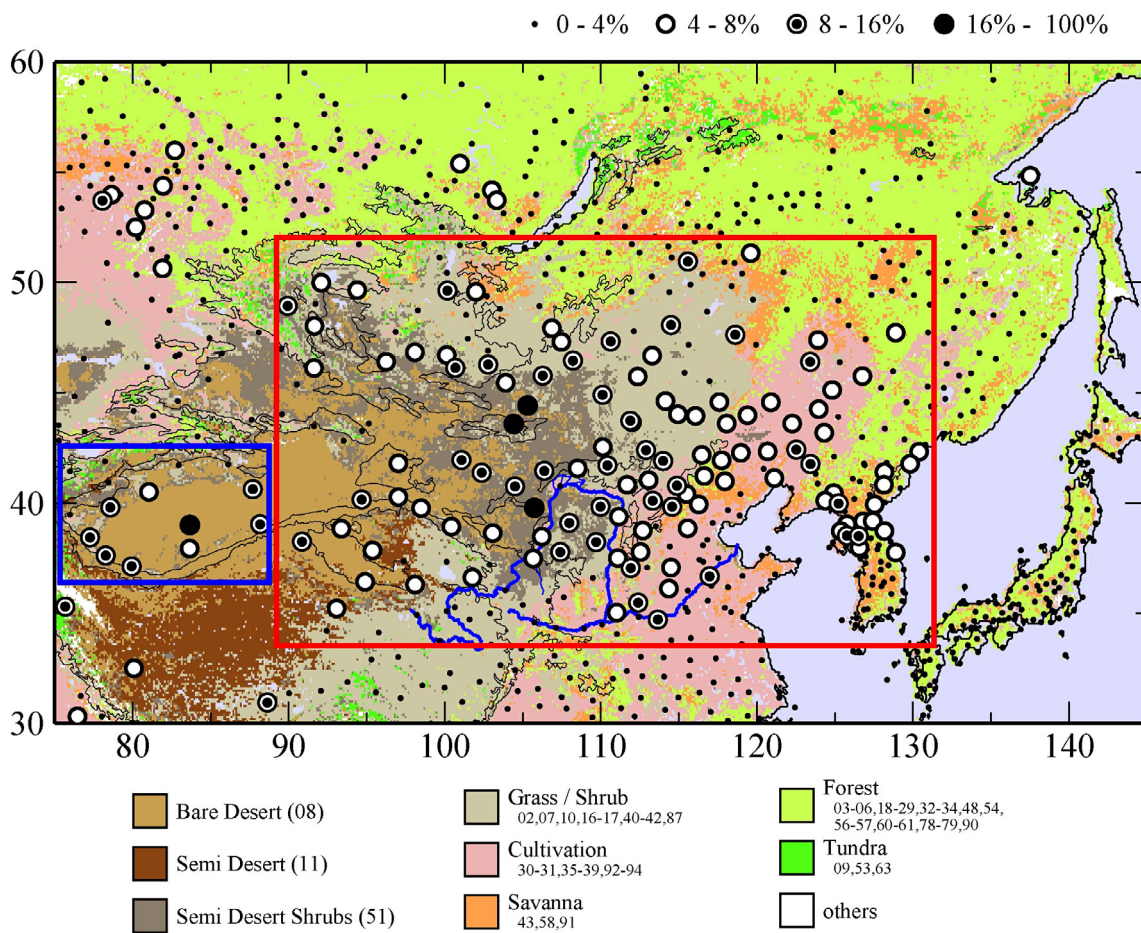
Fig. 4.1. The analysis regions "*around the Gobi Desert*" (Region I) shown by red box and "*the Taklimakan Desert*" (Region II) shown by blue box.
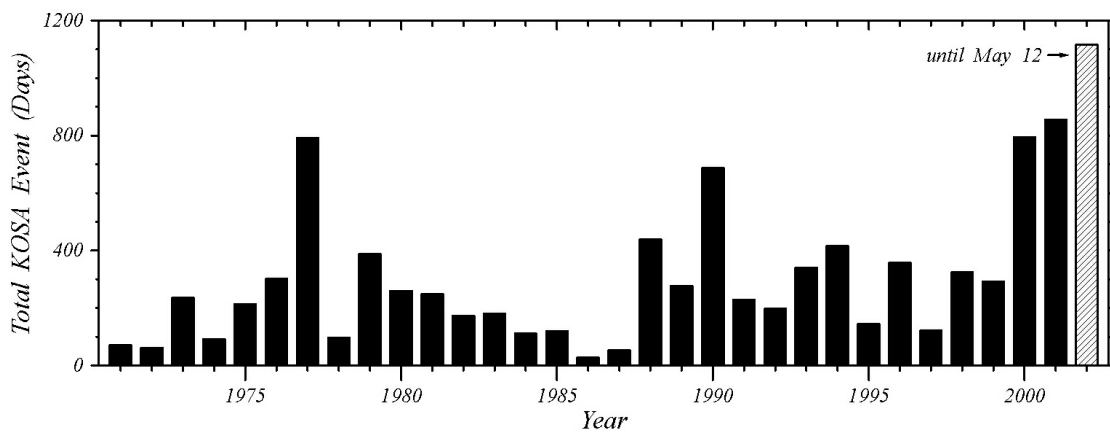
Fig. 4.2. Total number of days for which Kosa (i.e., yellow sand) events were observed at 123 observatories for each year in Japan. For example, the total number of Kosa days is five for any day when Kosa is observed at five observatories in one day. The result of 2002 includes data until May 12 of that year. (From a report for the press by Japan Meteorological Agency; http://www.jma.go.jp/JMA_HP/jma/press/0204/15a/kosa.pdf).
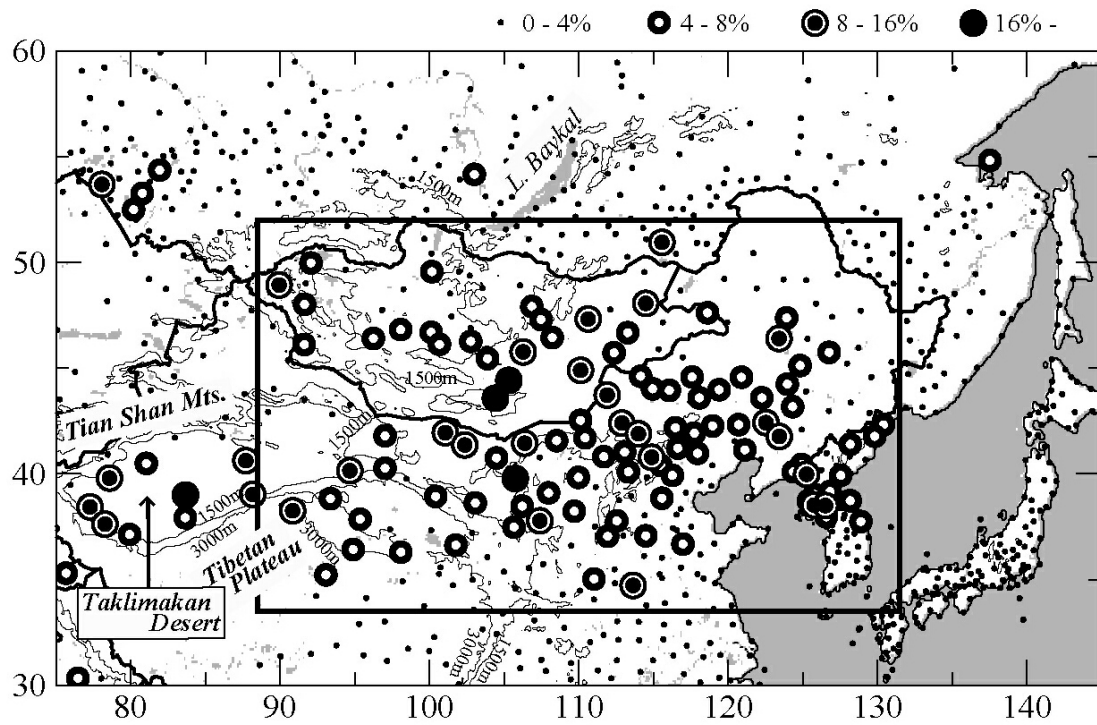
Fig. 4.3. Maximum monthly dust outbreak frequency during Jan. 1993 to Jun. 2002. The box indicates the analysis region. Thick solid lines indicate country boundaries. Thin solid lines indicate 1,500 m and 3,000 m topography contours. Gray shading indicates the sea and lakes.
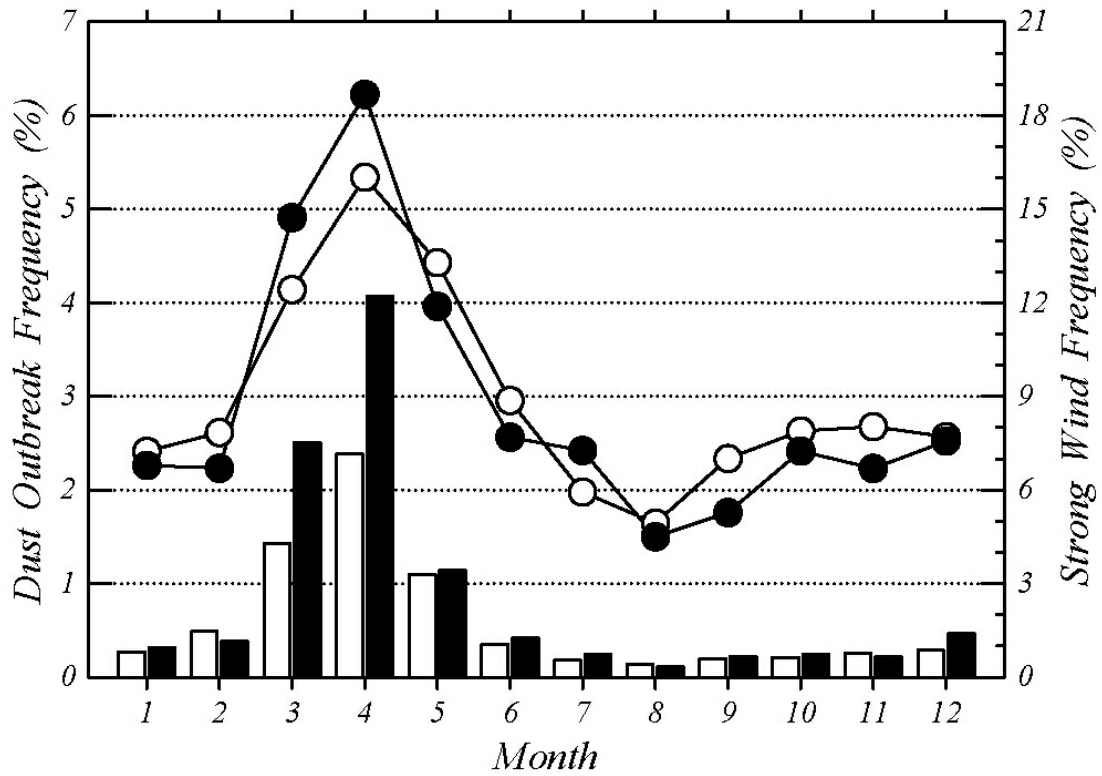
Fig. 4.4. Monthly dust outbreak frequency and strong wind frequency from Jan. 1993 to Jun. 2002 (white bars and white circles) and the same from Jan. 2000 to Jun. 2002 (black bars and black dots).
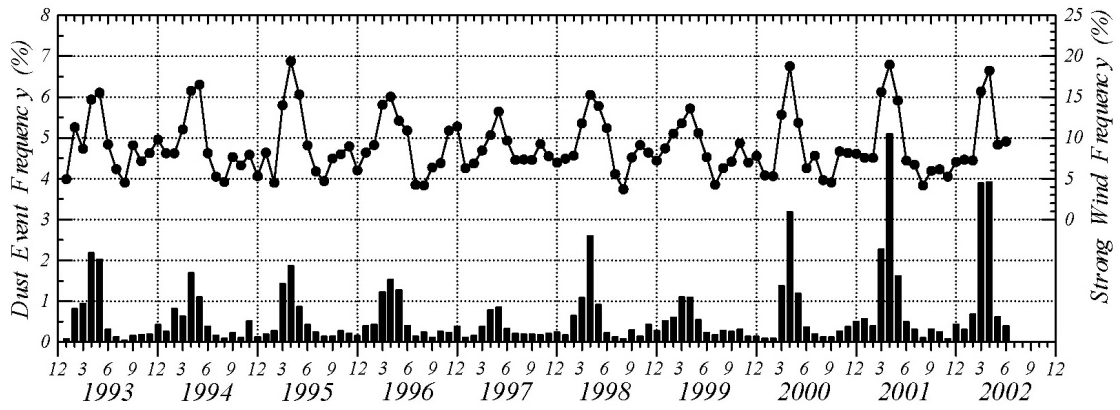
Fig. 4.5. Monthly dust outbreak frequency and strong wind frequency from Jan. 1993 to Jun. 2002. The black bar chart and line graph with black dots indicate dust outbreak frequency and strong wind frequency.
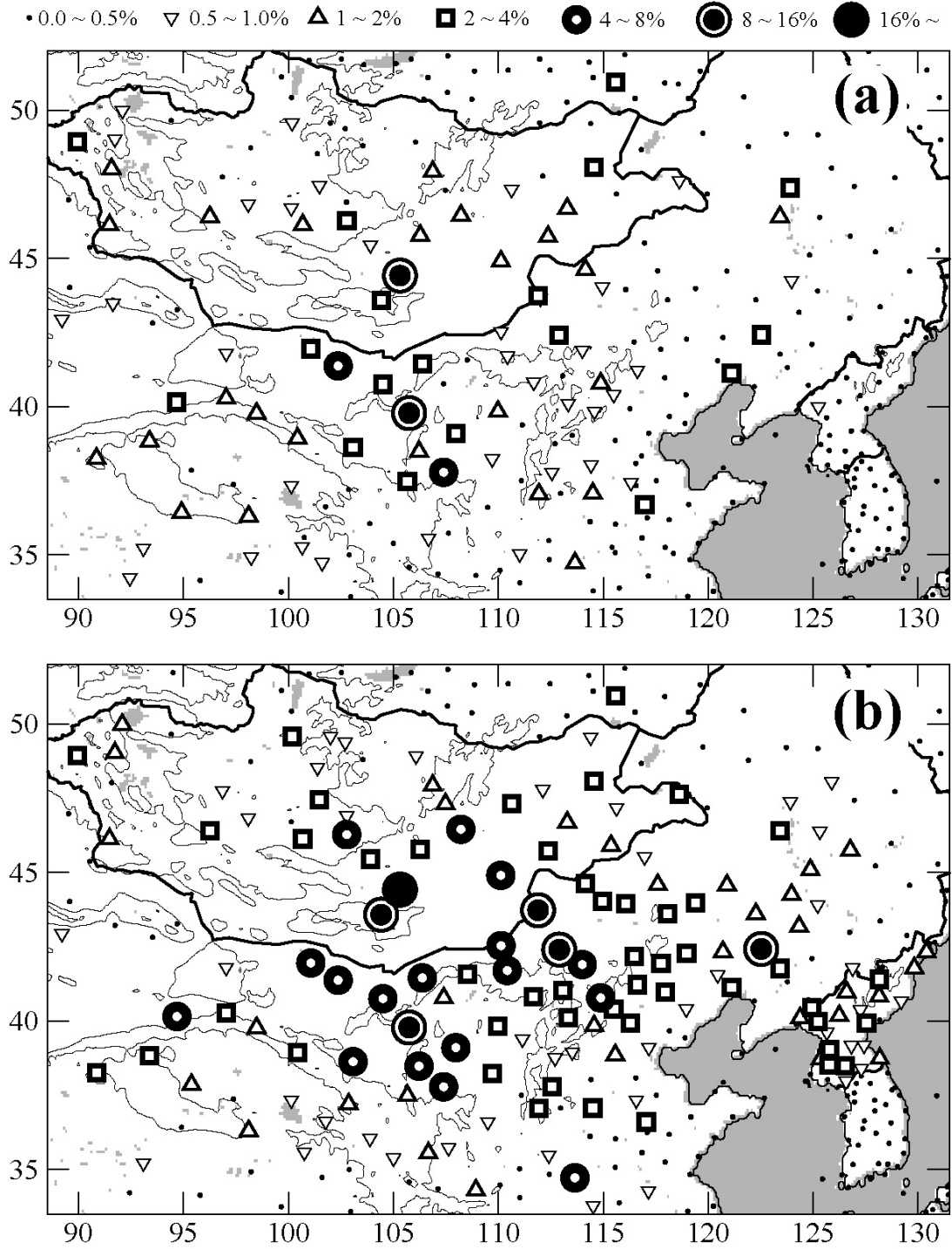
Fig. 4.6. Dust outbreak frequencies for March and April (a) in dust-normal years (1993 − 1999) and (b) in dust-frequent years (2000 − 2002). Thick and thin solid lines and gray shading are the same as in Fig. 4.3.
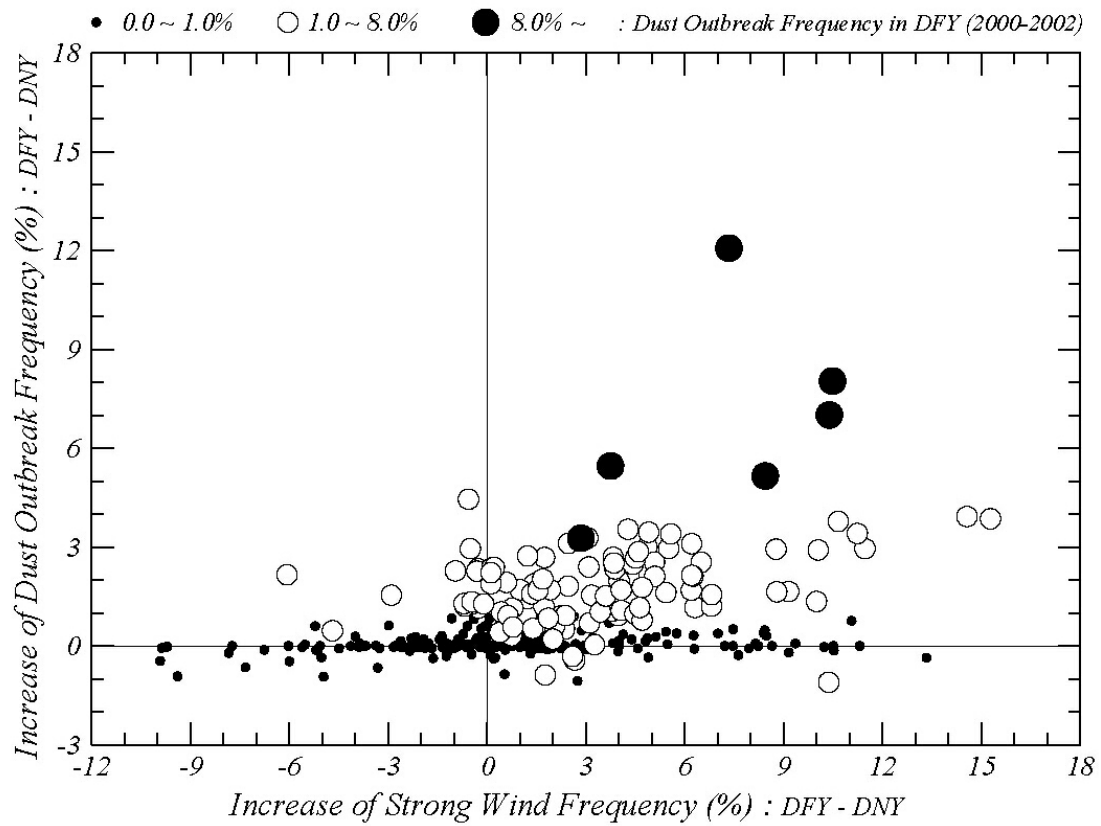
Fig. 4.7. Scatter diagram of increases in the frequency of strong winds (abscissa) and dust outbreaks (ordinate) for March to April at each observatory from the dust-normal years, DNY (1993 – 1999), to the dust-frequent years, DFY (2000 – 2002). Each symbol in this figure indicates the dust outbreak frequency in DFY.
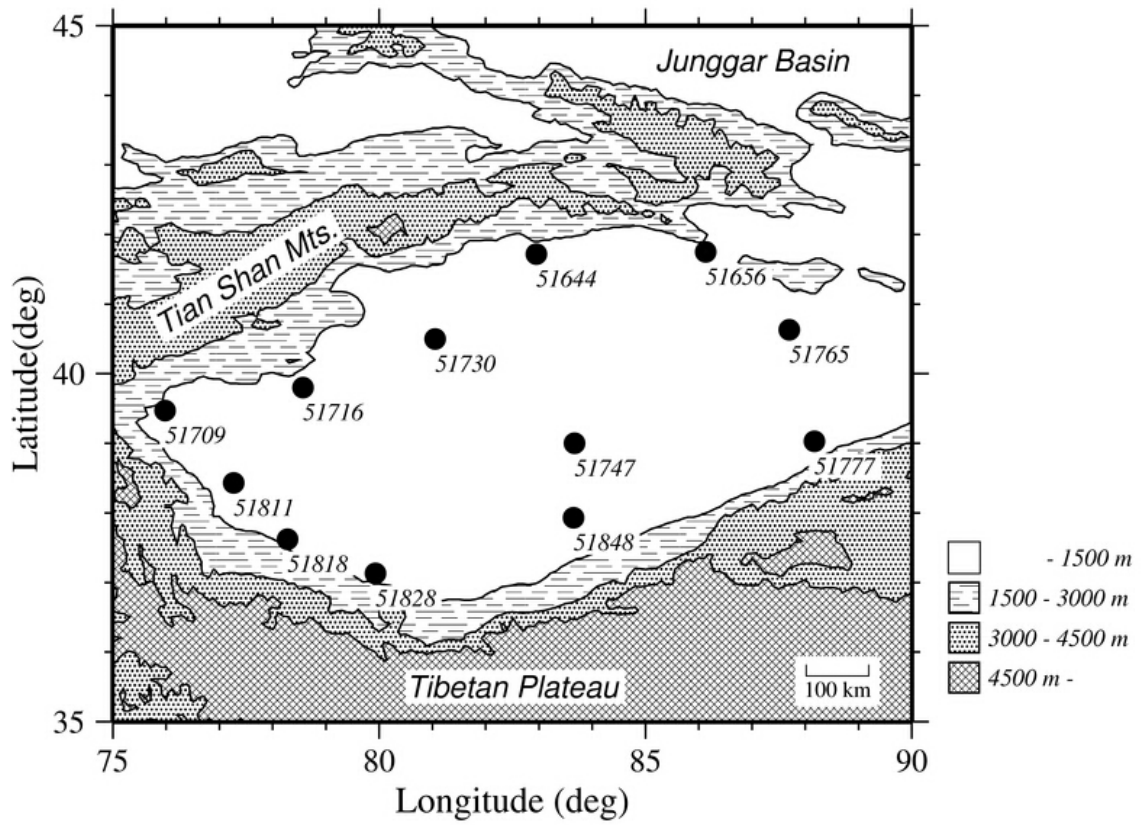
Fig. 4.8. Selected stations and topography around the Taklimakan Desert.
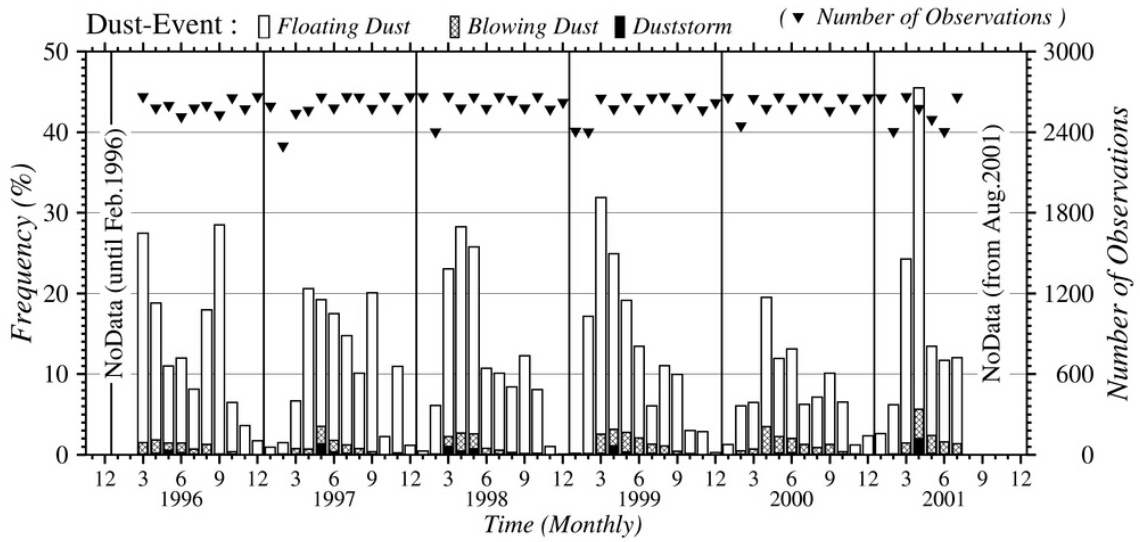
Fig. 4.9. Monthly time sequence of dust event frequency in the Taklimakan Desert from March 1996 to July 2001. The total number of observations for each month (▼) is shown by the right-side vertical axis.
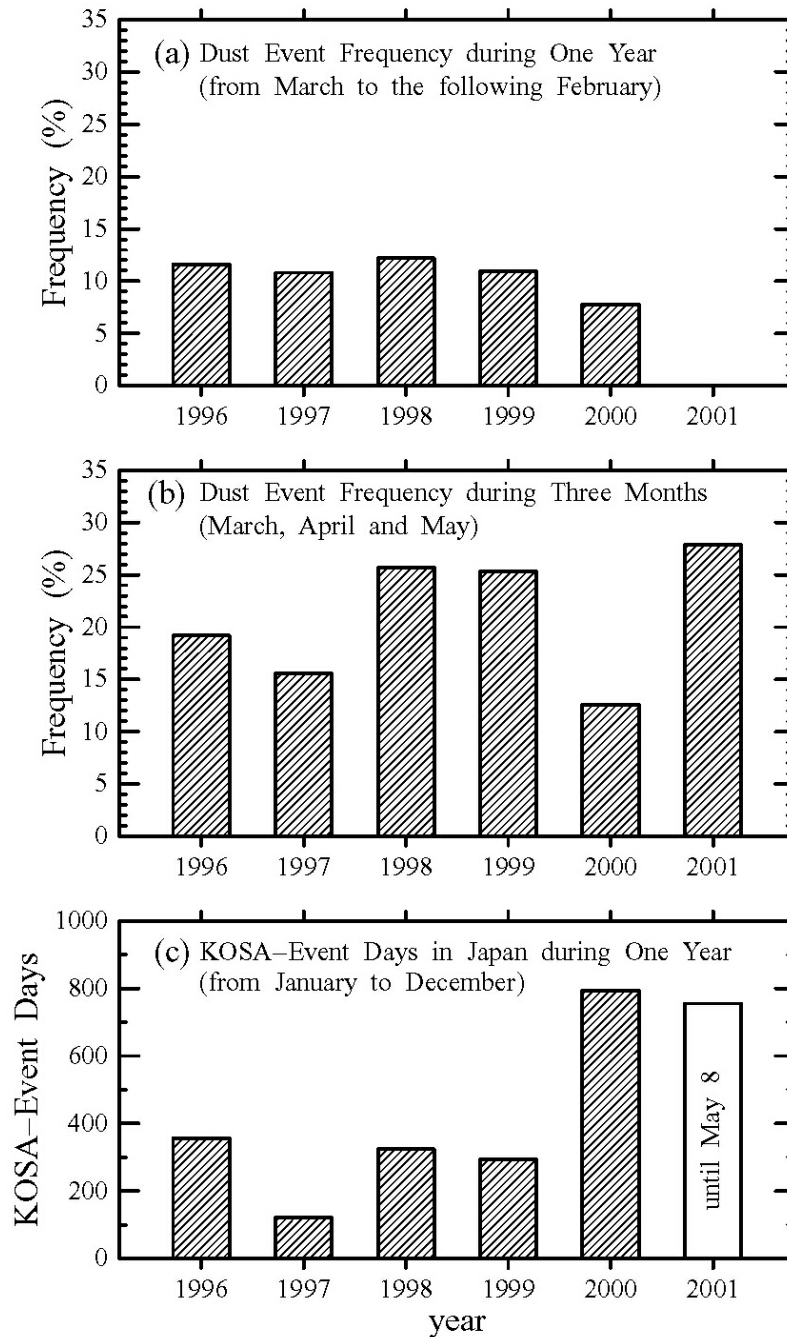
Fig. 4.10. (a) Annual change of dust event frequency during twelve months from March to the following February in the Taklimakan Desert. (b) Same as (a), but during three months, March, April, and May (MAM). (c) Annual change of KOSA-event days (date from Japan Meteorological Agency). This means the total number of days which floating dust was observed in Japan.
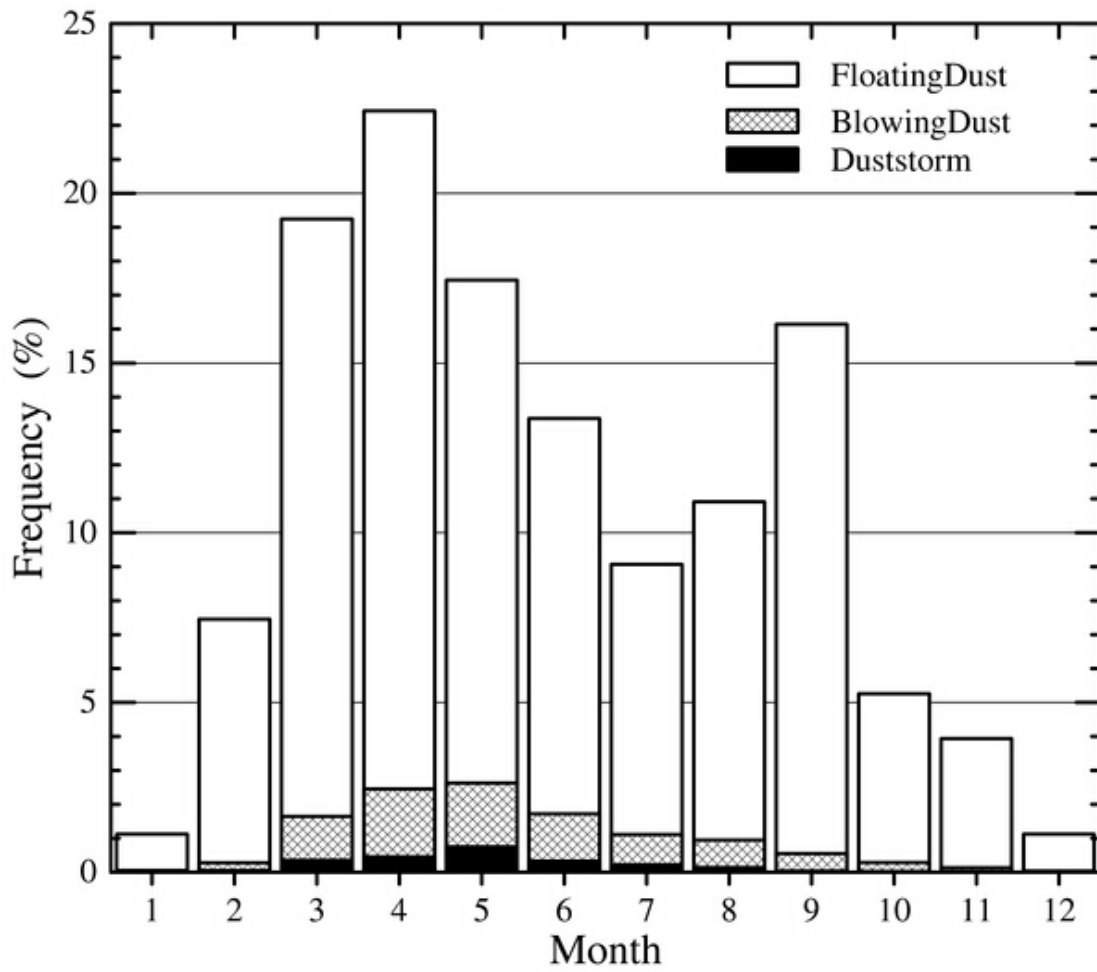
Fig. 4.11. Monthly dust event frequency in the whole Taklimakan Desert region during the five years from March 1996 to February 2001.

Fig. 4.12. Spatial distribution of dust event frequency during five years (central part of the figure). Monthly dust event frequency at each station (surrounding bar charts).

Fig. 4.13. Same as Fig. 4.12, but for the dust outbreak.

around the Gobi Desert
(Region I)

the Taklimakan Desert
(Region II)
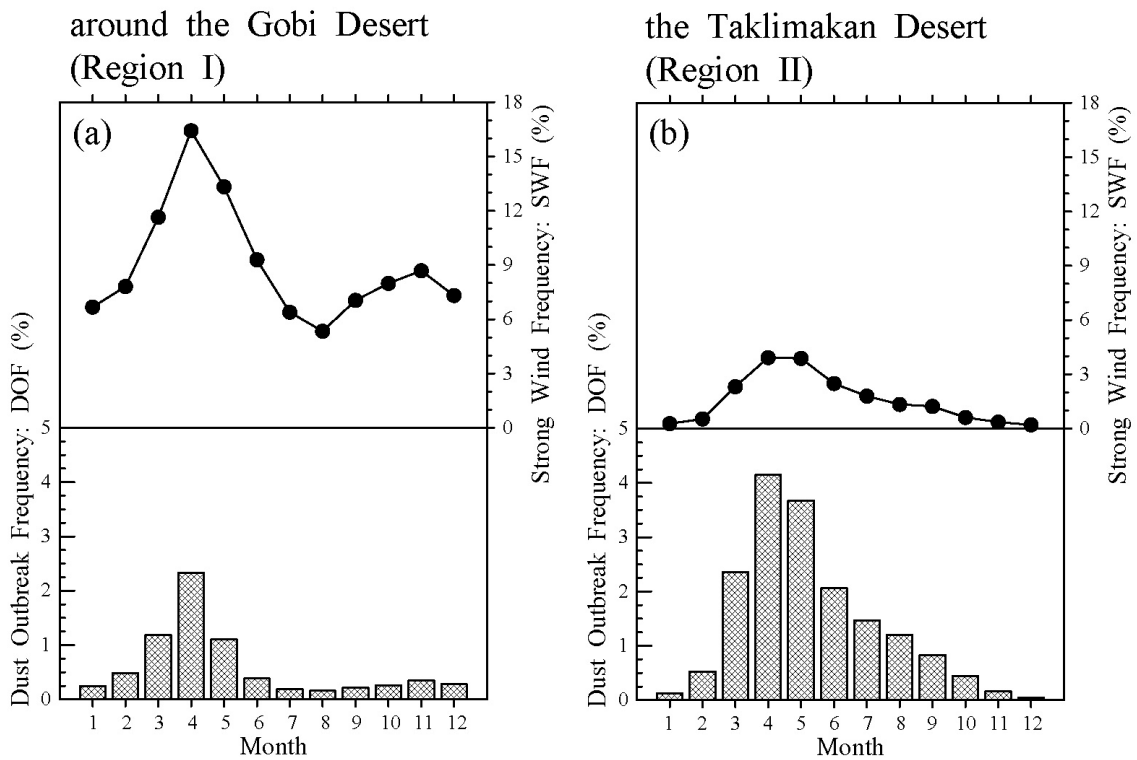
Fig. 4.14. Seasonal variations of dust outbreak frequency and strong wind frequency for the region around the Gobi Desert (a) and for the region in the Taklimakan Desert (b). Dust outbreak frequency and strong wind frequency are indicated by bar chart (left axis) and by line graph (right axis), respectively.
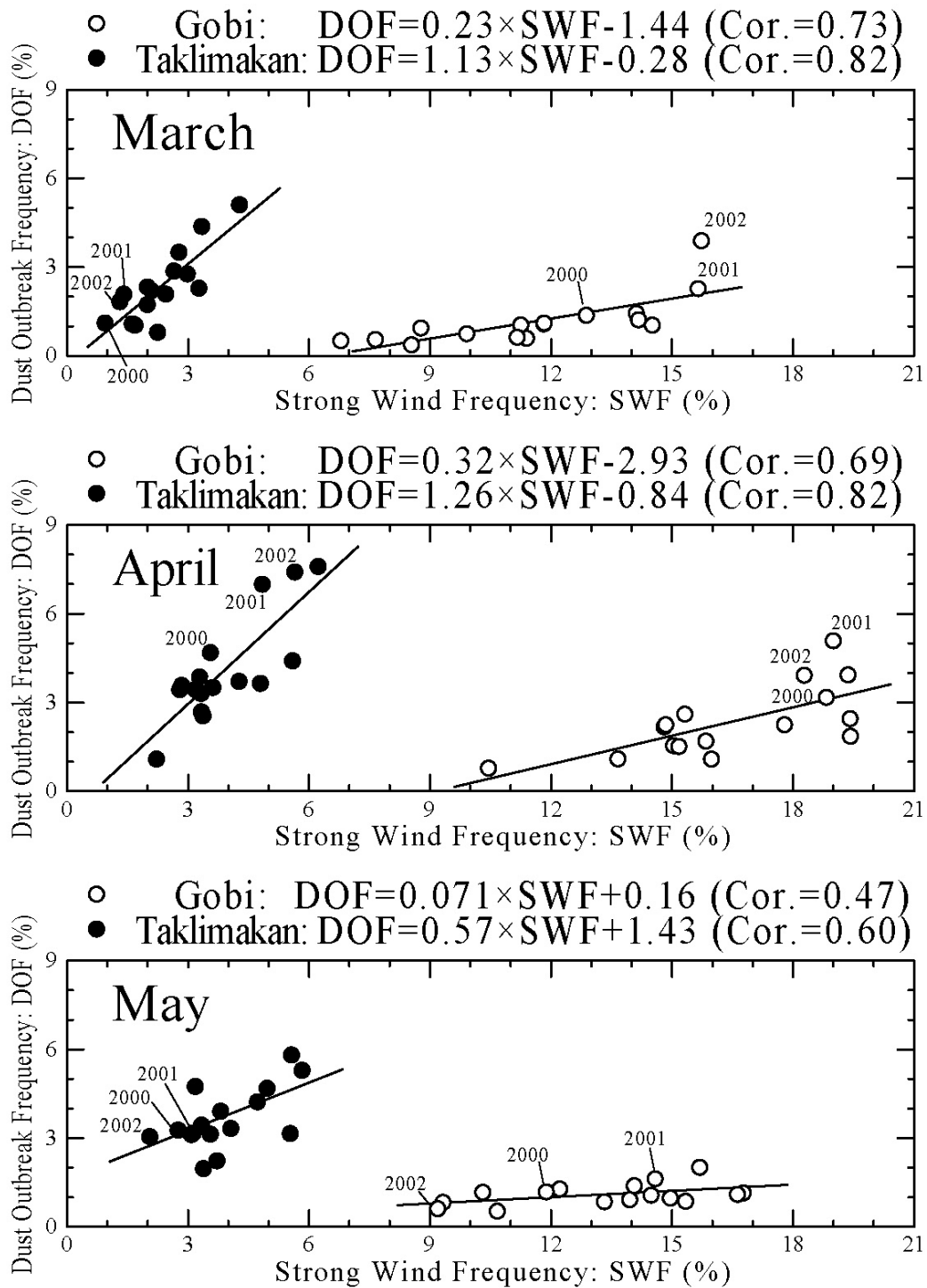
Fig. 4.15. Relations between strong wind frequency and dust outbreak frequency in March (upper panel), April (middle panel) and May (lower panel) of each year from 1988 to 2003. White and black circles indicate results for the regions around the Gobi Desert and in the Taklimakan Desert, respectively.
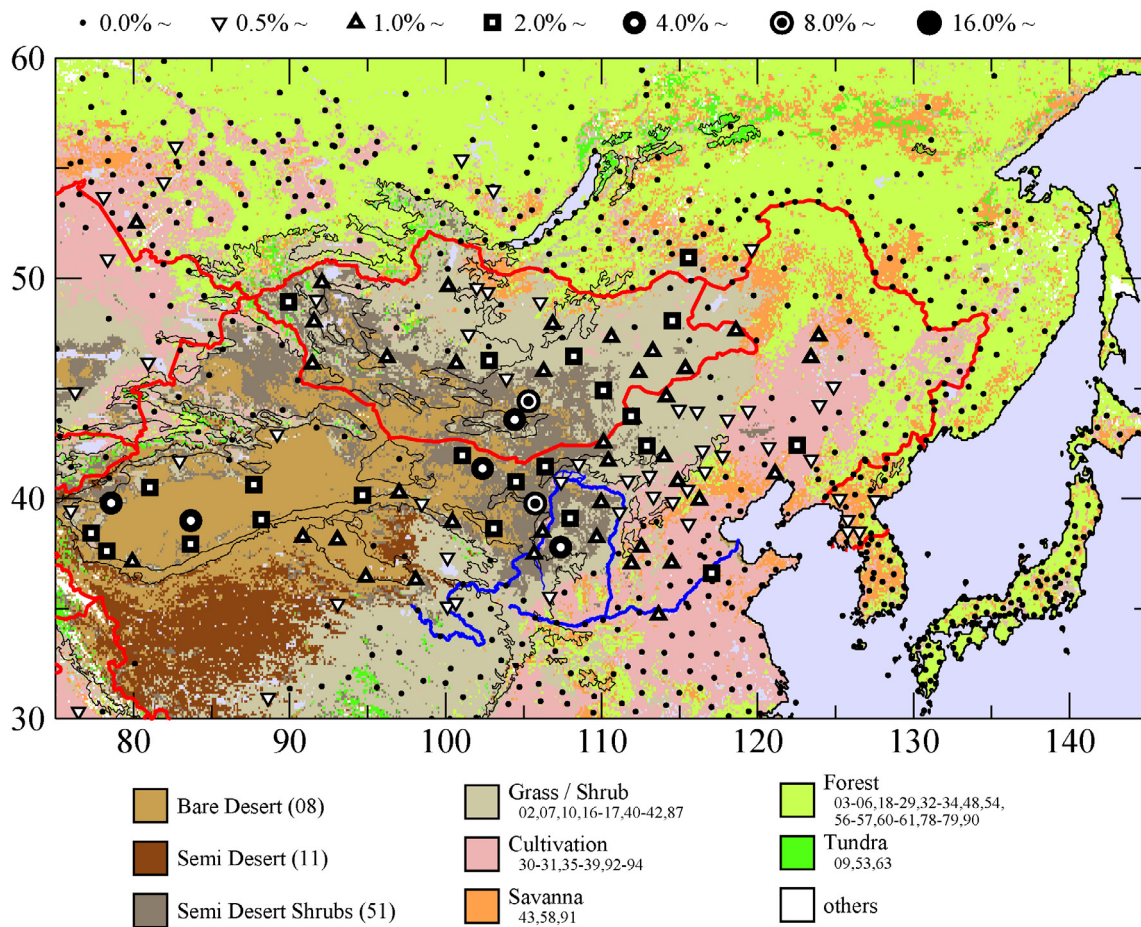
Fig. 4.16. Spatial distribution of dust outbreak frequency for March, April and May from 1988 to 2003.

Chapter 5

Threshold Wind Velocity of Aeolian Dust Outbreak

An aeolian dust outbreak occurs when a wind velocity exceeds a threshold, while the threshold wind velocity of aeolian dust outbreak has various values according to land surface conditions. Although threshold velocities have been measured in wind tunnel experiments and field experiments [*Bagnold*, 1941; *Gillette et al.*, 1980, 1982; *Shao and Raupach*, 1992; *Shao*, 2000; *Mikami et al.*, 2002], they are conducted in idealized conditions and the number of sites is limited. In numerical models, estimated threshold velocities are given with differing land surface conditions. However, it is not clear whether they are correctly estimated or not. This chapter presents maps of threshold velocity, which are obtained through a statistical analysis at each WMO synoptic observatory in the dust season (i.e., March, April and May) from 1988 to 2003. Regional variations in the threshold velocity are discussed and compared against land cover types.

5.1 Introduction

The aeolian dust outbreak occurs through two microphysical processes. In the first process, airflow mobilizes sand-sized particles in the direction of the prevailing wind and these particles begin to bounce when a wind velocity exceeds the threshold for each particle. This process is called as "*saltation*". The saltation threshold wind velocity depends on the soil particle size (Fig. 5.1). The optimal diameter of particles for

saltation is around 75 μm and these soil particles are categorized as "*sand*" (section 1.1). Sand-sized particles are too large to remain in suspension owing to their fall velocities. It is difficult for airflow to directly mobilize fine soil particles, which can be suspended for a long period, because their saltation threshold velocity is large as shown in Fig. 5.1. In the second process, bouncing sand-sized particles eject fine particles (i.e., dust particles) and this phenomenon is known as "*saltation bombardment*". Ejected dust particles are entrained into the atmosphere by turbulence.

Global and regional dust cycles, which are composed of three phases such as the outbreak, the transport and the deposition (section 1.1), have been simulated in many model studies. As far as the processes of aeolian dust outbreak are concerned, these models are divided into at least two distinct classes, simpler and more complex models. Complex models [e.g., *Marticorena and Bergametti*, 1995; *Shao et al.*, 1996; *Shao*, 2001] compute the horizontal flux for each particle size in proportion to the third power of the wind friction velocity. The vertical dust flux is obtained from the result of these horizontal fluxes. In these models, soil particle size distribution largely affects the vertical dust flux. In the study of *Marticorena and Bergametti* [1995], for example, the ratio of vertical to horizontal flux exponentially decreases with the decrease of the clay (< 4 μm) content when the percentage of clay (i.e., fine particles) is less than 20 %. On the contrary, when sand-sized particles (i.e., coarse particles) are scarce, although the land surface is rich in fine particles, little saltation flux causes little vertical dust flux. In simple models [e.g., *Tegen and Fung*, 1994; *Takemura et al.*, 2000; *Uno et al.*, 2001; *Ginoux et al.*, 2001; *Liu and Westphal*, 2001], the vertical dust flux is assumed to be proportional to the horizontal saltation flux. Furthermore, if the assumption of neutral atmospheric condition and the value of roughness length are given, the vertical dust flux is in proportion to the third power of the wind velocity when the wind velocity exceeds the threshold:

$$F = C \left(1 - u_t / u\right) u^3 \qquad\qquad (5.1)$$

where F is the vertical dust flux (kg m^{-2} s^{-1}), u is the wind velocity at a 10 m height (m

s^{-1}), u$_t$ is the threshold wind velocity of dust outbreak (m s^{-1}), and C is the coefficient (kg s^2 m^{-5}). If the wind velocity (u) is smaller than the threshold velocity (u$_t$), zero dust flux is given. In many models, the threshold velocity is set to be a constant, 6.5 m/sec, referring to *Kalma et al.* [1988] and the coefficient (C) depends on land surface conditions (e.g., soil particle size distribution, soil moisture, roughness length, vegetation activity, land cover type). On the other hand, according to the wind tunnel experiments and the field experiments, the threshold velocity depends on the land surface conditions [*Gillette*, 1978; *Shao*, 2000; *Mikami et al.*, 2002]. Referring to the equation (9.9) in *Shao* [2000][¶], the threshold wind velocity of dust outbreak (u$_t$) is indicated as,

$$u_t \doteqdot u_{td}\, f_\lambda(\lambda)\, f_\omega(\theta)\, f_{sc}(sc)\, f_{cr}(cr)\, \cdots \qquad (5.2)$$

where u$_{td}$ is the threshold wind velocity calculated from soil particle size distribution in the idealized situation when soil is dry, bare and free of crust and salt. In this equation, $f_\lambda(\lambda)$, $f_\omega(\theta)$, $f_{sc}(sc)$ and $f_{cr}(cr)$ are the correction functions for surface roughness elements (e.g., vegetation, pebbles), soil moisture, salt concentration and surface crust, respectively. All these multiplication functions are larger than 1.0.

5.2 Data and Method

5.2.1 Data

This chapter uses present weathers and wind velocities in SYNOP reports in the analysis region (30°N – 60°N, 75°E – 145°E) in the dust season (i.e., March, April and May) during the period from 1988 to 2003. An aeolian dust outbreak is defined as ww=07, 08, 09, 30, ⋯, 35, or 98. Land cover type data is used in the discussion of regional variations in the threshold wind velocity of aeolian dust outbreak. Details of

---

[¶] *Shao* [2000] discusses the threshold of saltation with the friction velocity (u$_*$=(τ / ρ)$^{0.5}$), which reflects the shear stress (τ) on a soil surface. This means that the threshold of saltation depends on not only land surface conditions but also the atmospheric stability. On the other hand, this study assumes that the threshold of saltation largely depends on land surface conditions in comparison with atmospheric condition.

these data are indicated in Chapter 2.

5.2.2 Regions

Regional variations in the threshold velocity are discussed in this chapter and they are compared against land cover types. For this purpose, WMO synoptic observatories are grouped into eight regions as shown in Fig. 5.2 by reference to land cover types around each observatory. These regions are *"Northern Mongolia"*, *"Inner Mongolia"*, *"Gobi Desert"*, *"Northeastern China"*, *"North China Plain"*, *"Loess Plateau"*, *"Hexi Corridor"*, and *"Taklimakan Desert"*. The major land cover types in each region are shown in Table 5.1. Several observatories are identified by different regional names instead of the usual names, because they are mainly grouped by land cover type. If an observatory is a non-dust-source (section 3.2) and/or less than 30 of dust outbreaks have been observed at an observatory for the analysis period, these observatories are not discussed in this chapter and they are indicated by symbols of dot and white star in Fig. 5.2.

5.2.3 Frequency distribution of wind velocity

A bar chart in the left panel of Fig. 5.3 is an example of frequency distribution of wind velocities at a WMO synoptic observatory (WMO No. 53231, 41.45°N, 106.38°E) located in the south of the Gobi Desert. Hatched and white bars indicate frequency distributions of wind velocities when dust outbreaks occurred and did not occur, respectively. A bar chart in the right panel is a vertical expansion of the left one. Each dot with error bar is a dust outbreak frequency at each wind velocity (right axis).

When the threshold wind velocity is assumed as a constant, 6.5 m/sec, frequency distributions of wind velocities and dust outbreak frequencies are shown as Fig. 5.4. When wind velocities are smaller than 6.5 m/sec, no dust outbreak occurs. Therefore, hatched bars cannot be found when the wind velocity is smaller than 6.5 m/sec. White bars similarly cannot be found when the wind velocity is larger than 6.5 m/sec. A dust outbreak frequency at each wind velocity jumps from 0 % to 100 % when the wind

velocity is 6.5 m/sec. In the real data (Fig. 5.3), however, there are many cases that a dust outbreak does not occur when a wind velocity exceeds 6.5 m/sec. The dust outbreak frequency gradually increases with an increase of wind velocity. The discrepancy between Fig. 5.3 and Fig. 5.4 means that the threshold wind velocity has various values in the real data. For example, many cases without dust outbreaks (i.e., a white bar) are found when a wind velocity is 12 m/sec in Fig. 5.3. This result means that there are many threshold velocities exceeding 12 m/sec.

Figure 5.5 shows frequency distributions of wind velocities and a dust outbreak frequency for each wind velocity at a WMO synoptic observatory (WMO No. 51818, 37.62°N, 78.28°E) located in the west of the Taklimakan Desert. The dust outbreak frequency gradually increases in the former case (Fig. 5.3) in comparison with this case (Fig. 5.5). This result indicates that the threshold velocity exhibits more various values at a WMO synoptic observatory (53231) than that at an observatory (51818). The variation of land surface conditions at these sites should affect these variations of threshold velocity.

5.2.4 Definitions of threshold wind velocity of dust outbreak

Two kinds of threshold velocity are defined here. They are the wind velocities when their dust outbreak frequencies are 5 % ($u_{t5\%}$) and 50 % ($u_{t50\%}$) at a given observatory, respectively. The former ($u_{t5\%}$) and the latter ($u_{t50\%}$) correspond to 5 percentile and 50 percentile (i.e., the median) of threshold velocities at this observatory for the analysis period. The 5 percentile of threshold velocities ($u_{t5\%}$) is the nearly minimum threshold velocity and this should be obtained when the land surface is in nearly the most favorable condition for dust outbreak at this observatory. Hereafter, this threshold velocity is called as the "*minimum threshold velocity*". The 50 percentile of threshold velocities ($u_{t50\%}$) should be obtained when the land surface is in a usual condition at this observatory. Hereafter, this threshold velocity is called as the "*practical threshold velocity*". Referring to the equation (5.2), these threshold velocities are expressed as,

$$u_{t5\%} \fallingdotseq u_{td} \min\{f_\lambda(\lambda) \, f_\omega(\theta) \, f_{sc}(sc) \, f_{cr}(cr) \, \cdots\} \qquad (5.3)$$

$$u_{t50\%} \fallingdotseq u_{td} \operatorname{med}\{f_\lambda(\lambda) \, f_\omega(\theta) \, f_{sc}(sc) \, f_{cr}(cr) \, \cdots\} \tag{5.4}$$

where u_{td} is the threshold wind velocity obtained from soil particle size distribution in the idealized situation. The "min" and "med" indicate the minimum and the median of the product of correction functions for several land surface elements between curly brackets. The difference between minimum and practical threshold velocities ($\Delta u_t = u_{t50\%} - u_{t5\%}$) indicates the variation of threshold velocities and this can be an index of the variation of land surface conditions.

The minimum and the practical threshold velocities are computed for each WMO synoptic observatory according to the following rules:

(i)   Observatories must be potential dust sources, which are defined in section 3.2. Furthermore, thirty or more dust outbreaks must be observed at such observatories during the analysis period (section 5.2.1). In other words, the minimum and practical threshold velocities are not computed at observatories, which are not potential dust sources or at which dust outbreaks have occurred less than 30 times during the analysis period.

(ii)   A dust outbreak frequency is computed for each wind velocity if such a wind velocity is counted six times or more during the analysis period. Even if this wind velocity is counted five times or less, this dust outbreak frequency is exceptionally assumed to be valid when dust outbreaks is counted three times or more at this wind velocity.

(iii)   The minimum and the practical threshold velocities (i.e., $u_{t5\%}$ and $u_{t50\%}$) are defined as the wind velocities when the dust outbreak frequencies are 5 % and 50 %, respectively. They are obtained by linear interpolation. As shown in Fig. 5.6, if there are two or more wind velocities when the dust outbreak frequency is 50 %, the minimum of these velocities is regarded as the practical threshold velocity ($u_{t50\%}$). Similarly, if there are two or more wind velocities when the dust outbreak frequency is 5 %, the minimum is regarded as the minimum threshold velocity ($u_{t5\%}$).

(iv)   When every dust outbreak frequency is less than 5 % and/or less than 50 % at an

observatory, the minimum and/or the practical threshold velocities ($u_{t5\%}$ and/or $u_{t50\%}$) and their difference (Δu_t) are not given. Figure 5.7 is an example of an observatory (WMO No. 54157, 43.18°N, 124.33°E) where the minimum threshold velocity ($u_{t5\%}$) is given but the practical threshold velocity ($u_{t50\%}$) is not given.

5.3 Results

5.3.1 Map of minimum threshold velocity ($u_{t5\%}$)

Figure 5.8 is the map of minimum threshold velocity ($u_{t5\%}$). Minimum threshold velocities are indicated at potential dust sources (section 3.2) in this map, while symbols of dot and white star indicate observatories, which are non-dust-sources (section 3.2) and at which dust outbreaks have occurred less than 30 times during the analysis period. White circles indicate observatories where the minimum threshold velocity cannot be obtained because the dust outbreak frequency is less than 5 % at every wind velocity.

The minimum threshold velocities exceed 9 m/sec at most observatories in Northern Mongolia (Grass/Shrub) and Inner Mongolia (Grass/Shrub). Thresholds are less than 8 m/sec at many observatories in the Gobi Desert (Semi Desert Shrubs), while they exceed 9 m/sec near the Grass/Shrub region. Thresholds are about 6 – 9 m/s in Northeastern China (Cultivation). Thresholds are about 4 – 7 m/sec in the North China Plain (Cultivation), the Loess Plateau (Grass/Shrub and Bare Desert Shrubs) and the Hexi Corridor (Bare Desert Shrubs and Bare Desert). Thresholds are 3 – 5 m/sec in the Taklimakan Desert (Bare Desert). There is a clear tendency in the Taklimakan Desert that threshold velocities are larger in the east than in the west although the difference of threshold velocities is no more than 1 m/sec.

5.3.2 Map of practical threshold velocity ($u_{t50\%}$)

Figure 5.9 is the map of threshold wind velocity ($u_{t50\%}$). Symbols of dot and white

star are the same as Fig. 5.8. White circles indicate observatories where the practical threshold velocity cannot be obtained because the dust outbreak frequency is less than 50 % at every wind velocity.

The practical threshold velocities exceed 15 m/sec at many observatories in Northern Mongolia (Grass/Shrub). Thresholds are larger than 11 m/sec in the Gobi Desert (Semi Desert Shrubs), Inner Mongolia (Grass/Shrub) and Northeastern China (Cultivation). Thresholds are larger than 9 m/sec at most observatories in the North China Plain (Cultivation), the Loess Plateau (Grass/Shrub and Semi Desert Shrubs) and the Hexi Corridor (Semi Desert Shrubs and Bare Desert) although they are less than 7 m/sec at some observatories. Thresholds are $6 - 9$ m/sec and $4 - 7$ m/sec in the east and in the west of the Taklimakan Desert, respectively. Same as the minimum threshold velocity (Fig. 5.8), a tendency can be found in Fig. 5.9 that thresholds are larger in the east than in the west.

5.3.3 Map of difference between minimum and practical threshold velocities

Figure 5.10 is the map of difference between the minimum and the practical threshold velocities (i.e., $\Delta u_t = u_{t50\%} - u_{t5\%}$). Symbols of dot, white star and white circle are the same as Fig. 5.9.

Differences of threshold velocity (Δu_t) exceed 6 m/sec at many observatories in Northern Mongolia (Grass/Shrub) and the Gobi Desert in Mongolia (Semi Desert Shrubs). On the other hand, Differences of threshold velocity are 1 m/sec in the west of the Taklimakan Desert. In other regions, they are about $2 - 5$ m/sec.

5.4 Discussion

The regional variation of the minimum threshold velocity ($u_{t5\%}$) roughly corresponds to that of the practical threshold velocity ($u_{t50\%}$). In other words, the minimum threshold velocity is large (small) where the practical threshold velocity is large (small) in most regions. Figure 5.11 is an illustration that shows the distribution of the threshold wind

velocity of aeolian dust outbreak. This illustration is drawn by reference to results in sections 5.3.1 and 5.3.2 (i.e., Figs. 5.8 and 5.9). In the region surrounded by thick orange lines, the minimum threshold velocity is larger than 9 m/sec. The practical threshold velocity is larger than 15 m/sec at many observatories in this region and most of these observatories are located in the Grass/Shrub region. In the region surrounded by thick blue lines, the practical threshold velocity ($u_{t50\%}$) is larger than 9 m/sec. These results indicate that the threshold velocities used in numerical models (i.e., 6.5 m/sec) are much smaller than the real values in these regions. In the Taklimakan Desert region, shown by a green ellipse, the minimum and the practical threshold velocities are smaller than those in the other regions. Both kinds of threshold velocities are smaller in the west than in the east. The minimum threshold velocities are $3 - 4$ m/sec in the west and 5 m/sec in the east. The practical threshold velocities are $4 - 7$ m/sec in the west and $6 - 9$ m/sec in the east. Both kinds of threshold velocities tend to decrease from the northeast (i.e., Mongolia and Inner Mongolia) to the southwest (i.e., the west of the Taklimakan Desert) and the land cover type gradually changes from Grass/Shrub (i.e., Northern Mongolia and Inner Mongolia), Semi Desert Shrubs (i.e., the Gobi Desert) to Bare Desert (i.e., the Taklimakan Desert).

The difference between the minimum and the practical threshold velocities ($\Delta u_t = u_{t50\%} - u_{t5\%}$) indicates the variation of threshold velocities and this can be an index of the variation of land surface conditions. Differences of threshold velocity are large in Mongolia. On the other hand, they are small in the Taklimakan Desert. These results suggest that the land surface conditions are largely variable in Mongolia and almost constant in the Taklimakan Desert.

5.5 Summary

In this chapter, we statistically evaluated the threshold wind velocities of aeolian dust outbreak at each observatory in East Asia and we presented the maps of them. We defined two kinds of threshold velocities. One is the minimum threshold velocity ($u_{t5\%}$), which is the threshold velocity at nearly the most favorable land surface condition for

aeolian dust outbreak. The other is the practical threshold velocity ($u_{t50\%}$), which is the threshold velocity at a usual land surface condition. We discussed the difference between the minimum and the practical threshold velocities ($\Delta u_t = u_{t50\%} - u_{t5\%}$) as well. The difference of the threshold velocity can be an index of the variation of land surface conditions. Results are summarized as follows:

1. Both kinds of threshold velocities (i.e., $u_{t5\%}$ and $u_{t50\%}$) are the largest in Northern Mongolia. On the other hand, they are the smallest in the west of the Taklimakan Desert. There is a tendency that thresholds decrease from the northeast (i.e., Mongolia and Inner Mongolia) to the southwest (i.e., the Taklimakan Desert).

2. From the viewpoint of land cover type, both kinds of threshold velocities are the largest in the Grass/Shrub region (i.e., Northern Mongolia and Inner Mongolia), the next largest in the Semi Desert Shrubs region (i.e., the Gobi Desert) and the smallest in the Bare Desert region (i.e., the Taklimakan Desert).

3. The practical threshold velocities ($u_{t50\%}$) are conspicuously larger than those used in simple dust models, which are 6.5 m/sec, in the regions except for the Taklimakan Desert.

4. Differences between the minimum and the practical threshold velocities (Δu_t) are large in Mongolia and small in the west of the Taklimakan Desert. This result indicates that land surface conditions are largely variable in Mongolia. On the other hand, land surface conditions are almost constant in the west of the Taklimakan Desert.

Region	Major Land Cover Types
Northern Mongolia	Grass/Shrub
Inner Mongolia	Grass/Shrub
Gobi Desert	Semi Desert Shrubs
Northeastern China	Cultivation
North China Plain	Cultivation
Loess Plateau	Grass/Shrub Semi Desert Shrubs
Hexi Corridor	Semi Desert Shrubs Bare Desert
Taklimakan Desert	Bare Desert

Table 5.1. Regions (left column) and their major land cover types (right column).
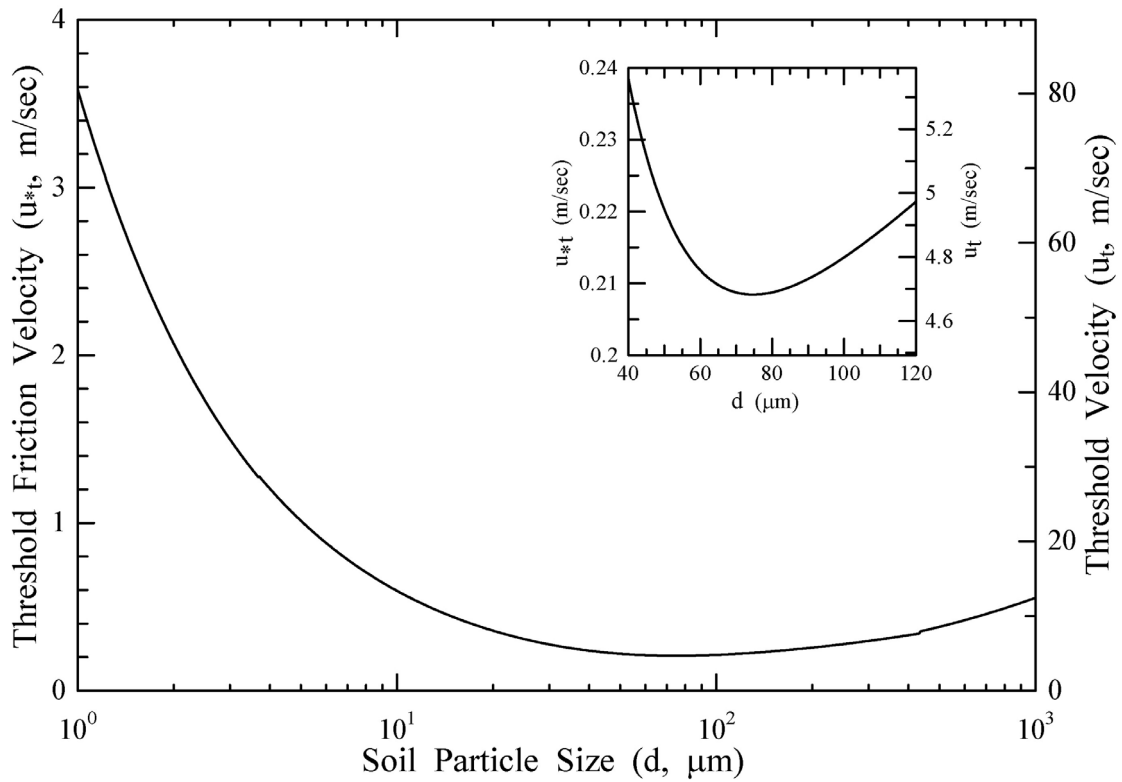
Fig. 5.1. The saltation threshold friction velocity (u_{*t}) as a function of soil particle diameter (d) from *Greeley and Iversen* [1985]. The minimum in the saltation threshold is around 75 μm. The threshold wind velocity (u_t) is shown as well in the right axis. In a neutrally buoyant surface layer the wind velocity varies with height in a logarithmic profile as $u(z) = \{u_* \ln(z/z_0)\}/\kappa$, where u is the wind velocity at the height z, u_* is the friction velocity, z_0 is the roughness length, and κ is the von Karman constant (0.41). Threshold wind velocity (u_t) in the right axis is given through this equation where the reference height (z) and the roughness length (z_0) are set as 10 m and 0.001 m, respectively.
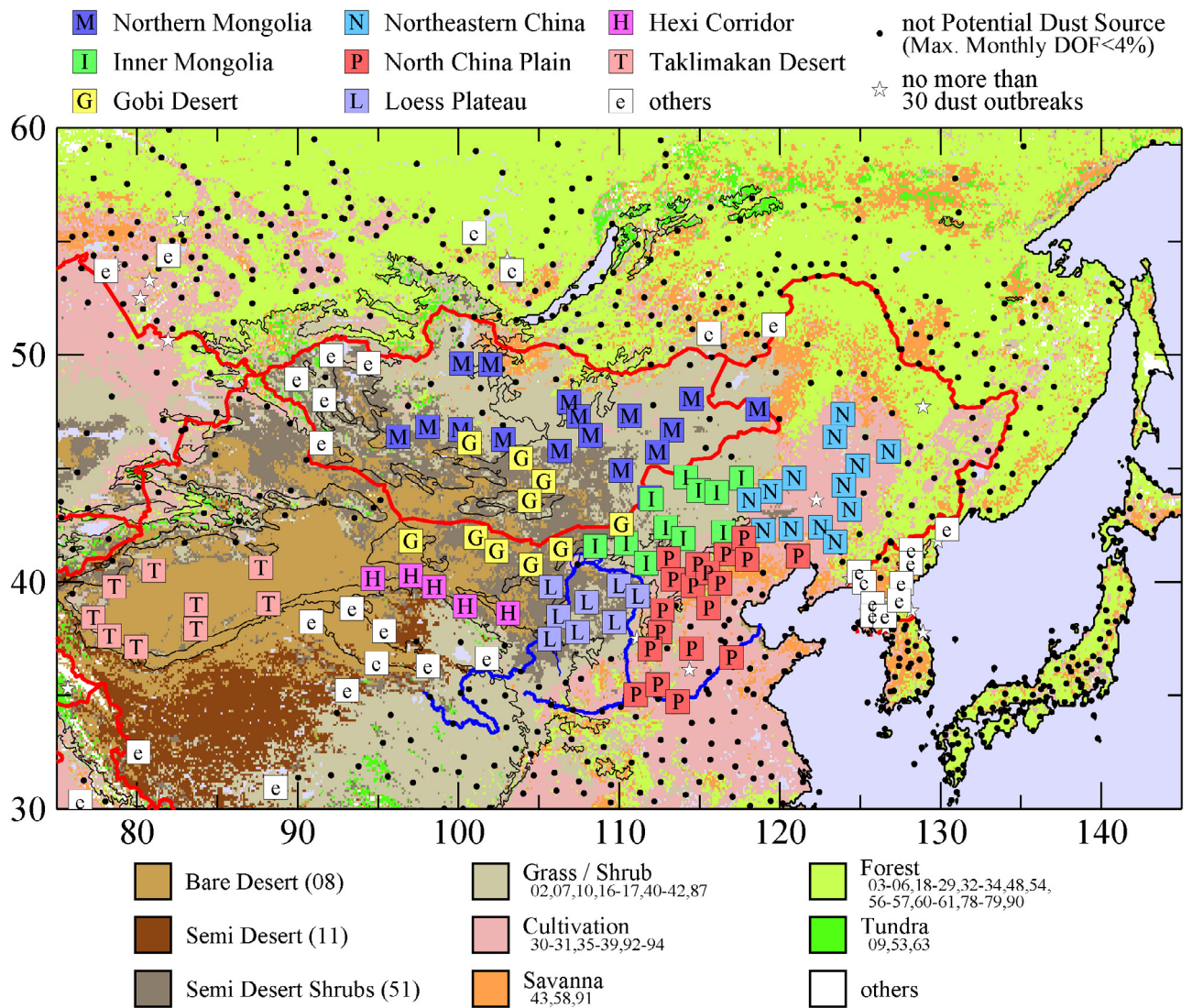
Fig. 5.2. The region name for each WMO synoptic observatory. Observatories plotted by dots are non-dust-sources, which are defined in section 3.2. Symbols of white star indicate observatories where less than 30 of dust outbreaks have occurred for the analysis period, which are March, April and May from 1988 to 2003. Color hatches represent land cover types.

WMO No.: 53231
41.45N, 106.38E

$u_{t50\%}=13.1$ m/s
$u_{t5\%}=9.6$ m/s
$\Delta u_t=3.5$ m/s

□ without Dust Outbreak
▨ with Dust Outbreak
—●— Dust Outbreak Frequency: DOF (%)
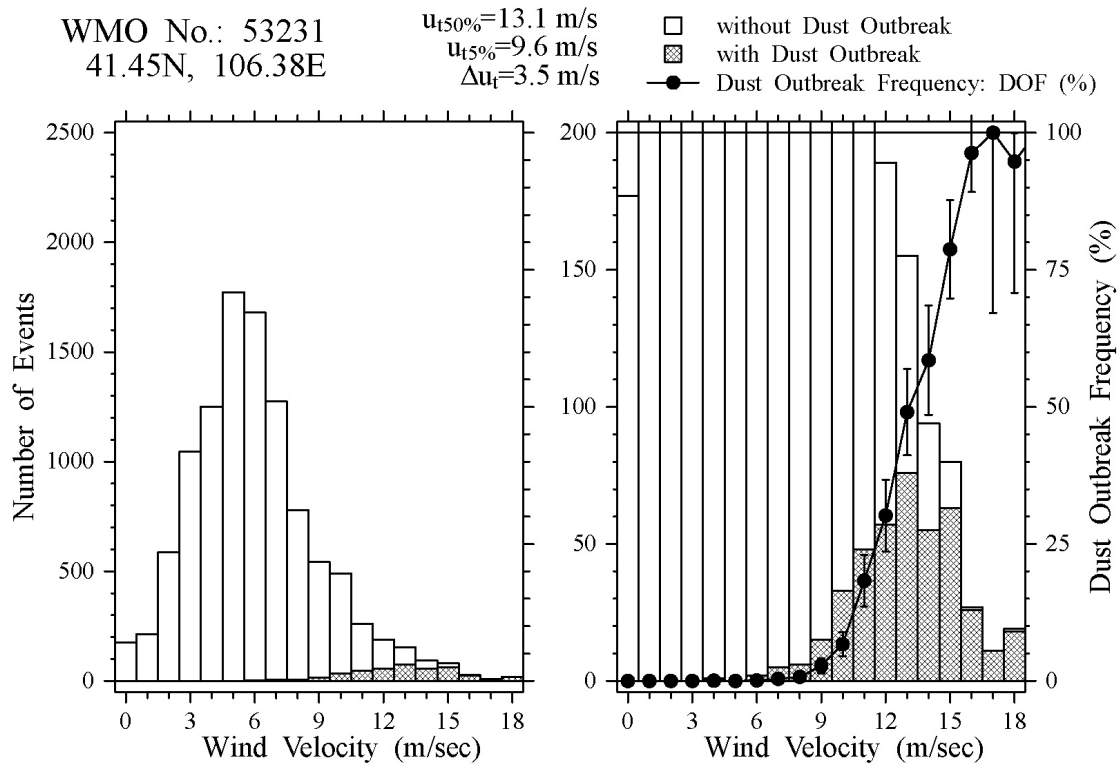
Fig. 5.3. An example of frequency distributions of wind velocity at a WMO synoptic site (53231) located at 41.45°N, 106.38°E. Hatched and white bars indicate frequency distributions of wind velocities when dust outbreaks occurred and did not occur, respectively. The bar chart in the right panel is a vertical expansion of the left panel. Each dot with an error bar shows a dust outbreak frequency at each wind velocity (right axis).

WMO No.: 53231
41.45N, 106.38E

$u_{t50\%}$=6.5 m/s
$u_{t5\%}$=6.5 m/s
Δu_t=0.0 m/s

☐ without Dust Outbreak
▨ with Dust Outbreak
●— Dust Outbreak Frequency: DOF (%)
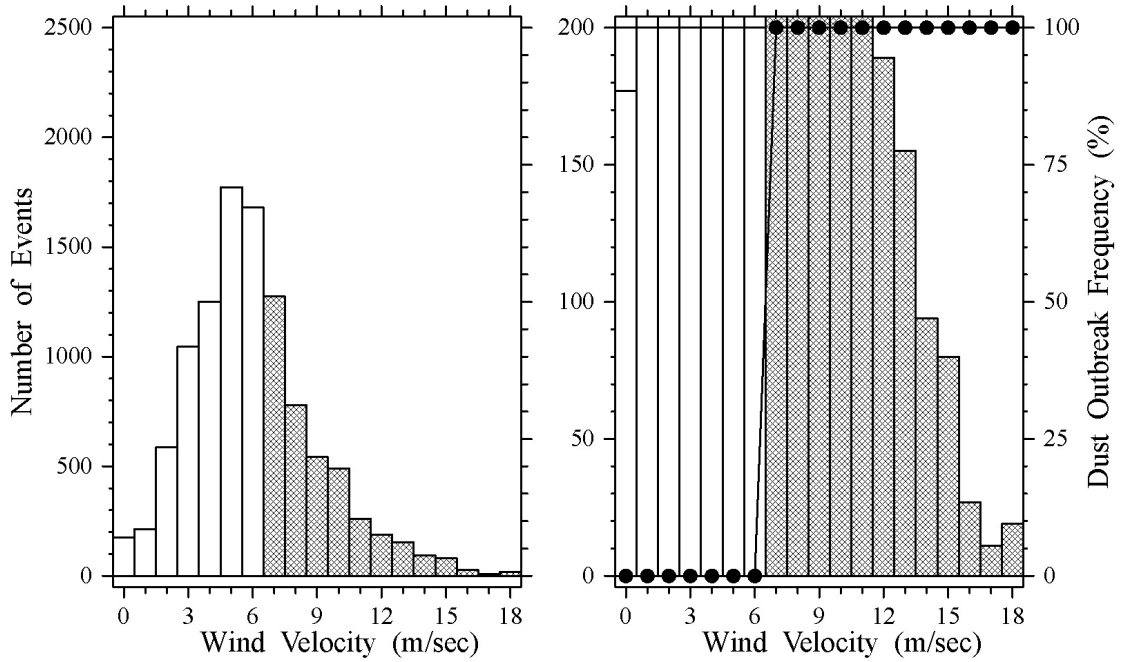
Fig. 5.4. Frequency distributions of wind velocity and dust outbreak frequencies are shown as Fig. 5.3 although the threshold velocity is assumed to be a constant, 6.5 m/sec. Under this assumption, hatched and white bars cannot be found when wind velocities are less than 6.5 m/sec and larger than 6.5 m/sec, respectively. The dust outbreak frequency jumps from 0 % to 100 % when the wind velocity is 6.5 m/sec.
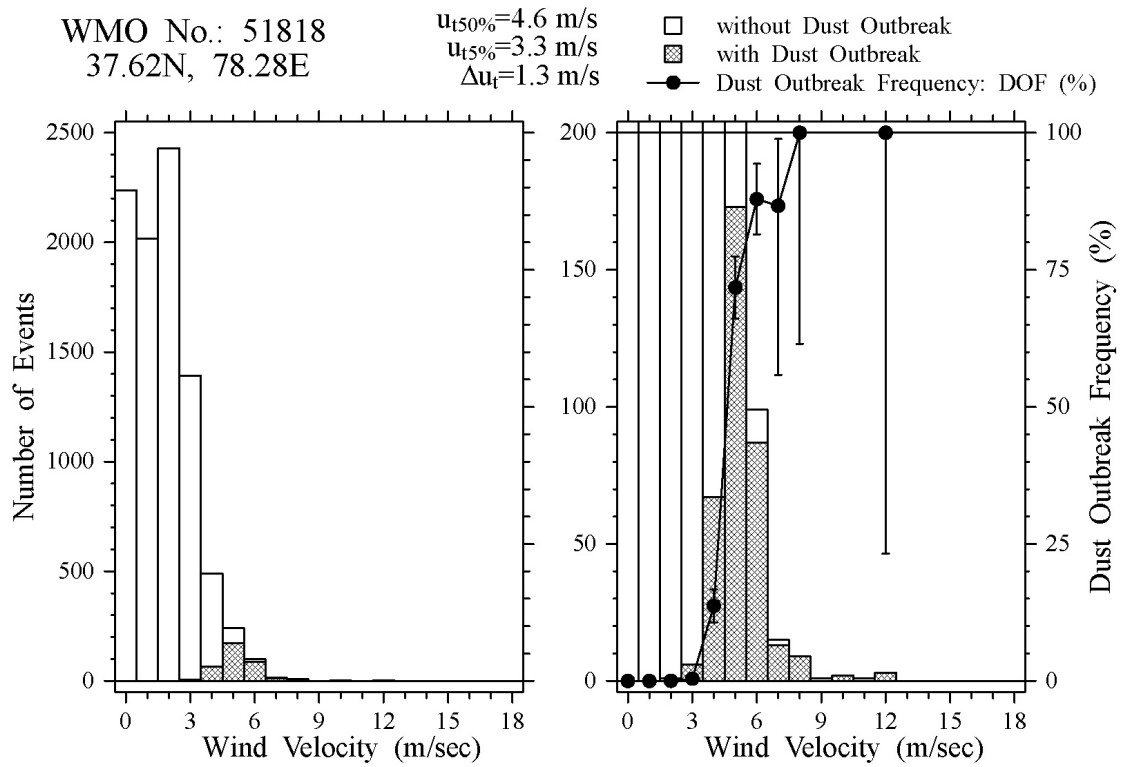
Fig. 5.5. An example of a frequency distribution of wind velocities at a WMO synoptic site (51828) located at 37.62°N, 78.28°E. White and hatched bars and dots with error bar are the same as in Fig. 5.3.

WMO No.: 53083
44.62N, 114.15E

$u_{t50\%}=13.8$ m/s
$u_{t5\%}=11.0$ m/s
$\Delta u_t=2.8$ m/s

□ without Dust Outbreak
▨ with Dust Outbreak
—●— Dust Outbreak Frequency: DOF (%)
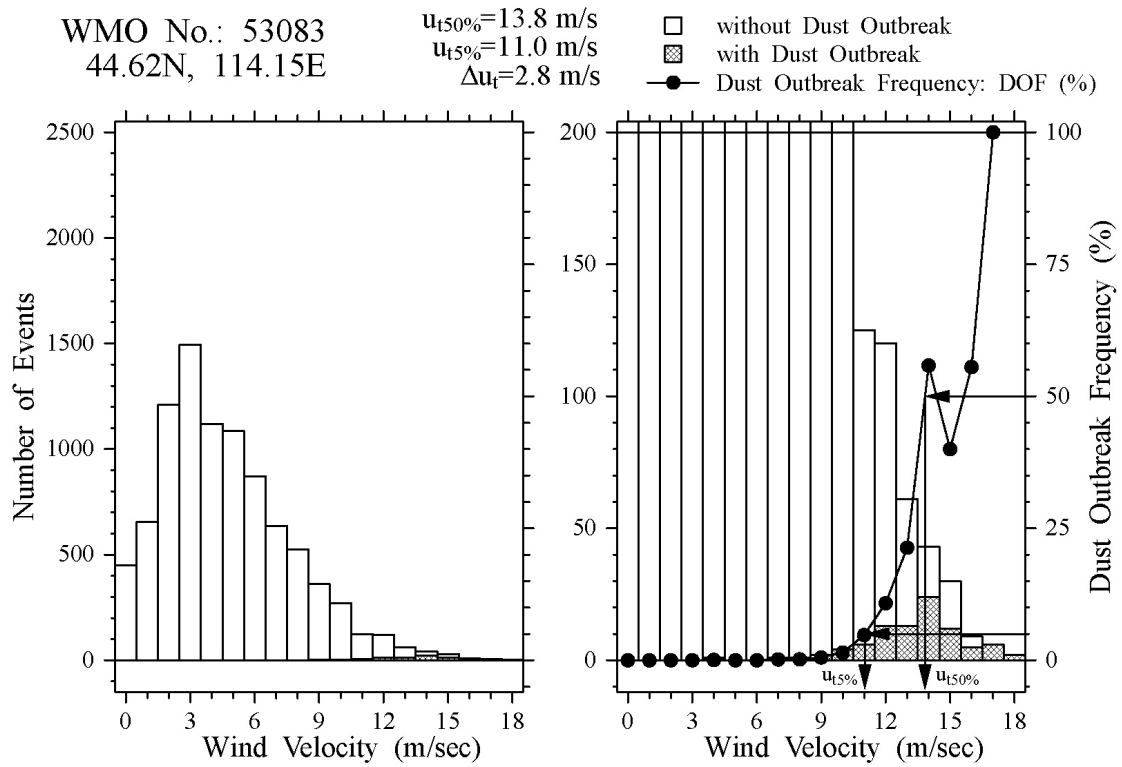
Fig. 5.6. An example of a frequency distribution of wind velocities at a WMO synoptic site (53083) located at 44.62°N, 114.15°E. White and hatched bars and dots with error bar are the same as in Fig. 5.3.
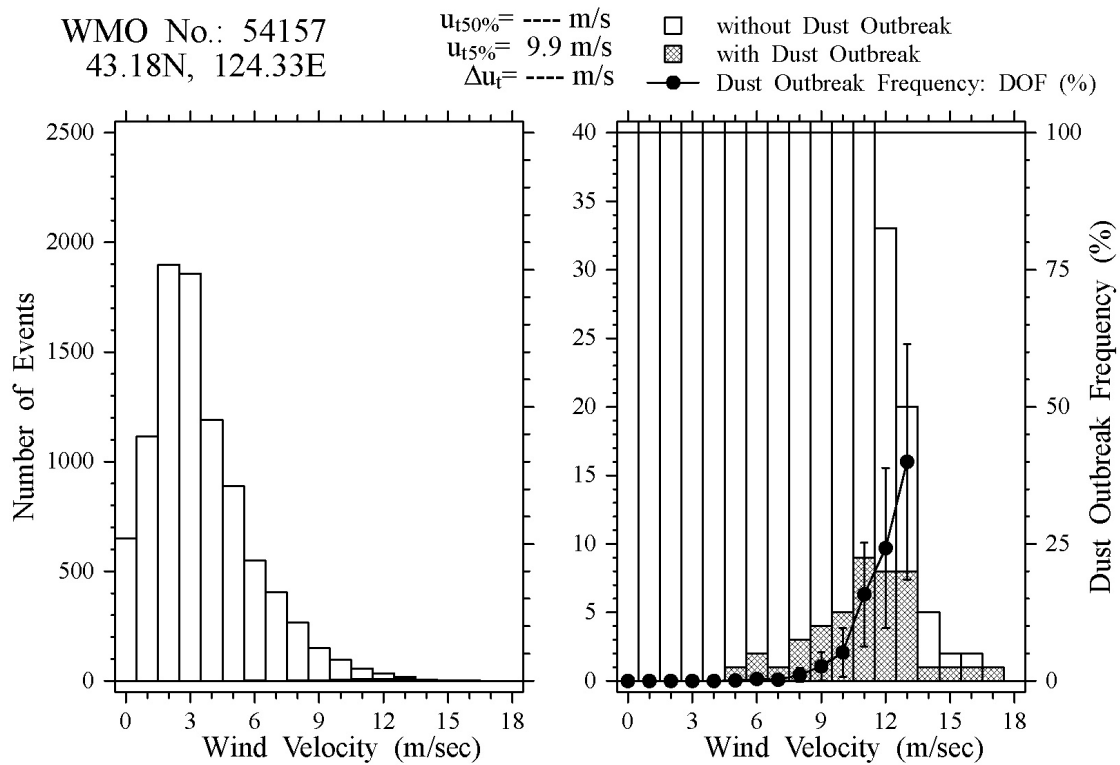
Fig. 5.7. An example of a frequency distribution of wind velocities at a WMO synoptic site (54157) located at 43.18°N, 124.33°E. White and hatched bars and dots with error bar are the same as in Fig. 5.3. The minimum threshold velocity is given (i.e., $u_{t5\%}$=9.9 m/sec) but the practical threshold velocity ($u_{t50\%}$) is not given at this observatory because every dust outbreak frequency is less than 50 %. The difference of threshold velocity ($\Delta u_t = u_{t50\%} - u_{t5\%}$) is not also given.
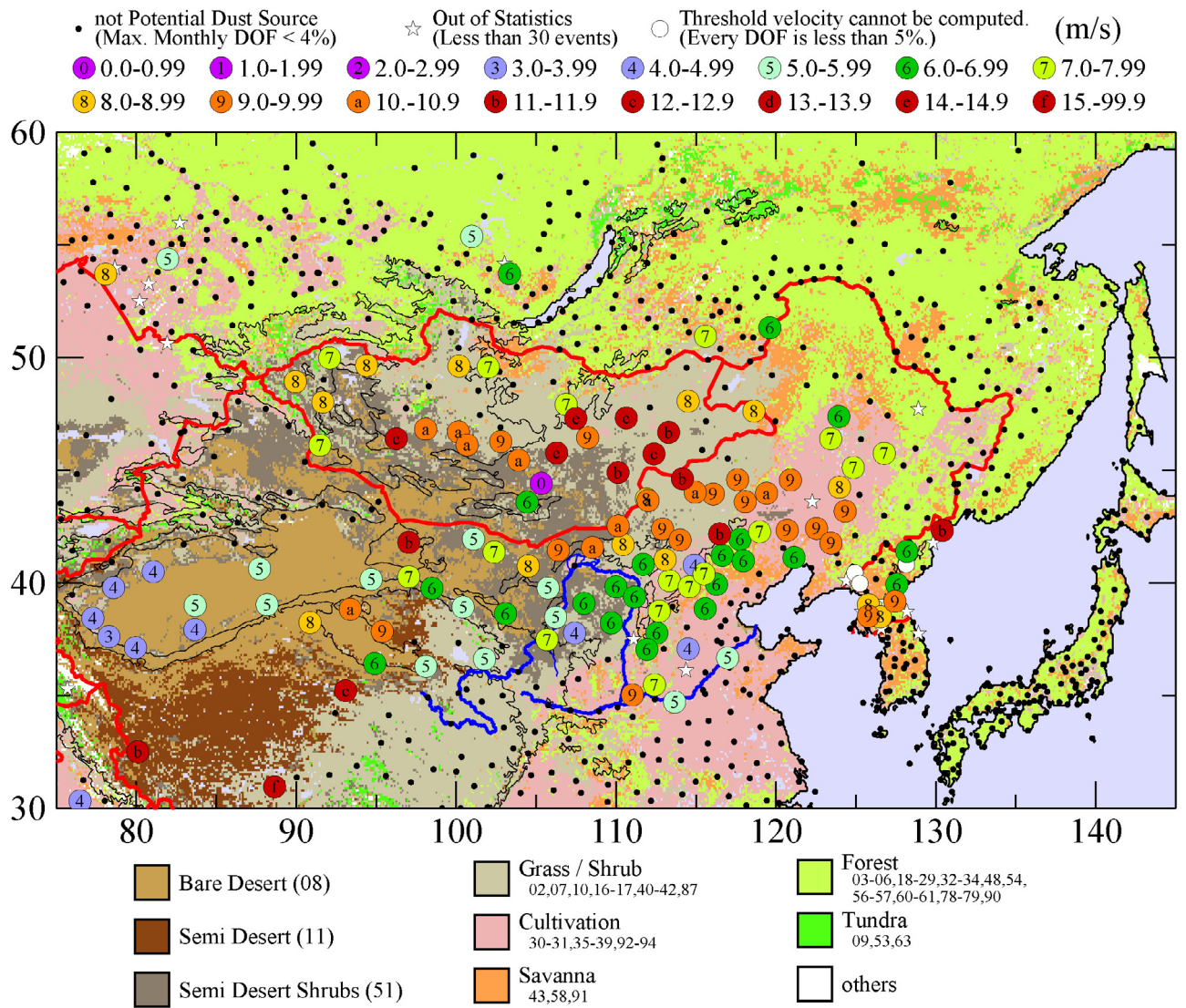
Fig. 5.8. The map of "*minimum threshold velocity*" ($u_{t5\%}$) (see also the definition in section 5.2.4). This threshold is obtained when the land surface is the nearly most favorable condition for dust outbreak. Color hatches represent land cover types.
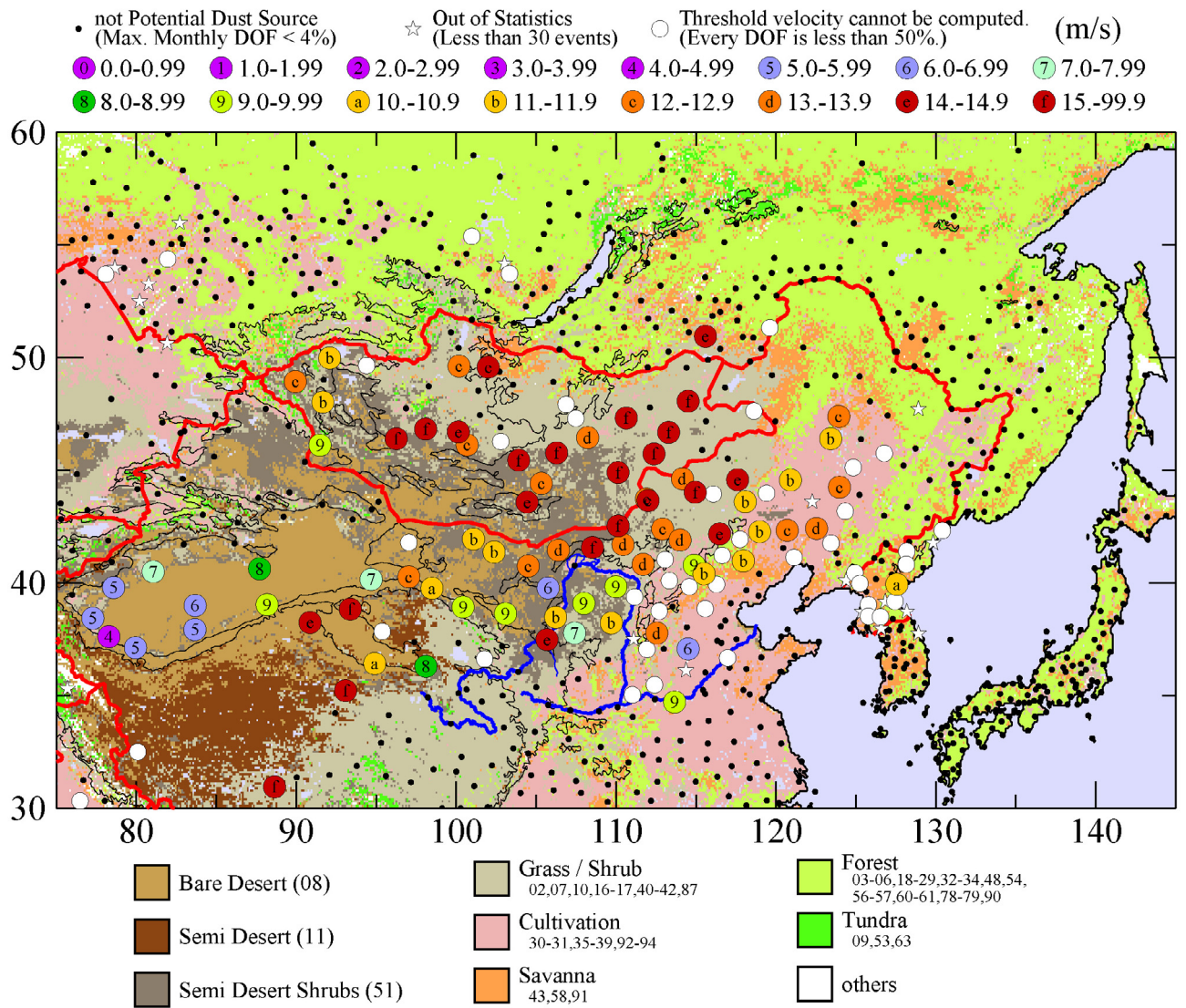
Fig. 5.9. The map of "*practical threshold velocity*" ($u_{t50\%}$) (see also the definition in section 5.2.4). This threshold is obtained when the land surface is the usual condition for dust outbreak. Color hatches represent land cover types.
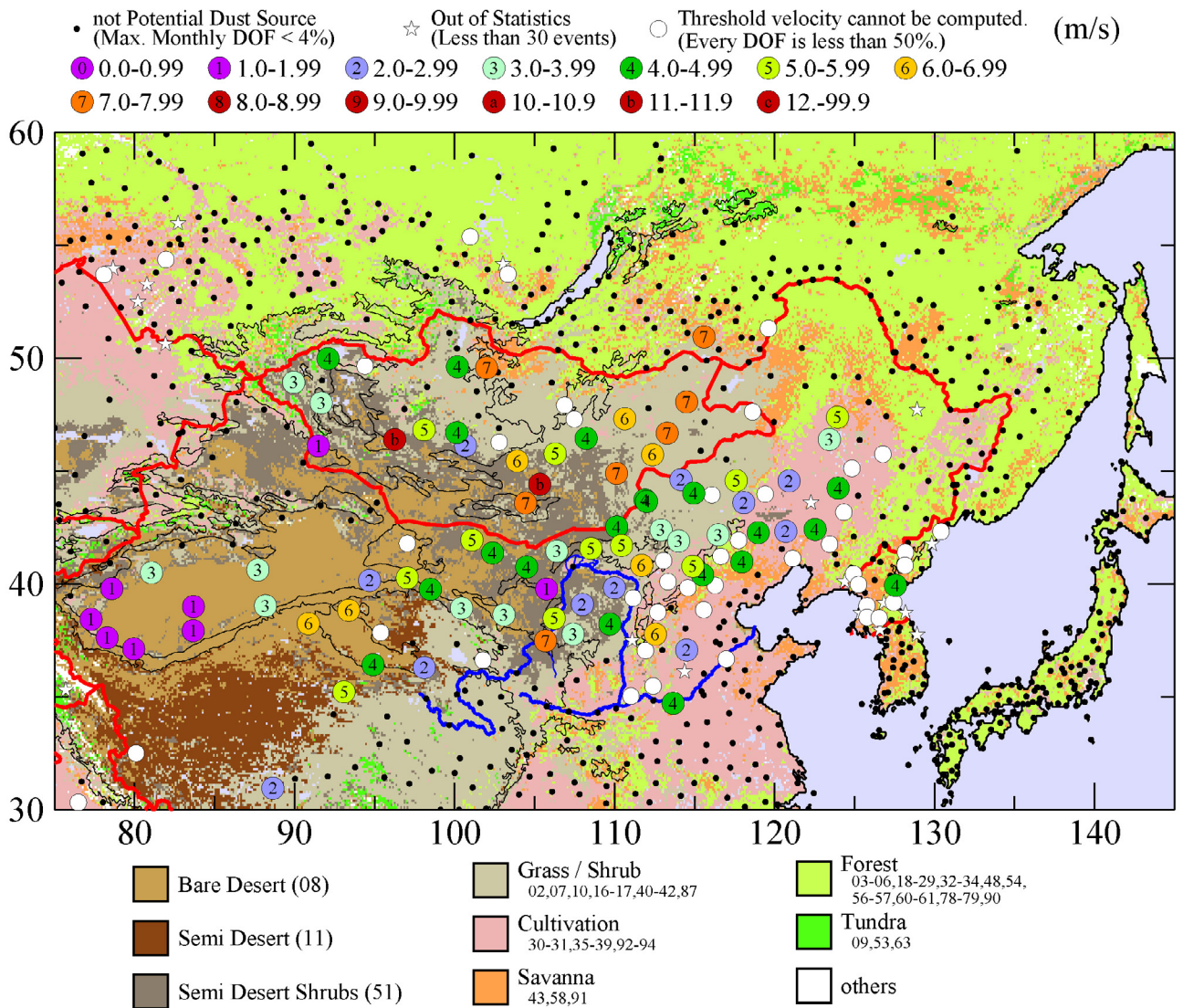
Fig. 5.10. The map of difference between the minimum and the practical threshold velocities ($\Delta u_t = u_{t50\%} - u_{t5\%}$). This indicates the variation of threshold velocity at each observatory and this can be an index of the variation of land surface conditions.
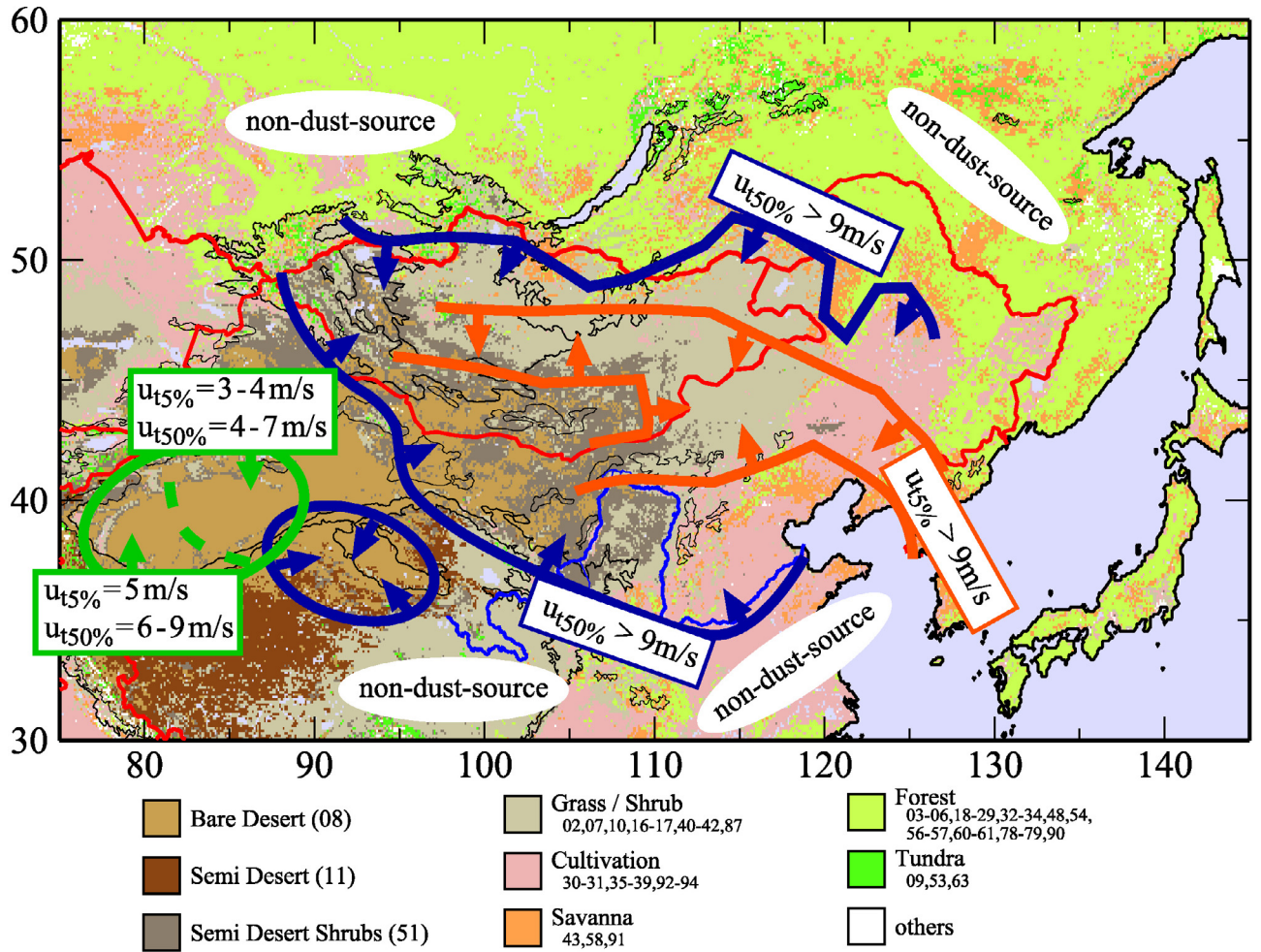
Fig. 5.11. The distribution of threshold wind velocity of aeolian dust outbreak. This illustration is drawn by reference to results of the minimum and the practical thresholds as shown in Figs. 5.8 and 5.9.

Chapter 6

Effect of Snow Cover on Aeolian Dust Outbreak

6.1 Introduction

The timing of a dust outbreak and the amount of vertical dust flux are largely controlled by surface wind and land surface conditions (e.g., soil wetness, land cover type, vegetation, snow cover, and soil size distribution). The effect of land surface conditions has been considered in some dust models for the simulation of global and regional dust cycles [e.g., *Tegen et al.*, 2002; *Shao et al.*, 2002; *Lunt and Valdes*, 2002a, 2002b; *Uno et al.*, 2003]. Although we recognize that recent dust models can reproduce the first-order patterns of dust distributions, *Tegen et al.* [2002] pointed out that oversimplification in the treatment of dust emission in these models has induced computational errors of dust transport and deposition. The effect of vegetation on dust outbreaks was studied in *Tegen et al.* [2002] and *Engelstaedter et al.* [2003].

Among land surface conditions, the effect of snow cover has not been discussed in detail, except in studies on dust in the glacial period [*Lunt and Valdes*, 2002a, 2002b]. This is probably because snow cover has been thought to have little effect on global dust distribution [*Woodward*, 2001; *Lunt and Valdes*, 2002b]. However, we believe snow cover affects dust outbreaks in East Asia, where arid and/or semiarid regions are frequently covered by snow in the season of dust events. Dust sources in East Asia are located in relatively high latitudes (around 35°N – 50°N) (section 3.1.3), and dust outbreaks frequently occur from March to May (sections 4.1 and 4.3). The areas of snow

cover differ every year, especially in high latitudes and early in the dust season (March and April). This fact makes it difficult to know the distribution of dust from East Asia.

In section 4.1, we showed year-to-year, seasonal and spatial variations of dust outbreak frequency (hereafter, DOF) correlate positively with those of strong wind frequency (hereafter, SWF) in East Asia, although we ignored the effect of land surface conditions on the threshold wind velocity of dust outbreak. This means that the surface wind, rather than land surface conditions, primarily controls dust outbreaks in East Asia. However, the DOF was low in April 1995, although the SWF was high. The reverse was true in April 1998. These facts suggest that land surface conditions largely controlled the dust outbreaks in these cases.

In simple dust models [e.g., *Tegen and Fung*, 1994], a vertical dust flux (F) is expressed by an equation, $F = C (u - u_t) \times u^2$, where C is a coefficient, u is a surface wind velocity at a height of 10 m, and u_t is the threshold wind velocity of dust outbreak. Although many researchers set a threshold velocity as a constant (6.5 m/sec), threshold velocities actually exhibit various values with differing land surface conditions. In this study, we made a statistical study of the effect of snow cover, one of these land surface conditions, on the threshold wind velocity. We will discuss the effect of snow cover on dust outbreaks in the cases of April 1995 and April 1998 in section 6.3.1. An equation of threshold wind velocity with snow cover will be proposed in section 6.3.2. The validity of this equation will be discussed in section 6.3.3.

6.2 Data and methods

We used the present weather code and surface wind velocity at a height of 10 m for calculating the DOF and the SWF. The data was obtained through observations at 105 meteorological sites in East Asia (33.5°N – 52.0°N, 88.5°E – 131.5°E) in the months of March and April from 1988 to 2003. They were distributed through SYNOP reports [*WMO*, 1974]. The code numbers of the present weather, ww=07, 08, 09, 30-35, and 98, are classified as the dust outbreaks. A strong wind, as discussed in section 3.1, is

defined as one with a velocity exceeding 6.5 m/sec. These definitions, the analysis region, and the 105 selected observatories are the same as those in section 4.1.

In this chapter, we would like to clarify the dependency of threshold wind velocity on snow cover. It is impossible, however, using the SYNOP data, to obtain threshold wind velocity in a dust emission model that refers to the minimum velocity required for emissions of dust particles [*Shao*, 2000]. The representative scale of dust outbreaks observed at a WMO synoptic site is too large (maybe a few hundred to thousands of meters) in comparison with the scale of the microphysical process of dust emission. Thus, we used a statistical approach for the snow cover dependency on the relation between wind velocity and DOF (sections 6.3.2 and 6.3.3).

The snow cover data used in this study is derived from the Special Sensor Microwave/Imager (SSM/I). This data set is distributed by the National Climatic Data Center (NCDC) as monthly and weekly snow cover fractions (hereafter, SCFs) [*Grody and Basist*, 1996; *Basist et al*, 1996]. Monthly and weekly SCFs refer to fractions of days with snow cover for a month and for a week, respectively. Monthly SCFs are used in section 6.3.1, and weekly SCFs are used in sections 6.3.2 and 6.3.3. Their grid interval is 1/3 degree (about 30 km). SCFs are not available for March 1991 and April of 1991, 1993, and 1996.

6.3 Results and discussion

6.3.1 Effect of snow cover on dust outbreaks in April of 1995 and 1998

Figures 6.1a and 6.1b present differences between SWFs in April 1995 and April 1998 (i.e., $SWF_{98} - SWF_{95}$; hereafter, ΔSWF) and between DOFs in April 1995 and April 1998 (i.e., $DOF_{98} - DOF_{95}$; hereafter, ΔDOF), respectively. Symbols in Fig. 6.2a (6.2b) indicate the DOF_{95} (DOF_{98}). Strong winds occurred less frequently in April 1998 than in April 1995 at most of the observatories in Mongolia (red ellipse), eastern China (blue ellipse), and the eastern Loess Plateau (green ellipse) in Fig. 6.1a. Dust outbreaks

occurred less frequently in April 1998 than in April 1995 at many observatories in eastern China. The ΔDOF positively correlates with the ΔSWF in this region. However, dust outbreaks occurred more frequently in April 1998 than in April 1995 in Mongolia and the eastern Loess Plateau, although the reverse was true about strong winds.

Color hatches in Fig. 6.1b indicate the difference between SCFs in April of 1995 and 1998 (i.e., SCF_{98} − SCF_{95}; hereafter, ΔSCF). Color hatches in Fig. 6.2a (6.2b) show the SCF in April 1995 (1998). Figure 6.1b spatiotemporally depicts more snow cover in April 1995 than in April 1998. This tendency is especially strong in Mongolia. Compared with the average of SCFs in April from 1988 to 2003 (not shown), SCF_{95} is greater throughout the analysis region. SCF_{98} is less than the average. SCF_{98} is almost the same as SCF_{95} around eastern China and the eastern Loess Plateau (Fig. 6.1b) because the SCF is small in both Aprils around these regions (Figs. 6.2a and 6.2b).

Table 6.1 illustrates the relations among the ΔSWF, the ΔDOF, and the ΔSCF in each region. While the correlation is negative between the ΔSWF and the ΔDOF in Mongolia, the ΔSCF is largely negative, suggesting that dust outbreaks were controlled by snow cover conditions rather than by surface winds. The similar tendency can be found in the eastern Loess Plateau. In eastern China, the correlation is positive between the ΔDOF and the ΔSWF. This is probably because little snow cover was observed around this region in either April, and the surface wind primarily controlled the dust outbreaks.

6.3.2 Threshold wind velocity of dust outbreak with snow cover

Figure 6.3 indicates the frequency distribution of wind velocity with a dust outbreak (hatched bar) and without a dust outbreak (no hatched bar) at all observatories when the weekly SCF is 0% for early spring (March and April) from 1988 to 2003. The right panel is a vertical expansion of the left one. Each dot with a solid line indicates the DOF for each wind velocity. This graph represents a reasonable conclusion that DOF increases with wind velocity.

The left panel of Fig. 6.4 depicts the DOF for each wind velocity in three cases (SCF=0%, 50%, and 100%). The DOF becomes smaller with an increase of SCF when wind velocity is constant at every value. The right panel shows cross sections of the left panel at three constant DOFs (4%, 8%, and 16%). This graph indicates that wind velocity increases to keep a DOF constant when the SCF increases. In addition, the increase rates among three different cross sections are almost the same between 0.027 and 0.030 (see Table 6.2). As threshold wind velocity expresses the wind velocity at some DOF criterion, this result means that a threshold wind velocity increases at a constant rate (0.027 to 0.030) with the SCF. When a threshold wind velocity under no snow cover condition is set as u_{t0}, a threshold wind velocity under snow cover condition (u_t) can be proposed as,

$$u_t = r \times f_{sc} + u_{t0} , \qquad\qquad\qquad (6.1)$$

where r is the increase rate (0.027 to 0.030), and f_{sc} is a SCF.

6.3.3 Validation of equation (6.1)

Figure 6.5 shows the relationship between SWFs and DOFs in March (upper panel) and April (lower panel) of each year from 1988 to 2003. Two types of SWFs are shown in Fig. 6.5. For the SWF_{cnst} (white symbol), a strong wind is defined by a constant value, 6.5 m/sec. For the SWF_{var} (black symbol), a strong wind is defined by equation (6.1) where r and u_{t0} are set 0.029 and 6.5, respectively   (i.e., $u_t = 0.029 \times f_{sc} + 6.5$).

The correlation of DOF with the SWF_{var} is greater than that with the SWF_{cnst} in both March and April. Therefore, equation (6.1) is certainly valid. Table 6.3 presents regression equations and correlation coefficients between SWFs and DOFs. The effect of snow cover shown by this equation can be seen in Fig. 6.5. For example, white triangles can be found where the SWF_{cnst} is 19% in April. There is no correlation between SWFs and DOFs, while there is a positive correlation when the SWF is computed using equation (6.1) (black triangles).

Despite the validity of equation (6.1) as shown above, some dispersion from the regression line remains between the SWF_{var} and the DOF. Some plots are still off the regression line (black symbols). For example, the SWF_{var} is still too large in April 1995.

The following reasons for this dispersion have been suggested. (1) Land surface conditions except for snow cover (e.g., soil wetness and vegetation) cause errors. Vegetation becomes active in some regions toward the end of April. That makes the threshold wind velocity increase even without snow cover conditions [*Shao et al.*, 2002]. (2) A SCF shows neither the amount nor the characteristics of snow. In some cases, therefore, when snow is rich before a thaw, soil becomes too wet for dust outbreaks even if the SCF is 0%. In contrast, when snow is powdery, strong wind can be expected to sweep away snow and entrain dust particles even if the SCF is 100%. (3) There are some cases in which snow does not cover the whole area in a grid even when SSM/I images show snow cover [*Basist et al.*, 1996]. The representative scale of dust observation at the surface (maybe a few hundred to thousands of meters) is much less than the grid scale of the SSM/I image (about 30 km). Therefore, a 100% SCF does not always mean total snow cover at an observatory. There can thus be errors due to the subgrid heterogeneity of the snow coverage.

The correlation coefficient between SWFs and DOFs is less in April than in March, and the improvement of the correlation coefficient by equation (6.1) is less in April than in March (Table 6.3). This is probably because a thaw is under way or has already finished in April, and soil wetness, vegetation, and errors due to subgrid heterogeneity of snow coverage, and so on affect dust outbreaks more remarkably in April than in March.

6.4 Summary

This study defines parameters for the threshold wind velocity of dust outbreak as affected by snow cover, and this formulation improves the correlation between the SWF and the DOF in East Asia in spring (March and April). Dust events frequently occur in this region in these months (section 4.1), while snow simultaneously covers a broad area.

Although this makes it difficult to know the timing of a dust outbreak and to estimate the dust flux, our equation to determine the threshold wind velocity should improve dust simulations in East Asia in the spring months.

Furthermore, this study suggests the importance of soil wetness, vegetation, and errors due to subgrid heterogeneity of snow coverage, as well as snow cover, especially in the season of thaw, which is around the latter half of April.

Region	ΔSWF (wind) $SWF_{98} - SWF_{95}$	ΔDOF (dust) $DOF_{98} - DOF_{95}$	Correlation between ΔSWF and ΔDOF	ΔSCF (snow) $SCF_{98} - SCF_{95}$
Mongolia	Negative (–)	Positive (+)	Negative (–)	Largely Negative (–)
Eastern Loess Plateau	Negative (–)	Positive (+)	Negative (–)	Negative (–)
Eastern China	Negative (–)	Negative (–)	Positive (+)	Negative (–)

Table 6.1. Relation among ΔSWF, ΔDOF, and ΔSCF in each region.

DOF (Dust Outbreak Frequency)	Regression equation between wind velocity, u (m/s) and SCF, f_{sc} (%)	Correlation Coefficient
4%	$u = 0.0276 \times f_{sc} + 6.04$	0.90
8%	$u = 0.0290 \times f_{sc} + 7.83$	0.92
16%	$u = 0.0295 \times f_{sc} + 9.44$	0.90

Table 6.2. Relations of surface wind velocity (u) with SCF (f_{sc}), when DOF takes values of 4%, 8%, and 16 %.

Month	Threshold of strong wind	Regression equation between DOF and SWF	Correlation Coefficient
March	constant	$DOF = 0.22 \times SWF_{cnst} - 1.43$	0.73
March	variable	$DOF = 0.36 \times SWF_{var} - 1.27$	0.90
April	constant	$DOF = 0.32 \times SWF_{cnst} - 2.83$	0.70
April	variable	$DOF = 0.47 \times SWF_{var} - 3.88$	0.83

Table 6.3. Relations of DOFs with SWF_{cnst} and SWF_{var}.
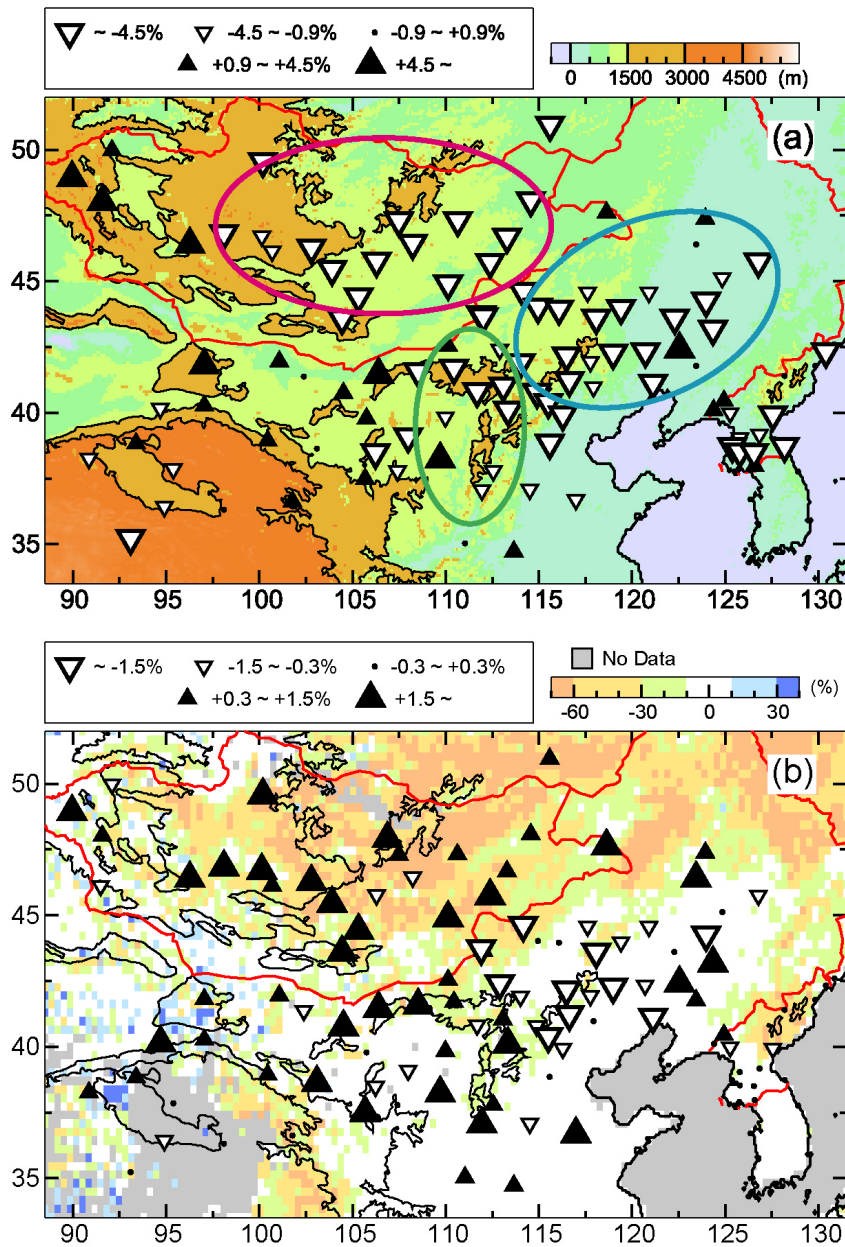
Fig. 6.1. Symbols in (a) and (b) shows differences between SWFs in April 1995 and April 1998 (i.e., $SWF_{98} - SWF_{95}$) and between DOFs in April 1995 and April 1998 (i.e., $DOF_{98} - DOF_{95}$), respectively. Color hatches in (b) show differences between SCFs in April 1995 and April 1998 (i.e., $SCF_{98} - SCF_{95}$). Color hatch in (a) and black solid line show topography, and this black solid line indicates 1500 m and 3000 m A.S.L. Red solid line indicates the national border. Red, blue, and green ellipses in (a) indicate regions of Mongolia, the eastern China, and the eastern Loess Plateau, respectively.
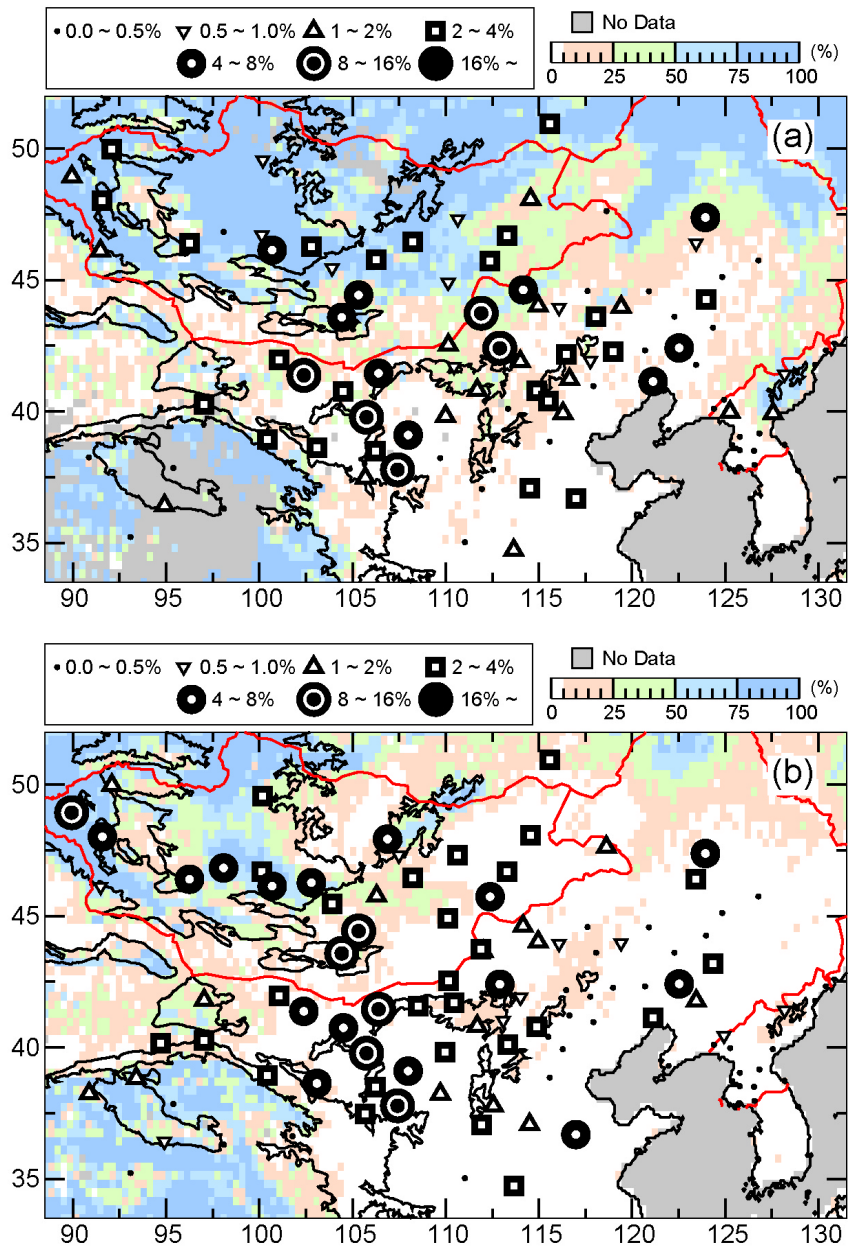
Fig. 6.2. Symbols in (a) and (b) shows DOFs in April 1995 and April 1998, respectively. Similarly, color hatches show SCFs. Solid lines are the same as Fig. 6.1.
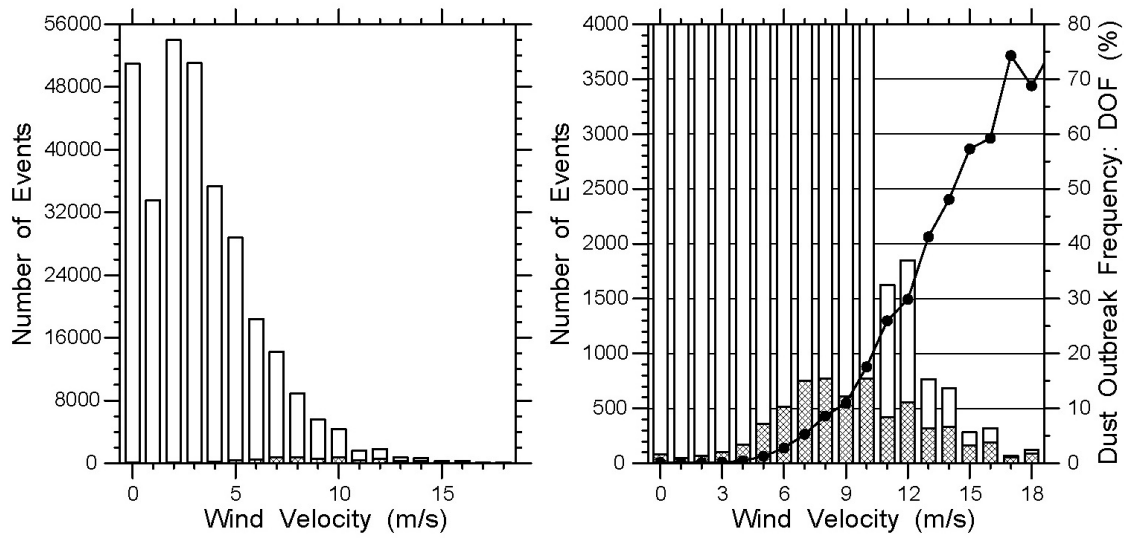
Fig. 6.3. Frequency distributions of wind velocities with a dust outbreak (hatched bar) and without a dust outbreak (no hatched bar) at all observatories when a weekly SCF is 0% for March and April from 1988 to 2003 (left panel). The right panel is a vertical expansion of the left panel. A solid line with dots indicates each DOF for each wind velocity in right panel.
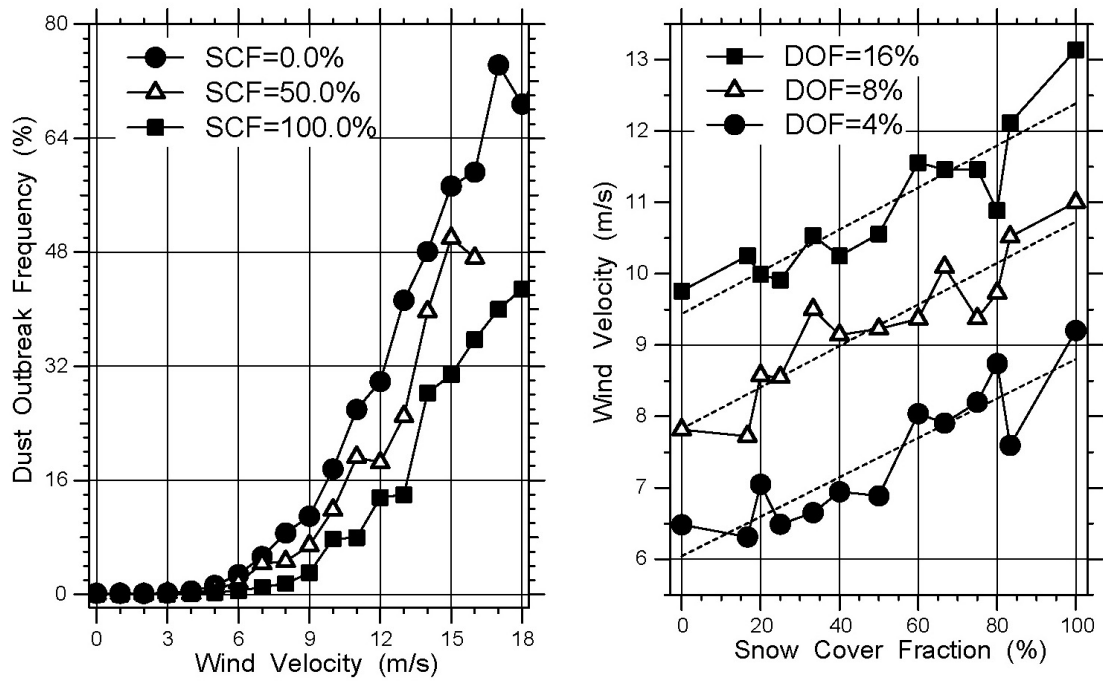
Fig. 6.4. The left panel is the DOF for each wind velocity, when SCFs are 0%, 50%, and 100%. The right panel is cross sections of the left panel at three constant DOFs (4%, 8%, and 16%) and their regression lines (dash line).
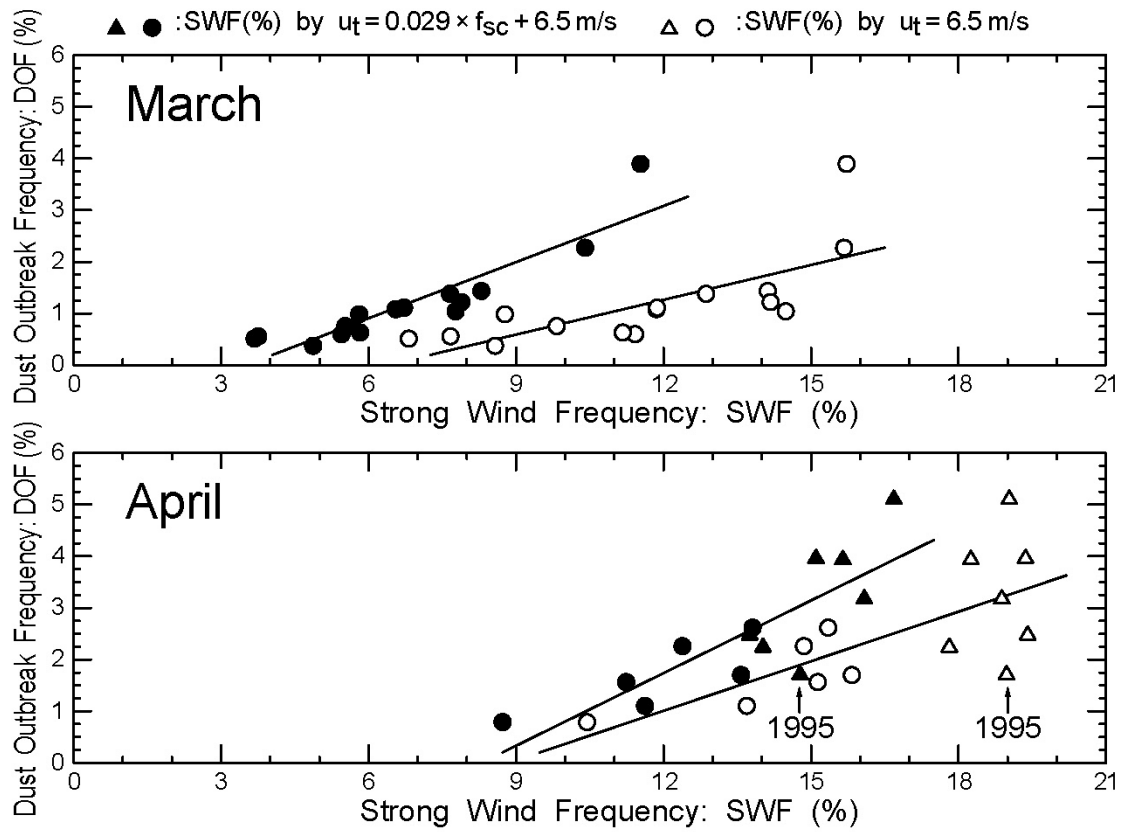
Fig. 6.5. Relations between the SWF and the DOF in March (upper panel) and in April (lower panel) of each year from 1988 to 2003. Two kinds of SWFs are shown here. For the SWF$_{cnst}$ (open circles and triangles), a strong wind is defined by a constant value, 6.5 m/sec; for the SWF$_{var}$ (closed circles and triangles), a strong wind is defined by the equation (1). Both open and closed plots in March 1991 and Aprils 1991, 1993, and 1996 are not shown because snow cover data are absent for these periods.

Chapter 7

Conclusions

This study conducted statistical analyses by use of surface meteorological data, land cover type data and snow cover data in East Asia for the period from March 1988 to June 2003 in order to clarify (i) the relation between aeolian dust sources and land cover types, (ii) which largely control aeolian dust outbreaks, surface winds or land surface conditions, (iii) the spatial distribution of threshold wind velocities of aeolian dust outbreak, and (iv) the effect of snow cover on aeolian dust outbreak.

For the first purpose, the potential dust source is defined in Chapter 3 as that the maximum monthly dust outbreak frequency exceeds 4% from March 1988 to June 2003. The summary for the first purpose is as follows:

1. Potential dust sources distribute in regions where land cover types are Bare Desert, Semi Desert Shrubs, Grass/Shrub and Cultivation. The northern boundary of potential dust sources almost corresponds to the southern boundary of the Forest regions. The southern boundary of potential dust sources distribute around the Huang He River. The southern boundary of potential dust sources is located around the southern boundaries of Bare Desert and Semi Desert Shrubs regions in middle and upper reaches of the Huang He River. This result suggests that deforestation and desertification will cause an expansion of dust source.

For the second purpose, two analysis regions are given as "around the Gobi Desert" and "the Taklimakan Desert" in Chapter 4. Seasonal, year-to-year and spatial

variations of dust outbreak frequencies were discussed with reference to strong wind frequencies in both regions. The results are summarized as follows:

2. Dust outbreaks frequently occur at months of frequent strong winds in both regions. The months of frequent dust outbreaks are limited in March, April and May around the Gobi Desert, while dust outbreaks frequently occur from March to July and/or August in the Taklimakan Desert.

3. The ratio of dust outbreaks to strong winds is small around the Gobi Desert when a strong wind is defined as one with a velocity exceeding 6.5 m/sec. This tendency is remarkable in April that both dust outbreaks and strong winds occur the most frequently around the Gobi Desert and in the Taklimakan Desert. The probability of dust outbreak is about one seventh when a strong wind occurs in April around the Gobi Desert, although these frequencies are almost the same in the Taklimakan Desert. This suggests that the threshold velocity of aeolian dust outbreak should be around 6.5 m/sec in the Taklimakan Desert while it should be larger than 6.5 m/sec around the Gobi Desert.

4. The correlation between strong wind frequency and dust outbreak frequency is always higher in the Taklimakan Desert than that around the Gobi Desert from March to May. In both regions, the correlation between these frequencies is large in March and April in comparison with May. These results mean that the surface wind primarily controls dust outbreaks in March and April especially in the Taklimakan Desert. On the other hand, land surface conditions such as soil wetness and vegetation activity should largely affect dust outbreaks in May around the Gobi Desert.

5. Major regions of frequent dust outbreaks are the southern Mongolia (about 44°N, 105°E), the Badain Jaran Desert (about 42°N, 102°E), the western Loess Plateau (about 40°N, 105°E) and the Taklimakan Desert for the period of March, April and May from 1988 to 2003.

6. The remarkable frequent dust outbreaks were observed around the Gobi Desert during 2000 – 2002. Although March, April, and May are the most active months for

dust outbreaks, remarkable increases of dust outbreaks occurred only in March and April. Furthermore, frequencies of strong wind and dust outbreak correlate in March and April. Dust outbreaks frequently occurred around the northeastern region of China and the North China Plain during the same period although these regions include small dust sources in other years.

For the third purpose, two kinds of threshold velocities are defined in Chapter 5. One is the minimum threshold velocity ($u_{t5\%}$), which is the threshold velocity at nearly the most favorable land surface condition for aeolian dust outbreak. The other is the practical threshold velocity ($u_{t50\%}$), which is the threshold velocity at a usual land surface condition. The results are summarized as follows:

7. Both kinds of threshold velocities (i.e., $u_{t5\%}$ and $u_{t50\%}$) are the largest in Northern Mongolia. On the other hand, they are the smallest in the west of the Taklimakan Desert. There is a tendency that thresholds decrease from the northeast (i.e., Mongolia and Inner Mongolia) to the southwest (i.e., the Taklimakan Desert).

8. From the viewpoint of land cover type, both kinds of threshold velocities are the largest in the Grass/Shrub region (i.e., Northern Mongolia and Inner Mongolia), the next largest in the Semi Desert Shrubs region (i.e., the Gobi Desert) and the smallest in the Bare Desert region (i.e., the Taklimakan Desert).

9. The practical threshold velocities ($u_{t50\%}$) are conspicuously larger than those used in simple dust models, which are 6.5 m/sec, in the regions except for the Taklimakan Desert.

10. Differences between the minimum and the practical threshold velocities ($\Delta u_t = u_{t50\%} - u_{t5\%}$) are large in Mongolia and small in the west of the Taklimakan Desert. This result indicates that land surface conditions are largely variable in Mongolia. On the other hand, land surface conditions are almost constant in the west of the Taklimakan Desert.

For the fourth purpose, statistical analyses were conducted about snow cover, surface wind and aeolian dust outbreak in Chapter 6. The results are summarized as

follows:

11. As mentioned in the fourth conclusion, the dust outbreak frequency positively correlate with the strong wind frequency in April around the Gobi Desert. However, the dust outbreak frequency is low in April 1995 although the strong wind frequency is high. The reverse is true in April 1998. The reason of these is snow cover especially in Mongolia. In April 1995, snow covers larger area than in usual April. The reverse is true in April 1998.

12. This study statistically analyzed the relation between the threshold wind velocity of dust outbreak and snow cover. It is found that the threshold velocity linearly increases with snow cover fraction. The threshold velocity is well parameterized with snow cover fraction. This formulation improves the correlation between the strong wind frequency and the dust outbreak frequency in East Asia in March and April.

This study deepened the understanding about the aeolian dust outbreak in East Asia from the viewpoint of surface wind and land surface conditions such as land cover type and snow cover. These results should improve representations of numerical models of aeolian dust in East Asia and we will obtain more precise spatial and temporal distributions of aeolian dust. This contributes to the high level scientific understanding about the impact of aeolian dust on climate. Moreover, aeolian dust outbreaks occur by the conditions of surface wind and land surface (e.g., soil wetness, vegetation activity, land cover type, snow cover) and this study provided many of these conditions. Therefore, the monitoring aeolian dust from East Asia plays an important role in understanding current environment in East Asia such as climate, desertification, deforestation, water resource, food resource and so on.

Appendix 1

Present Weather in SYNOP

---

ww = 00 – 49   *No precipitation at the station at the time of observation*

---

ww = 00 – 19   No precipitation, fog, ice fog (except for 11 and 12), duststorm, sandstorm, drifting or blowing snow at the station* at the time of observation or, except for 09 and 17, during the preceding hour

---

ww

00   Cloud development not observed or not observable

01   Clouds generally dissolving or becoming less developed

02   State of sky on the whole unchanged

03   Clouds generally forming or developing

} characteristic change of the state of sky during the past hour

04   Visibility reduced by smoke, e.g., veldt or forest fires, industrial smoke or volcanic ashes

05   Haze

06   Widespread dust in suspension in the air, not raised by wind at or near the station at the time of observation

07   Dust or sand raised by wind at or near the station at the time of observation, but no well-developed dust whirl(s) or sand whirl(s), and no duststorm or sandstorm seen; or, in the case of ships, blowing spray at the station

08   Well-developed dust whirl(s) or sand whirl(s) seen at or near the station during the preceding hour or at the time of observation, but no duststorm or sandstorm

09   Duststorm or sandstorm within sight at the time of observation, or at the station during the preceding hour

} Haze, dust, sand or smoke

10   Mist

11 { Patches of

12 { More or less continuous

} shallow fog or ice fog at the station, whether on land or sea, not deeper than about 2 metres on land or 10 metres at sea

---

* The expression "at the station" refers to a land station or a ship.

13   Lightning visible, no thunder heard

14   Precipitation within sight, not reaching the ground or the surface of the sea

15   Precipitation within sight, reaching the ground or the surface of the sea, but distant, i.e., estimated to be more than 5 km, from the station

16   Precipitation within sight, reaching the ground or the surface of the sea, near to, but not at the station

17   Thunderstorm, but no precipitation at the time of observation

18   Squalls

19   Funnel cloud(s)*

⎫ at or within sight of the station during the preceding hour or at the time of observation

---

ww = 20 – 29   Precipitation, fog, ice fog or thunderstorm at the station during the preceding hour but not at the time of observation

---

ww

20   Drizzle (not freezing) or snow grains

21   Rain (not freezing)

22   Snow

23   Rain and snow or ice pellets

24   Freezing drizzle or freezing rain

25   Shower(s) of rain

⎫ not falling as shower(s)

26   Shower(s) of snow, or of rain and snow

27   Shower(s) of hail** or of rain and hail**

28   Fog or ice fog

29   Thunderstorm (with or without precipitation)

---

ww = 30 – 39   Duststorm, sandstorm, drifting or blowing snow

---

ww

30   ⎫

31   ⎬ Slight or moderate duststorm or sandstorm

32   ⎭

⎧ − has decreased during the preceding hour

− no appreciable change during the preceding hour

⎩ − has begun or has increased during the preceding hour

---

* Tornado cloud or waterspout.
** Hail, small hail, snow pellets.

33			− has decreased during the preceding hour
34	Severe duststorm or sandstorm		− no appreciable change during the preceding hour
35			− has begun or has increased during the preceding hour

36	Slight or moderate drifting snow	
37	Heavy drifting snow	Generally low (below eye level)
38	Slight or moderate blowing snow	
39	Heavy blowing snow	Generally high (above eye level)

---

ww = 40 – 49   Fog or ice fog at the time of observation

---

ww

40   Fog or ice fog at a distance at the time of observation, but not at the station during the preceding hour, the fog or ice fog extending to a level above that of the observer

41   Fog or ice fog in patches

42   Fog or ice fog, sky visible

43   Fog or ice fog, sky invisible   has become thinner during the preceding hour

44   Fog or ice fog, sky visible

45   Fog or ice fog, sky invisible   no appreciable change during the preceding hour

46   Fog or ice fog, sky visible

47   Fog or ice fog, sky invisible   has begun or has become thicker during the preceding hour

48   Fog, depositing rime, sky visible

49   Fog, depositing rime, sky invisible

---

ww = 50 – 99   *Precipitation at the station at the time of observation*

---

ww = 50 – 59   Drizzle

---

ww

50   Drizzle, not freezing, intermittent

51   Drizzle, not freezing, continuous   slight at time of observation

52   Drizzle, not freezing, intermittent

53   Drizzle, not freezing, continuous   moderate at time of observation

54	Drizzle, not freezing, intermittent	
55	Drizzle, not freezing, continuous	heavy (dense) at time of observation

56 Drizzle, freezing, slight

57 Drizzle, freezing, moderate or heavy (dense)

58 Drizzle and rain, slight

59 Drizzle and rain, moderate or heavy

---

ww = 60 – 69   Rain

---

ww

60	Rain, not freezing, intermittent	
61	Rain, not freezing, continuous	slight at time of observation
62	Rain, not freezing, intermittent	
63	Rain, not freezing, continuous	moderate at time of observation
64	Rain, not freezing, intermittent	
65	Rain, not freezing, continuous	heavy at time of observation

66 Rain, freezing, slight

67 Rain, freezing, moderate or heavy

68 Rain or drizzle and snow, slight

69 Rain or drizzle and snow, moderate or heavy

---

ww = 70 – 79   Solid precipitation not in showers

---

ww

70	Intermittent fall of snowflakes	
71	Continuous fall of snowflakes	slight at time of observation
72	Intermittent fall of snowflakes	
73	Continuous fall of snowflakes	moderate at time of observation
74	Intermittent fall of snowflakes	
75	Continuous fall of snowflakes	heavy at time of observation

76 Diamond dust (with or without fog)

77 Snow grains (with or without fog)

78 Isolated star-like snow crystals (with or without fog)

79 Ice pellets

ww = 80 – 99	Showery precipitation, or precipitation with current or recent thunderstorm

ww

80	Rain shower(s), slight
81	Rain shower(s), moderate or heavy
82	Rain shower(s), violent
83	Shower(s) of rain and snow mixed, slight
84	Shower(s) of rain and snow mixed, moderate or heavy
85	Snow shower(s), slight
86	Snow shower(s), moderate or heavy

| 87 | Shower(s) of snow pellets or small hail, with or without rain or rain and snow mixed | – slight |
| 88 | | – moderate or heavy |

| 89 | Shower(s) of hail, with or without rain or rain and snow mixed, not associated with thunder | – slight |
| 90 | | – moderate or heavy |

91	Slight rain at time of observation	
92	Moderate or heavy rain at time of observation	
93	Slight snow, or rain and snow mixed or hail*, at time of observation	thunderstorm during the preceding hour but not at time of observation
94	Moderate or heavy snow, or rain and snow mixed or hail* at time of observation	

95	Thunderstorm, slight or moderate, without hail* but will rain and/or snow at time of observation	
96	Thunderstorm, slight or moderate, with hail* at time of observation	
97	Thunderstorm, heavy, without hail* but with rain and/or snow at time of observation	thunderstorm at time of observation
98	Thunderstorm combined with duststorm or sandstorm at time of observation	
99	Thunderstorm, heavy, with hail* at time of observation	

---

* Hail, small hail, snow pellets.

Appendix 2

USGS Global Land Cover Characteristics Data Base Version 2.0

Global Ecosystems Legend

Value   Description

01	Urban		20	Cool Rain Forest
02	Low Sparse Grassland		21	Conifer Boreal Forest
03	Coniferous Forest		22	Cool Conifer Forest
04	Deciduous Conifer Forest		23	Cool Mixed Forest
05	Deciduous Broadleaf Forest		24	Mixed Forest
06	Evergreen Broadleaf Forests		25	Cool Broadleaf Forest
07	Tall Grasses and Shrubs		26	Deciduous Broadleaf Forest
08	Bare Desert		27	Conifer Forest
09	Upland Tundra		28	Montane Tropical Forests
10	Irrigated Grassland		29	Seasonal Tropical Forest
11	Semi Desert		30	Cool Crops and Towns
12	Glacier Ice		31	Crops and Town
13	Wooded Wet Swamp		32	Dry Tropical Woods
14	Inland Water		33	Tropical Rainforest
15	Sea Water		34	Tropical Degraded Forest
16	Shrub Evergreen		35	Corn and Beans Cropland
17	Shrub Deciduous		36	Rice Paddy and Field
18	Mixed Forest and Field		37	Hot Irrigated Cropland
19	Evergreen Forest and Fields		38	Cool Irrigated Cropland

39	Cold Irrigated Cropland	70	Glacier Rock

39 Cold Irrigated Cropland

40 Cool Grasses and Shrubs

41 Hot and Mild Grasses and Shrubs

42 Cold Grassland

43 Savanna (Woods)

44 Mire, Bog, Fen

45 Marsh Wetland

46 Mediterranean Scrub

47 Dry Woody Scrub

48 Dry Evergreen Woods

49 Volcanic Rock

50 Sand Desert

51 Semi Desert Shrubs

52 Semi Desert Sage

53 Barren Tundra

54 Cool Southern Hemisphere Mixed Forests

55 Cool Fields and Woods

56 Forest and Field

57 Cool Forest and Field

58 Fields and Woody Savanna

59 Succulent and Thorn Scrub

60 Small Leaf Mixed Woods

61 Deciduous and Mixed Boreal Forest

62 Narrow Conifers

63 Wooded Tundra

64 Heath Scrub

65 Coastal Wetland, NW

66 Coastal Wetland, NE

67 Coastal Wetland, SE

68 Coastal Wetland, SW

69 Polar and Alpine Desert

70 Glacier Rock

71 Salt Playas

72 Mangrove

73 Water and Island Fringe

74 Land, Water, and Shore

75 Land and Water, Rivers

76 Crop and Water Mixtures

77 Southern Hemisphere Conifers

78 Southern Hemisphere Mixed Forest

79 Wet Sclerophylic Forest

80 Coastline Fringe

81 Beaches and Dunes

82 Sparse Dunes and Ridges

83 Bare Coastal Dunes

84 Residual Dunes and Beaches

85 Compound Coastlines

86 Rocky Cliffs and Slopes

87 Sandy Grassland and Shrubs

88 Bamboo

89 Moist Eucalyptus

90 Rain Green Tropical Forest

91 Woody Savanna

92 Broadleaf Crops

93 Grass Crops

94 Crops, Grass, Shrubs

95 Evergreen Tree Crop

96 Deciduous Tree Crop

99 Interrupted Areas (Goodes Homolosine Projection)

100 Missing Data

Acknowledgments

References

Aoki, I. (2003), *The process of dust storm generation in Tarim Basin, Northwest China*, Master Degree Thesis, Univ. Tsukuba, Tsukuba, Japan, 114 pp. (in Japanese)

Aoki, T., M. Mikami, W.-J. Liu (2002), Spectral albedos of desert surfaces and size distributions of soil particles measured around Qira and Aksu in the Taklimakan Desert, *J. Arid Land Studies*, **11**, 259-266.

Bagnold, R. A. (1941), *The Physics of Blown Sand and Desert Dunes*, 265 pp., Methuen, New York.

Basist, A., D. Garrett, R. Ferraro, N. Grody, and K. Mitchell (1996), A comparison between snow cover products derived from visible and microwave satellite observations, *J. Appl. Meteor., 35*, 163-177.

Bullard, J. E., D. S. G. Thomas, I. Livingstone, and G. F. S. Wiggs (1997), Dunefield activity and interactions with climatic variability in the southwest Kalahari Desert, *Earth Surface Processes and Landforms*, **22**, 165-174.

Canadian Society of Soil Science (2002), *Soil and environmental science dictionary*, edited by Gregorich, E. G., L. W. Turchenek, M. R. Carter, and D. A. Angers, 577pp., CRC press, Boca Raton.

Chen, S.-J., Y.-H. Kuo, P.-Z. Zhang, and Q.-F. Bai (1991), Synoptic climatology of cyclogenesis over east Asia, *Mon. Weather Rev.*, **119**, 1407-1418.

Chiapello, I., J. M. Prospero, J. R. Herman, and N. C. Hsu (1999), Detection of mineral

dust over the North Atlantic Ocean and Africa with the Nimbus 7 TOMS, *J. Geophys. Res.*, **104**, 9277-9292.

Chun, Y., K.-O. Boo, J. Kim, S.-U. Park, and M. Lee (2001), Synopsis, transport, and physical characteristics of Asian dust in Korea, *J. Geophys. Res.*, **106**(D16), 18461-18469.

Chun, Y., S.-W. Kim, K.-M. Cho, and J.-S. Kim (2002), Saikin 100 nenkan no Kankoku niokeru Kosa kansoku nissu (Asian dust events in Korea during the recent hundred years), *Chikyu Kankyo*, **7**, 225-231. (in Japanese)

Duce, R. A., C. K. Unni, B. J. Ray, J. M. Prospero, and J. T. Merrill (1980), Long-range atmospheric transport of soil dust from Asia to the tropical North Pacific: Temporal variability, *Science*, **209**, 1522-1524.

Engelstaedter, S., K. E. Kohfeld, I. Tegen, and S. P. Harrison (2003), Controls of dust emissions by vegetation and topographic depressions: An evaluation using dust storm frequency data, *Geophys. Res. Lett.,* **30**(6), 1294, doi:10.1029/2002GL016471.

Gao, X.-Q., S. Yabuki, Z. Qu, and Z.-N. Qian (2002), Some characteristics of dust storm in northwest China, *J. Arid Land Studies*, **11**, 235-243.

Gao, Y., R. Arimoto, M. Y. Zhou, J. T. Merrill, and R. A. Duce (1992), Relationships between the dust concentrations over Eastern Asia and the remote North Pacific, *J. Geophys. Res.*, **97**(D9), 9867-9872.

Gillette, D. (1978), A wind tunnel simulation of the erosion of soil: effect of soil texture, sandblasting, wind speed, and soil consolidation on dust production, *Atmos. Environ.*, **12**, 1735-1743.

Gillette, D. A., J. Adams, A. Endo, and D. Smith (1980), Threshold velocities for input of soil particles into the air by desert soils, *J. Geophys. Res.*, **85**(C85), 5621-5630.

Gillette, D. A., J. Adams, D. Muhs, and R. Kihl (1982), Threshold friction velocities and

rupture moduli for crusted desert soils for the input of soil particles into the air, *J. Geophys. Res.*, **87**(C11), 9003-9015.

Ginoux, P., M. Chin, I. Tegen, J. M. Prospero, B. Holben, O. Dubovik, and S.-J. Lin (2001), Sources and distributions of dust aerosols simulated with the GOCART model, *J. Geophys. Res.*, **106**(D17), 20255-20273.

Glickman, T. S. (Eds.) (2000), *Glossary of meteorology, second edition*, American Meteorological Society, Boston, Massachusetts.

Goudie, A. S., and N. J. Middleton (1992), The changing frequency of dust storms through time, *Clim. Change*, **20**, 197-225.

Gove, P. B., and the Merriam-Webster editorial staff (Eds.) (1981), *Webster's Third New International Dictionary of the English Language Unabridged*, G. & C. Merriam Company, Publishers, Springfield.

Grody, N. C., and A. N. Basist (1996), Global identification of snowcover using SSM/I measurements, *IEEE Trans. Geosci. Remote Sens., 34*, 237-249.

He, Q. and J. Zhao (1999), Studies on distribution of floating dust in Tarim Basin, *Chinese. J. Arid Land Research*, **12**, 35-42.

He, Q., J. Zhao, and H. Nagashima (1996), The distribution of sandstorms in Taklimakan Desert, *J. Arid Land Studies*, **5**, 185-193.

Hedin, L. O., and G. E. Likens (1996), Atmospheric dust and acid rain, *Scientific American*, **275**, 88-92.

Herman, J. R., P. K. Bhartia, O. Torres, C. Hsu, C. Seftor, and E. Celarier (1997), Global distribution of UV-absorbing aerosols from Nimbus-7/TOMS data, *J. Geophys. Res.*, **102**, 16911-16922.

Hsu, N. C., J. R. Herman, O. Torres, B. N. Holben, D. Tanre, T. F. Eck, A. Smirnov, B.

Chatenet, and F. Lavenu (1999), Comparisons of the TOMS aerosol index with Sun-photometer aerosol optical thickness: Results and applications, *J. Geophys. Res.*, **104**, 6269-6280.

Husar, R.B., D.M. Tratt, B.A. Schichtel, S.R. Falke, F. Li, D. Jaffe, S. Gasso, T. Gill, N.S. Laulainen, F. Lu, M.C. Reheis, Y. Chun, D. Westphal, B.N. Holben, C. Gueymard, I. McKendry, N. Kuring, G.C. Feldman, C. McClain, R.J. Frouin, J. Merrill, D. DuBois, F. Vignola, T. Murayama, S. Nickovic, W.E. Wilson, K. Sassen, N. Sugimoto, and W.C. Malm (2001), Asian dust events of April 1998, *J. Geophys. Res.*, **106**(D16), 18317-18330.

Husar, R. B., J. M. Prospero, and L. L. Stowe (1997), Characterization of tropospheric aerosols over the oceans with the NOAA advanced very high resolution radiometer optical thickness operational product, *J. Geophys. Res.*, **102**, 16889-16909.

Intergovernmental Panel on Climate Change (IPCC) (2001), *Climate change 2001: The scientific basis*, edited by J. T. Houghton et al., 896 pp., Cambridge Univ. Press, New York. (http://www.ipcc.ch/)

Iwasaka, Y., H. Minoura, and K. Nagaya (1983), The transport and special scale of Asian dust-storm clouds: A case study of the dust-storm event of April 1979, *Tellus*, **35B**, 189-196.

Kalma, J. D., J. G. Speight, and R. J. Wasson (1988), Potential wind erosion in Australia: A continental perspective, *J. Climatol.*, **8**, 411-428.

Kanayama, S., S. Yabuki, F. Yanagisawa, and R. Motoyama (2002), The chemical and strontium isotope composition of atmospheric aerosols over Japan: the contribution of long-range-transported Asian dust (Kosa), *Atmos. Environ.*, **36**, 5159-5175.

Kurosaki, Y., and M. Mikami (2002), Seasonal and regional characteristics of dust event in the Taklimakan Desert, *J. Arid Land Studies*, **11**, 245-252.

Kurosaki, Y., and M. Mikami (2003), Recent frequent dust events and their relation to surface wind in East Asia, *Geophys. Res. Lett.*, **30**(14), 1736, doi:10.1029/2003GL017261.

Kurosaki, Y., and M. Mikami (2004), Effect of snow cover on threshold wind velocity of dust outbreak, *Geophys. Res. Lett.*, **31**(3), L03106, doi:10.1029/2003GL018632.

Littmann, T. (1991), Dust storm frequency in Asia: Climatic control and variability, *Int. J. Climatol.*, **11**, 393-412.

Liu, M. and D. L. Westphal (2001), A study of the sensitivity of simulated mineral dust production to model resolution, *J. Geophys. Res.*, **106**(D16), 18099-18112.

Liu, M., D. L. Westphal, S. Wang, A. Shimizu, N. Sugimoto, J. Zhou, and Y. Chen (2003), A high-resolution numerical study of the Asian dust storms of April 2001, *J. Geophys. Res.*, **108**(D23), 8653, doi:10.1029/2002JD003178.

Loveland, T. R., B. C. Reed, J. F. Brown, D. O. Ohlen, J. Zhu, L. Yang and J. W. Merchant (2000), Development of a Global Land Cover Characteristics Database and IGBP DISCover from 1-km AVHRR Data: *Int. J. Remote Sens.*, **21**, 1303-1330.

Lunt, D. J. and P. J. Valdes (2002a), Dust deposition and provenance at the last glacial maximum and present day, *Geophys. Res. Lett.*, **29**(22), 2085, doi:10.1029/2002GL015656.

Lunt, D. J., and P. J. Valdes (2002b), The modern dust cycle: Comparison of model results with observations and study of sensitivities, *J. Geophys. Res.*, **107**(D23), 4669, doi:10.1029/2002JD002316.

Marticorena, B., and G. Bergametti (1995), Modeling the atmospheric dust cycle: 1. Design of a soil-derived dust emission scheme, *J. Geophys. Res.*, **100**(D8), 16415-16430.

Middleton, N. J., and D. S. G. Thomas. (Eds.) (1997), *World Atlas of Desertification,*

Second Edition, Published by United Nations Environment Programme (UNEP), 182 pp., Arnold, London.

Mikami, M., O. Abe, M. Du, M. Chiba, K. Fujita, M. Hayashi, Y. Iwasaka, K. Kai, K. Masuda, T. Nagai, T. Ootomo, J. Suzuki, A. Uchiyama, S. Yabuki, Y. Yamada, M. Yasui, G. Shi, X. Zhang, Z. Shen, W. Wei, and J. Zhou (2002), The impact of aeolian dust on climate: Sino-Japanese cooperative project ADEC, *J. Arid Land Studies*, **11**, 211-222.

Mikami, M., T. Fujitani, and X. Zhang (1995), Basic characteristics of meteorological elements and observed local wind circulation in Taklimakan Desert, China, *J. Meteor. Soc. Japan*, **73**, 899-908.

Murayama, N. (1991), Kosa hassei no kisyou. Water Research Institute of Nagoya University ed., *Kosa*, Kokon Shoin, Tokyo. (in Japanese)

Okada, K., J. Heintzenberg, K. Kai and Y. Qin (2001), Shape of atmospheric mineral particles collected in three Chinese arid-regions, *Geophys. Res. Lett.*, **28**(16), 3123-3126.

Olson, J. S. (1994a), Global ecosystem framework-definitions: *USGS EROS Data Center Internal Report*, Sioux Falls, SD, 37p.

Olson, J. S. (1994b), Global ecosystem framework-translation strategy: *USGS EROS Data Center Internal Report*, Sioux Falls, SD, 39p.

Parungo, F., Z. Li, X. Li, D. Yang, and J. Harris (1994), Gobi dust storms and the great green wall, *Geophys. Res. Lett.*, **21**, 999-1002.

Prospero, J. M., P. Ginoux, O. Torres, S. E. Nicholson, and T. E. Gill (2002), Environmental characterization of global sources of atmospheric soil dust identified with the NIMBUS 7 Total Ozone Mapping Spectrometer (TOMS) absorbing aerosol product, *Rev. Geophys.*, **40**(1), 1002, doi:10.1029/2000RG000095.

Pye, K. (1987), *Aeolian Dust and Dust Deposits*, 334 pp., Academic Press, London.

Qian, W., L. Quan, and S. Shi (2002), Variations of the dust storm in China and its climatic control, *J. Clim.*, **15**, 1216-1229.

Rodwell, M. J. and B. J. Hoskins (1996), Monsoons and the dynamics of deserts, *Q. J. R. Meteorol. Soc.*, **122**, 1385-1404.

Sasaki, A. (2002), *A numerical study of synoptic disturbance over Mongolian arid region*, Master Degree Thesis, Univ. Tsukuba, Tsukuba, Japan, 60 pp. (in Japanese)

Sato, T., and F. Kimura (2004), *Subsidence over East Asia responded by diabatic heating of Tibetan Plateau*, Proceedings of the 2nd International Workshop on Terrestrial Change in Mongolia, 90-95.

Shaw, G. E. (1980), Transport of Asian desert aerosol to the Hawaiian Islands, *J. Appl. Mteorol.*, **19**, 1254-1259.

Shao, Y. (2000), *Physics and Modeling of Wind Erosion*, 393pp., Kluwer Academic Publishers, Norwell.

Shao, Y. (2001), A model for mineral dust emission, *J. Geophys. Res.*, **106**(D17), 20239-20254.

Shao, Y., E. Jung, and L. M. Leslie (2002), Numerical prediction of northeast Asian dust storms using an integrated wind erosion modeling system, *J. Geophys. Res.,* **107**(D24), 4814, doi:10.1029/2001JD001493.

Shao, Y., and M. R. Raupach (1992), The overshoot and equilibration of saltation, *J. Geophys. Res.,* **97**, 20559-20564.

Shao, Y., M. R. Raupach, and J. F. Leys (1996), A model for predicting aeolian sand drift and dust entrainment on scales from paddock to region, *Aust. J. Soil Res.*, **34**, 309-342.

Squires, V. R. (2001), Dust and sandstorms: An early warning of impending disaster. In: *Global Alarm: Dust and Sandstorms from the World's Drylands*, edited by Youlin, Y., V. R. Squires, and L. Qi, pages 15-28, a publication of UNCCD and CCICCD on the web-site, http://www.unccd.int/publicinfo/duststorms/menu.php.

Sun, J., M. Zhang, and T. Liu (2001), Spatial and temporal characteristics of dust storms in China and its surrounding regions, 1960-1999: Relations to source area and climate, *J. Geophys. Res.*, **106** (D10), 10325-10333.

Sun, J., T. Liu, and Z. Lei (2000), Sources of heavy dust fall in Beijing, China on April 16, 1998, *Geophys. Res. Lett.*, **27**(14), 2105-2108.

Takemura, T., H. Okamoto, Y. Murayama, A. Numaguti, A. Higurashi, and T. Nakajima (2000), Global three-dimensional simulation of aerosol optical thickness distribution of various origins, *J. Geophys. Res.*, **105** (D14), 17853-17873.

Takemura, T., I. Uno, T. Nakajima, A. Higurashi, and I. Sano (2002), Modeling study of long-range transport of Asian dust and anthropogenic aerosols from East Asia, *Geophys. Res. Lett.*, **29** (24), 2158, doi:10.1029/2002GL016251.

Tegen, I., and I. Fung (1994), Modeling of mineral dust in the atmosphere: Sources, transport, and optical thickness, *J. Geophys. Res.*, **99** (D11), 22897-22914.

Tegen, I., and I. Fung (1995), Contribution to the atmospheric mineral aerosol load from land surface modification, *J. Geophys. Res.*, **100** (D9), 18707-18726.

Tegen, I., S. P. Harrison, K. Kohfeld, I. C. Prentice, M. Coe, and M. Heimann (2002), Impact of vegetation and preferential source areas on global dust aerosol: Results from a model study, *J. Geophys. Res.*, **107**(D21), 4576, doi:10.1029/2001JD000963.

Torres, O., P. K. Bhartia, J. R. Herman, Z. Ahmad, and J. Gleason (1998), Derivation of aerosol properties from a satellite measurements of backscattered ultraviolet radiation: Theoretical basis, *J. Geophys. Res.*, **103**, 17099-17110.

Uematsu, M., R. A. Duce, J. M. Prospero, L. Chen, J. T. Merrill, and R. L. McDonald (1983), Transport of mineral aerosol from Asia over the North Pacific Ocean, *J. Geophys. Res.*, **88**, 5343-5352.

Uno, I., G. R. Carmichael, D. G. Streets, Y. Tang, J. J. Yienger, S. Satake, Z. Wang, J.-H. Woo, S. Guttikunda, M. Uematsu, K. Matsumoto, H. Tanimoto, K. Yoshioka, and T. Iida (2003), Regional chemical weather forecasting system CFORS: Model descriptions and analysis of surface observations at Japanese island stations during the ACE-Asia experiment, *J. Geophys. Res.,* **108**(D23), 8668, doi:10.1029/2002JD002845.

Uno, I., H. Amano, S. Emori, K. Kinoshita, I. Matsui, and N. Sugimoto (2001), Trans-Pacific yellow sand transport observed in April 1998: A numerical simulation, *J. Geophys. Res.*, **106** (D16), 18331-18344.

Watts, I. (1969), Climates of China and Korea. In: *Climates of Northern and Eastern Asia, World Survey Climatology 8*, edited by Arakawa, H., 1-118, Amsterdam, Elsevier.

World Meteorological Organization (WMO) (1974), Manual on Codes, Vol. I. International Codes, *WMO Publ., 306*, WMO, Geneva.

Woodward, S. (2001), Modeling the atmospheric life cycle and radiative impact of mineral dust in the Hadley Centre climate model, *J. Geophys. Res.,* **106**, 18155-18166.

Xuan, J. (1999), Dust emission factors for environment of Northern China, *Atmos. Environ.*, **33**, 1767-1776.

Xuan, J., G. Liu, and K. Du (2000), Dust emission inventory in northern China, *Atmos. Environ.*, **34**, 4565-4570.

Yabuki, S., S. Kanayama, F.-F. Fu, M. Honda, F. Yanagisawa, W.-S. Wei, F.-J. Zeng, M.-Z.

Liu, Z.-B. Shen, and L.-C. Liu (2002), Physical and chemical characteristics of aeolian dust collected over Asian dust source regions in China – Comparison with atmospheric aerosols in an urban area at Wako, Japan, *J. Arid Land Studies*, **11**, 273-289.

Yoshino, M. (1997), *Desertification in China*, Taimeido, Tokyo. (in Japanese)

Yoshino, M. (2002), Kosa (Asian dust) related to Asian monsoon system, *Korean J. Meteorol. Soc.*, **5**, 93-100.

Youlin, Y. (2001), Progress of research on understanding sand and dust storms in the world. In: *Global Alarm: Dust and Sandstorms from the World's Drylands*, edited by Youlin, Y., V. R. Squires, and L. Qi, pages 29-48, a publication of UNCCD and CCICCD on the web-site, http://www.unccd.int/publicinfo/duststorms/menu.php.